Taphonomy of exceptional Cambrian fossil Lagerstätten of China exemplified by the Chengjiang Biota and the Guanshan Biota

Dott. (Dipl.-Geol.) Angela Forchielli

Dissertation

submitted in partial fulfillment of the requirements
for the degree Doctor of Science in Geology and Paleontology
presented at the Department of Geosciences, Freie Universität Berlin

eingereicht in teilweiser Erfüllung der Anforderungen
für die Promotion zum Doktor *rer. nat.* in Geologie und Paläontologie
vorgelegt am Fachbereich Geowissenschaften der Freien Universität Berlin

Berlin, October 2013

Date of defense of the thesis/

Tag der Disputation: 20. 12. 2013

First Referee (Erstgutachter):   Prof. Dr. Helmut Keupp

Freie Universität Berlin

Institut für Geologische Wissenschaften

Fachrichtung Paläontologie

Malteserstrasse 74-100, Haus D

12249 Berlin

Germany

Second Referee (Zweitgutachter):   Prof. Dr. Gerhard Franz

Technische Universität Berlin

Fachgebiet Mineralogie-Petrologie

Ackerstrasse 75,

13355 Berlin

Germany

IV

Declaration of Authenticity

I hereby certify sole authorship of the thesis "Taphonomy of exceptional Cambrian fossil Lagerstätten of China exemplified by the Chengjiang Biota and the Guanshan Biota" as submitted to the Department of Earth Sciences of the "Freie Universität Berlin" for the conferral of a doctorate, and that no sources other than those indicated have been used in its preparation. Parts of this thesis that have been drawn on the work of others with regard to contents or by literal quotation have been appropriately marked through indication of source. Where any collaboration has taken place with other researchers, I have clearly stated my own personal share in the investigation.
This work in the same or a similar form has not been submitted to any other examining body.

Erklärung zur Originalität (Ehrenwörtliche Erklärung)

Hiermit versichere ich an Eides statt, dass ich die der Fachrichtung Geowissenschaften der Freien Universität Berlin zur Promotion eingereichte Arbeit „Taphonomy of exceptional Cambrian fossil Lagerstätten of China exemplified by the Chengjiang Biota and the Guanshan Biota" selbstständig verfasst und keine anderen als die angegebenen Hilfsmittel verwendet habe. Teile der vorliegenden Arbeit, die anderen Werken wörtlich oder inhaltlich entnommen sind, wurden durch Angaben der Quellen gekennzeichnet. In allen Fällen einer Zusammenarbeit mit anderen Forschenden habe ich meinen persönlichen Arbeitsanteil klar dargestellt.
Diese Arbeit wurde in gleicher oder ähnlicher Form noch keiner Prüfungsbehörde vorgelegt.

Wien, den 3.09.2013

Angela Forchielli

VI

Extended Abstract

The preservation of highly delicate tissues and soft parts is exceptional in Earth history, but provides a huge amount of information on early metazoan bauplans. Deposits in which these soft-bodied fossils occur are termed fossil Lagerstätten and can be excellent in quantity (concentration deposits) or in quality (conservation deposits). The conservation deposit of Chengjiang represents one of the oldest fossil deposits conserving both metazoan stem- and crown-group bauplans directly after the most rapid diversification event of Metazoa ("Cambrian bioradiation event").

Although extensive studies have been conducted on the systematic of taxa of this Lagerstätte, the major mechanisms of preservation of this exceptional soft-tissued fossil Lagerstätte remain controversial. The present contribution takes previous models of Burgess Shale-type preservation into account. Alteration and weathering processes play a pivotal role in the taphonomy of the Chengjiang Biota, but no overview of its taphonomic pathways using material with little or no weathering influence was available. The dearth of information that all the previous models have due to weathering is analyzed, and the gap in information is bridged by analysing unweathered material.

Iron mineral precipitation onto organic carcasses of Chengjiang-type fossils is mostly confined to later diagenetic processes and thus is not crucial for the early fixation of highly decayable tissues in Burgess Shale-type faunas. This statement is based on several facts. Energy dispersive X-ray (EDX) analyses and elemental mapping of fresh fossil material from a variety of facies settings indicate that pyrite crystals are located only surrounding the fossils. Organic carbon is detected in all taxa, independently of their weathering/alteration stage, whereas pyrite is not. The systematic and detailed geochemical screening of various fossil groups such as brachiopods, priapulids, arthropods, sponges – mainly based on the geochemical screening of body fossils and entombing clay matrix – indicate a more complex preservational history than hitherto expected. The presence of apatite in sclerites of palaeoscolecids, shells of brachiopods, and bradoriids in unweathered samples supports the conclusion that these organisms were primary biomineralizers. Besides sub-recent oxidation processes during modern weathering, other processes such as clay mineral formation and/ or alteration, carbonization, phosphatization, and perhaps pyritization played key roles in the preservation of the exceptional soft-bodied organisms. Using different geochemical proxies such as various redox indicators and iron speciation, statistics on framboid sizes, along with classical geological observation and clay mineralogy reveal that iron mineral precipitation

onto organic carcasses of the Chengjiang-type fossils is mostly confined to later diagenetic processes during weathering: the occurrence of Fe crystallites and framboides on soft tissues and within dissolved skeletal parts underlines a later diagenetic origin or even latest replacement during relatively recent weathering. Accordingly, such precipitation is not crucial for the early fixation of highly decayable tissues. The different preservational traits of tissues in same individuals (carbonization, phosphatization etc.) are mostly due to the ambient geochemical micro-environment and the primary biochemistry of different tissues itself. The analyzed material demonstrates that pyrite does not replace the morphology of the fossils in unweathered material, as it does in the weathered material. This is one piece of evidence that anything replacing the altered fossils (in this case iron oxides) appeared successively, probably from the Cretaceous onward, and thus is not important for the early fixation of delicate tissues.

The samples are classified into three groups with different degrees of alteration and reveal that the chemistry of these groups differs fundamentally. The implications of the sedimentological and mineralogical composition of the fossil Lagerstätten in the exceptional preservation of the Chengjiang Fauna and of the similar but younger Guanshan Fauna are investigated in detail. The Chengjiang fossil Lagerstätte is characterized by the presence of clay-dominated couplets of background beds (BGB) and event beds (EB), containing mostly shell accumulations or soft-tissue preservation. The specific clay mineral composition varies slightly between the different types of beds, hinting at variations in the source of clastics or the hydrochemical environment during the deposition of strata. This study shows that late-stage chemical alteration/weathering plays a much more prominent role in the taphonomy of the Chengjiang and Guanshan Biotas than previously recognized. The chemistry of UW (unweathered) and SW (slightly weathered) +W (weathered) groups is significantly different due to chemical alteration, which is likely linked to intense faulting since the Cretaceous. This thesis analyzes, for the first time, the whole spectrum of weathering stages in relation to the fossils. Its main contribution is the analysis of the effects of extensive subsurface weathering on the early Cambrian Lagerstätten of Yunnan Province. It resolves the extensive late diagenetic history of weathering, and peels that back to reveal the complex early diagenetic history of these deposits and their fossils.

The role of anoxia and possible alternative explanations for the preservation of these exceptional faunas are also thoroughly investigated. The role of benthic anoxia in promoting exceptional preservation in Burgess Shale-type deposits has been and continues to be an issue of debate. Redox parameters for least weathered samples do not indicate deposition under

anoxic conditions. Bottom-water anoxia conditions were apparently not permanently present during the deposition. A rapid deposition in finest claystones is here considered more important for the preservation of highly delicate tissues than the presence of bottom-water anoxia, although bottom-water anoxia and microbial sealing may further increase the probability for soft-tissue preservation.

Finally, all these new data led to the development of an updated taphonomic pathway for Burgess Shale-type preservation.

x

Erweiterte Kurzfassung

Die Erhaltung von Weichteilen und fragilem Gewebe ist in der Erdgeschichte außergewöhnlich und, die Baupläne früher Metazoa betreffend, sehr aufschlussreich. Aufschlüsse, die Fossilien mit Weichteilerhaltung führen, werden Fossillagerstätten genannt, und in Konzentratlagerstätten (die eine hohe Quantität an Funden aufweisen) oder Konservatlagerstätten (bei welchen die herausragende Qualität im Vordergrund steht) unterschieden.

Die Konservatlagerstätte von Chengjiang gehört zu den ältesten Fossillagerstätten und liefert sowohl Fossilien von Stamm- als auch von Kronengruppen der Metazoa. Die hier erhaltenen Baupläne sind unmittelbar nach dem größten Diversifizierungsevent in der Geschichte der Metazoa, dem "Cambrian bioradiation event", entstanden. Trotz der intensiven Arbeit über die systematische Stellung der in dieser Lagerstätte vorkommenden Arten bleiben die die außergewöhnlich gute Weichteilerhaltung ermöglichenden Faktoren weiterhin unklar. Frühere Modelle zu diesem speziellen Erhaltungszustand, einer "Burgess-Shale preservation", wurden in Betracht gezogen. Verwitterung und Veränderung der Komponenten spielen eine zentrale Rolle in der Taphonomie der Chengjiang Biota. Bisher ist es nicht gelungen, an nicht oder wenig verwittertem Material einen Überblick über die taphonomischen Prozesse zu bekommen. Der aus Verwitterungsprozessen resultierende Informationsverlust bisheriger Modelle wurde analysiert. Dank der Verfügbarkeit unverwitterten Materials konnten Informationslücken vermieden werden. Der Eintrag von Eisen –auf Chengjiang Fossilien ist eher als ein spätdiagenetischer Prozess zu betrachten und demnach nicht für die Fixierung von Weichteilen, wie man es aus "Burgess - Shale" - Typ Lagerstätten kennt, verantwortlich zu machen.

Diese Behauptung kann mit den folgenden Fakten untermauert werden: "Energy dispersive X-ray" (EDX) Analysen und Spurenelementanalysen an frischem Fossilmaterial aus einer Vielzahl verschiedener Fazies zeigen ausschließlich das Fossil einsäumende Pyrit-Kristalle. Organischer Kohlenstoff kann, im Gegensatz zu Pyrit, unabhängig des Verwitterungs- oder Umbaustadiums in allen Taxa nachgewiesen werden. Eine detaillierte und systematische geochemische Untersuchung verschiedener Fossilgruppen, darunter Brachiopoden, Priapuliden, Arthropoden und Schwämme, deren Hauptaugenmerk auf der geochemischen Analyse der Körperfossilien und der einschließenden Ton Matrix liegt, lässt weitaus komplexere der Erhaltung zugrunde liegende Mechanismen vermuten, als bisher angenommen.

In nicht verwitterten Proben kann Apatit in den Skleriten von Palaeoscoleciden, Brachiopodenschalen und Bradoriiden nachgewiesen werden, was die Annahme nahelegt, dass es sich hier um Bildner von Biomineralisaten handelt.

Neben sub-rezenten Oxidationsprozessen im Rahmen moderner Verwitterungsprozesse spielten Tonmineral-Bildung, Kalk- oder Phosphat-Bildung sowie möglicherweise Pyritisierung eine Schlüsselrolle für die Erhaltung dieser außergewöhnlichen Weichteilorganismen. Unter Berücksichtigung verschiedener geochemischer Proxies - neben klassischen geochemischen Beobachtungen und Tonmineral Analysen - wie beispielsweise verschiedenster Redox Indikatoren und Eisenbildung, sowie statistischer Analysen an den Framboid Größen, konnte festgestellt werden, dass Eisenmineral-Niederschlag auf Chengjiang- Typ Organismen sich hauptsächlich als spät-diagenetischer, während der Verwitterung auftretender Prozess darstellt:

Das Auftreten von Eisenkristallen und Framboiden auf Weichteilen und in gelösten Skelettelementen zeigt den spätdiagenetischen Ursprung oder sogar ein jüngstes Ersetzen durch rezentere Verwitterungsprozesse und kann deshalb nicht als maßgeblich wichtig für die frühzeitliche Fixierung von hoch verderblichem Gewebe angesehen werden.

Verschiedene Merkmale in der Erhaltung von Geweben desselben Individuums (Kalzifizierung, Phosphatierung, etc...) sind hauptsächlich auf das äußere geochemische Mikro-Environment und die primäre Biochemie der unterschiedlichen Gewebe selbst zurückzuführen.

Das kann als Beweis erachtet werden, dass alle Ersetzungsvorgänge in veränderten Fossilien (in diesem Fall Eisenoxid) als nacheinander, wahrscheinlich seit der Kreide andauernder Prozess abgelaufen sein muss, und deshalb nicht für die frühe Fixierung von fragilem Gewebe relevant sein kann.

Die Proben wurden in 3 Gruppen geteilt, die jeweils unterschiedliche Stadien der Veränderung aufweisen und fundamental unterschiedliche chemische Eigenschaften aufweisen. Schlüsse, die sich aus der sedimentologischen und mineralogischen Zusammensetzung der Fossillagerstätten, die solch außerordentliche Erhaltungen zeigen wie in Chengjiang sowie der ähnlichen, aber erdgeschichtlich jüngeren Guanshan Fauna ziehen lassen, wurden im Detail untersucht. Die Chengjiang Lagerstätte kann durch das Auftreten ton dominierter Wechsellagen von Event-Horizonten und Hintergrundsedimentation charakterisiert werden, die hauptsächlich Ansammlungen von Schalen beziehungsweise Weichteilerhaltungen führen.

Zwischen den verschiedenen Schichten variiert die Zusammensetzung der Tonmineralien geringfügig, was ein Hinweis auf Unterschiede im Ursprung der klastischen Sedimente oder dem hydrothermischen Environment während der Ablagerung der Schichten ist.

Diese Studie legt nahe, dass die späte chemische Änderung oder Verwitterung eine größere Rolle in der Taphonomie der Chengjiang und Guanshan Biota spielt als bisher angenommen. Chemischer Veränderung, die wahrscheinlich mit intensiver Verfaltung seit der Kreide in Zusammenhang steht, ist es auch zuzuschreiben, dass die chemischen Eigenschaften der UW (unverwittert) und SW (leicht verwittert)+W (verwittert) Gruppen sich signifikant unterscheiden.

Zum ersten Mal wird in dieser Arbeit das volle Spektrum der Verwitterungsstadien in Bezug auf das Fossilmaterial analysiert, sowie eine genaue Auswertung der Effekte extensiver Tiefen-Verwitterung in Lagerstätten des frühen Kambriums aus der Yunnan Provinz durchgeführt.

Dieses Werk befasst sich mit der umfassenden Beschreibung und der gesonderten Betrachtung spätdiagenetischer Verwitterung, um die Begebenheiten der früheren Diagenese dieser Ablagerungen und Fossilien zu beleuchten.

Weiters wird die Rolle von Anoxia und anderen möglichen Erklärungen für die Erhaltung dieser außergewöhnlichen Faunen intensiv untersucht.

Welche Rolle benthische Anoxia für den außergewöhnlichen Erhaltungszustand in Burgess-Shale Typ Lagerstätten spielten und spielen, steht zur Diskussion. Redox Parameter für die am wenigsten verwitterten Proben zeigen keine Anzeichen einer Ablagerung unter anoxischen Bedingungen. Demnach kann angenommen werden, dass anoxische Konditionen der Bodenwässer nicht während des gesamten Ablagerungsprozesses vorherrschten.

Die schnelle Ablagerung in feinsten Tonsteinen kann hier eher als entscheidend für die Erhaltung von Weichteilen angenommen werden als das Auftreten anoxischer Bedingungen in den Bodenwässern. Dennoch könnten letztere, sowie ein mikrobielles Versiegeln, die Wahrscheinlichkeit für die Überlieferung von Weichteilen erhöhen.

Resümierend ist zu sagen, dass all diese neuen Erkenntnisse zur Entwicklung eines aktualisierten taphonomischen Konzeptes für Lagerstätten, die einen der Burgess-Shale Lagerstätte ähnlichen Zustand der Erhaltung zeigen, führten.

Acknowledgments

Contents

Preamble

This thesis deals with the "Taphonomy of exceptional Cambrian fossil Lagerstätten of China exemplified by the Chengjiang Biota and the Guanshan Biota", within the scope of the German Science Foundation (DFG) project FOR 736 "The Precambrian-Cambrian Ecosphere (R)evolution: Insights from Chinese microcontinents". Sub-project 3 (Grant No. Ke 322/34-1)

Structure

The thesis presented is written in a cumulative style and comprises four chapters including three scientific papers:

> Chapter 1: Introduction
> Chapter 2: Material and methods
> Chapter 3: Scientific Papers
> Chapter 4: References
> Curriculum vitae

Chapter 1 is subdivided into two subchapters and presents an introduction to the fossil Lagerstätten, the scientific background of the topic, original goals, working hypotheses and developments of the thesis.

Chapter 2 provides an overview of material, area of sampling and methods used for this thesis.

Chapter 3.1 is published in Volume 87 number 1 of 2012 of the Bulletin of Geosciences as: FORCHIELLI, A., STEINER, M., HU SHIXUE & KEUPP, H. 2012. Taphonomy of Cambrian (Stage 3/ 4) sponges from Yunnan (South China). Bulletin of Geosciences 87(1), 133-142 (7 figures). Czech Geological Survey, Prague. ISSN 1214-1119. Manuscript received September 12, 2010; accepted in revised form October 10, 2011; published online February 21, 2012; issued February 29, 2012.

All the authors contributed to fieldwork. Angela Forchielli carried out the analyses, wrote the paper and produced all the figures. Michael Steiner contributed to the discussion with suggestions that improved the quality of the paper. The personal work input of Angela Forchielli for this publication exceeds 90%.

Chapter 3.2 is in press in Acta Palaeontologica Polonica as: Angela Forchielli, Michael Steiner, Shixue Hu, Carsten Lüter, and Helmut Keupp. Taphonomy of the earliest Cambrian linguliform brachiopods. Acta Palaeontologica Polonica in press; Received 28 November 2011, accepted 25 April 2012, available online 4 May 2012 doi: http://dx.doi.org/10.4202/app.2011.0182

Angela Forchielli, Michael Steiner, Hu Shixue and Helmut Keupp contributed to fieldwork. Angela Forchielli carried out the analyses, wrote the paper and drew the figures, so that her personal work input for this publication makes up more than 85% of the concept, content, writing and editing including resins preparation and the "SEM images-maps" of recent specimens of figures 4 and 5 (each map consists of more than 150 SEM images). Michael Steiner performed the analysis shown in Fig. 6G and 7 and contributed to the discussion with useful suggestions. Carsten Lüter provided the histological material (used for photos and figures made by Angela Forchielli) and Fig. 7B.

Chapter 3.3 is in press in Palaeogeography, Palaeoclimatology, Palaeoecology as: Forchielli, A., Steiner, M., Kasbohm, J., Hu, S., Keupp H. Taphonomic traits of clay-hosted early Cambrian Burgess Shale-type fossil Lagerstätten in South China. Palaeogeography, Palaeoclimatology, Palaeoecology (2013), http://dx.doi.org/10.1016/j.palaeo.2013.08.001; Received 1 February 2013; received in revised form 30 July 2013; accepted 1 August 2013; available online 9 August 2013.

Angela Forchielli, Michael Steiner, Hu Shixue and Helmut Keupp contributed to fieldwork. Angela Forchielli prepared all the material for the analyses, carried out part of them (Jörn Kasbohm was paid to make the clay matrix analyses), wrote the paper and made the figures, yielding a personal input for this publication of 85% concerning concept, content, writing and editing. Michael Steiner made Fig. 5 and contributed to the discussion. Both Angela Forchielli and Michael Steiner worked on PCA analyses.

Extra publication related to the theme (not included in this thesis):

An extra work is published in the Austrian Journal of Earth Science Volume 106 of 2013 as: Forchielli A. and Pervesler P. Phosphatic cuticle in thylacocephalans: a taphonomic case study of *Austriocaris* (Arthropoda, Thylacocephala) from the Fossillagerstätte Polzberg (Raingraben shales, Carnian, Upper Triassic, Lower Austria). Austrian Journal of Earth Science 106, 46-61.

Angela Forchielli conducted the analyses, wrote the paper and produced all the figures (except Fig. 1), yielding a personal work input for this publication of about 95%. Peter Pervesler wrote the German abstract and provided Fig. 1.

This work analyzes a group of bivalved arthropods having a phosphatic cuticle. Thylacocephala is a recently established group of bivalved arthropods that existed since the Cambrian and was geographically widely distributed. This group was extensively studied with respect to its taxonomy, morphology and ecology, but the taphonomic pathways involved in its preservation have not received the same attention. The cuticle of the thylacocephalan *Austriocaris* from Polzberg is analyzed and compared with material (bradoriids, a group of bivalve arthropod with phosphatic cuticle too) from the Cambrian Chengjiang and Guanshan Lagerstätten (Stage 3 and 4) and with other members of the Thylacocephala.

1. Introduction

1.1. State of the art

Exceptionally preserved fossils are rare: the conservation of highly delicate tissues and soft parts is unusual in the history of the Earth, but provides a huge amount of information. Deposits containing such soft-bodied fossils are known as Fossillagerstätten (sensu Seilacher 1970) and can be excellent in quantity (Konzentrat Lagerstätten, normally accumulation layers) or in quality (Konservat Lagerstätten, where soft-bodied fossils occur) (Seilacher, 1990). Taphonomy deals with the information content of the fossil record and the processes by which fossils are incorporated into the fossil record (Martin, 1999). It has been estimated that from 66 to 79% of the biota of a marine community does not appear in the fossil record (Martin, 1999 and references therein); shelly organisms represent only 21% to 33% of a marine community (Allison and Briggs, 1993). For example, 98% of the individuals of the Burgess Shale fossil Lagerstätte were soft bodied and therefore would not have been preserved in the shelly organism record (Briggs, 2003 and references therein). The rise of the Metazoa at the beginning of the Cambrian and the diversification of complex ecosystems are best recorded by fossil Lagerstätten because they yield preserved soft tissues and along with the relevant information. This work deals with Konservat Lagerstätten and with the preservation of organisms that are otherwise not documented in the normal fossil record. Konservat Lagerstätten can be the result of several events, such as rapid burial, and represent an instant in geological time. The settings in which Konservat-Lagerstätten are preserved extend from offshore marine (the Cambrian Burgess Shale, e.g. Conway Morris, 1989), through shallow water (most Ediacaran biotas; e.g. Glaessner, 1984), shelf (Kaili Biota, Zhao et al., 2005), outer shelf to slope (the Chengjiang Biota, e.g. Hou et al., 1988) to restricted marine basins (the Jurassic Solnhofen Limestone; e.g. Barthel et al., 1990), and transitional facies (Grès à Voltzia, Briggs and Gall, 1990), to name but few examples. A number of different taphonomic pathways can produce fossil Lagerstätten. The preservation of organisms in phosphate is known as Orsten-type preservation and Doushantuo-type preservation (e.g. Butterfield, 2003); carbonaceous films are the result of Burgess Shale-type preservation (e.g. Butterfield, 1990), whilst Bitter Springs-type preservation preserves them in silica (e.g. Butterfield, 2003). Superb details are shown, replicated in pyrite, in Beecher's Trilobite-type preservation (e.g. Briggs et al., 1991) and in the Hunsrück Slate (Briggs et al., 1996), and casts and moulds are preserved in the Ediacaran-type with the aid of microbial mats (e.g. Gehling, 1999; Laflamme et al., 2011). Non-biomineralized tissues display a large

spectrum of resistance to decay; robust structural tissues, such as arthropod cuticles, are decay resistant and may be incorporated into the fossil record as organic remains. Decay-prone tissues, such as muscle or gut, which degrade very rapidly, are preserved only when they are replicated very rapidly in authigenic minerals (see e.g. the fish muscle in the Cretaceous Santana Formation). Both organic and inorganic preservation may occur in the same deposit, or even in the same fossil (Briggs and Crowther, 2001).

This work focuses on the taphonomic pathways of the early Cambrian Burgess Shale-type Lagerstätten of the Yunnan Province (South China).

The preservation of soft-bodied organisms and highly volatile tissues as organic or iron-mineralized imprints in shales is not well understood. Taphonomic alterations of morphological patterns pose a challenge to the palaeobiological interpretation of early metazoan fossils. This work therefore explores the taphonomic pathways in soft-bodied Chengjiang and Guanshan Biota, and may have a direct bearing on the interpretation of the Cambrian bioradiation event and the reconstruction of early metazoan evolution.

Figure 1- The discovery outcrop of the Chengjiang Fauna at the Maotianshan hill. Now it is a protected site within the "Chengjiang Fossil National Geopark" and since 2012 is inscribed on the Word Heritage List.

Burgess Shale-type preservation is defined as the "exceptional" preservation of non-mineralizing organisms as carbonaceous compressions in marine siliciclastic sediments (Butterfield 1995). The Chengjiang Fauna represents a taxonomically, temporally and spatially specific case of a Burgess Shale-type Fauna (Steiner et al. 2005) (Fig. 1). The Chengjiang Fauna (Cambrian Stage 3) is widely exposed in the Yunnan Province. Exceptionally preserved soft-bodied fossils of the Chengjiang Biota occur in the Yuanshan Formation.

The conservation deposit of Chengjiang, characterized by couplets of background beds (BGBs) and event beds (EBs), represents one of the key fossil deposits to understand and reconstruct the metazoan bauplans at the very beginning of metazoan evolution. Fossil preservation varies considerably in the two different depositional settings, with soft-tissue preservation occurring preferentially in EBs, whereas skeletal accumulations are typical of BGBs (Fig. 2).
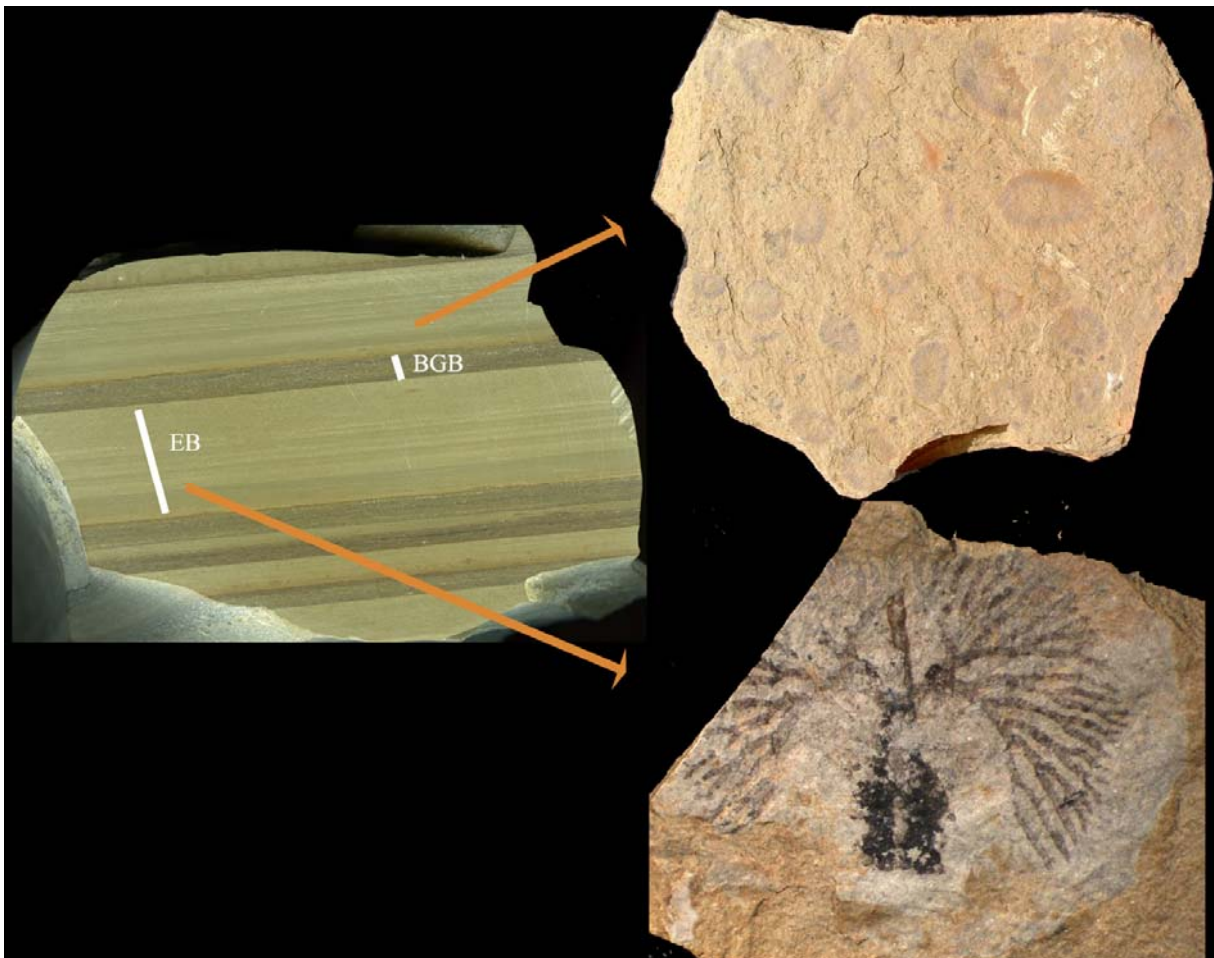

Figure 2- Differences in BGB and EB preservation.

1. Introduction

The Chengjiang Fauna comprises an extremely diverse and exceptionally preserved faunal assemblage, with a prevalence of arthropods, sponges and brachiopods. In Chengjiang fossil Lagerstätte, arthropods comprise 44% in the event beds and the 84% in the background beds (individuals), with the prevalence of the species *Kunmingella douvillei* (81%); sponges comprise more than 8% (individuals) of the Chengjiang Fauna (Hu 2005; table 1 in Zhao et al. 2009), with 15 genera and 30 species among demosponges and hexactinellids (Li et al. 1998). Brachiopods represent 24% of the individuals of the Chengjiang Fauna in the event beds (EB) and 0.7% in the background beds (BGB) in a section near Haikou, Kunming (Zhao et al. 2009).

The Guanshan Fauna (ca. Cambrian Stage 4) is a slightly younger fauna than the Chengjiang Fauna, which is widely exposed in the eastern part of Yunnan Province. Exceptionally preserved soft-bodied fossils of the Guanshan Biota occur in the Wulongqing Formation. A large number of exceptional fossils (belonging to more than 10 metazoan groups) have been discovered from the Guanshan Fauna in recent years, including arthropods (Luo et al. 1999, 2006, 2007, 2008; Liu Q et al. 2006), brachiopods (Luo et al. 2008, Hu et al. 2010 and personal unpublished data), sponges (Forchielli et al., 2012: chapter 3.1), eocrinoid echinoderms (Hu et al. 2007), cnidarians, hyolithids, vetulicoliids (Luo et al. 2005), paleoscoleciids (Hu et al. 2008, 2012), chancelloriids, anomalocaridids, lobopods (Steiner et al., 2012), Ediacaran-type organisms (Zhang & Babcock, 2001), eldonioids, algae, several problematic taxa, and trace fossils (Weber et al., 2012).

The quality of the preservation of soft-tissues in some metazoan groups of the Guanshan Fauna, such as the trilobites (often with antennae preserved) and brachiopods, rivals that of the Chengjiang Fauna and the Burgess Shale Fauna. Furthermore, the Guanshan Fauna fills the gap between the early Cambrian Chengjiang Fauna and the middle Cambrian Kaili Biota, the Burgess Shale Fauna, and the Utah fossil Lagerstätten and sheds new light into marine biodiversity and community dynamics before the Early-Middle Cambrian transition.

In Guanshan fossil Lagerstätten, arthropods are the most dominant animal group in terms of both individuals and species, including trilobites (the most abundant) and non-trilobite arthropods, bivalved arthropods (bradoriids are the most abundant in this sub-group), and some additional taxa. Brachiopods rank second in terms of both abundance and diversity. Hu et al. (2010) list at least 6 taxa of brachiopods, 4 of which with soft-part preservation. Unlike the composition of the Chengjiang Fauna, sponges are relatively rare and low in diversity. Although not predominant, priapulid worms are common elements of the Guanshan Fauna, as in the Chengjiang Fauna. Hu et al. (2010) report that besides the described *Guanduscolex*

minor (Hu et al., 2008), several undescribed species of palaeoscolecids and an undescribed species of corynetid have been collected. They also suggest that the abundant and diverse priapulids of the Chengjiang and Guanshan biotas indicate a possible radiation center of this animal group on the soft-substratum shelf of the western part of the Yangtze Platform during the early Cambrian.

1.2. Original goals, working hypotheses and developments of the thesis

The Cambrian bioradiation event of metazoans represents a phenomenon that can be recognized only by investigating the fossil record. Therefore, the modes of fossilization, possible selective processes in fossilization (primary biomineralization and histological preferences for ion attachment) and additionally the reasons for the non-fossilization of some dead organisms, are crucial in reconstructing the evolutionary history of metazoans. Despite extensive studies on the systematic of taxa of these Lagerstätten, the major mechanisms of preservation remain controversial. The available hypotheses on the causes for soft-bodied preservation in Burgess Shale-type deposits embrace various models because the preservation of these early Cambrian fossils has been particularly controversial; several taphonomic pathways have been proposed to account for the exceptional preservation of these fossils. Under present-day conditions, labile tissues and skeletal material of the Burgess Shale-type fossils from Chengjiang and Guanshan deposits are replaced by iron minerals. An early iron adsorption onto surfaces of organic carcasses was considered to be a key factor for the preservation of soft-tissued fossils (Petrovich, 2001). This model has also been applied to the Chengjiang fossil Lagerstätte, where extensive replacements of organic structures by iron oxides were interpreted as pseudomorphic alteration of early diagenetic framboidal pyrite stabilizing the labile organic tissues (e.g., Gabbott et al., 2004). Zhu et al. (2005) also emphasized the role of other authigenic minerals such as apatite and late diagenetic Fe-rich aluminosilicate in replacing parts of the exceptionally well-preserved Chengjiang fossils. Meanwhile, it has been variously discussed that the recorded mineral replacements may not be of an earliest diagenetic origin, but may even be a product of the weathering process itself (Hu, 2005; Gaines et al., 2008; Forchielli et al., 2012 in press: Chapter 3.2). It was also proposed that clay minerals acted as templates to replicate labile tissues (Orr et al., 1998) or as binding substances for enzymes to inhibit autolytic decay (Butterfield, 1995). Recently, Gaines et al. (2012b) suggested that Burgess Shale-type deposits resulted from early inhibitions of microbial activity in the sediment by means of oxidant deprivation. Rapid

entombment of fossils in fine-grained sediments and early sealing of sediments by pervasive carbonate cements of bed tops restricted oxidant flux into the sediments.

Furthermore, alteration and later weathering plays a pivotal role in the taphonomy of the Chengjiang Biota, but an overview of this biota's taphonomic pathways using material with little or no weathering influence is still missing. Specimens analyzed here embrace for the first time the complete spectrum of alteration/weathering stages. This approach avoids the strong influence of weathering and generates more accurate taphonomic pathways.

The main goal of this work is to investigate the taphonomy of exceptional Early Cambrian fossil Lagerstätten of the Yunnan Province. In order to achieve this, three main aims were proposed:

1. To document the detailed chemistry of key Chengjiang-type fossils of different phyla from different depositional settings by SEM-EDX and electron microprobe.
2. To investigate the importance and extent of the influence of suboxic bottom water for the preservation of Chengjiang organisms.
3. To develop a hypothesis that describes the diagenetic history of Chengjiang-type fossils.

Analyses performed for this work were based on both Chengjiang and Guanshan faunas. I focused my attention on the sponges (see Chapter 3.1), linguliform brachiopods (see Chapter 3.2), arthropods (parts of data on bradoriids are published in Forchielli and Pervesler, 2013) and worms (parts of the data are published in several abstracts and posters, see appendix). I also extensively analyzed the lithogeochemistry of the host matrix (see Chapter 3.3).

In chapter 3.1, sponges from four Burgess Shale-type fossil associations from several palaeogeographic settings are analyzed in order to investigate the possible influence of facies on their taphonomic pathways. The classical Chengjiang Fauna of Yunnan Province is compared to fossils from the Guanshan Fauna (*ca* Cambrian Stage 4; Yunnan Province), the Chengjiang-type Fauna from Zunyi (Cambrian Stage 3; Guizhou Province) and the Sancha Fauna from Hunan Province (*ca* Cambrian Stage 3). Analyses were performed on specimens with a broad spectrum of weathering grades among the Chengjiang and Guanshan faunas and also a few specimens from the Zunyi. The material comes from different palaeogeographic settings. The Guanshan and Chengjiang faunas from Yunnan and the Chengjiang-type Fauna from Guizhou represent nearshore shallow-water and slope facies, whereas the Sancha Fauna from Hunan area represents a deeper shelf-basin facies of the Yangtze Platform. These differences in settings can be linked to different taphonomic models. The Chengjiang sponges

(Cambrian Stage 3) have a taphonomic pathway similar to that of the slightly younger Guanshan sponges (Canglangpuan Stage). Weathering is crucial in the Chengjiang Lagerstätte and, as in other groups, the sponges show different results due to the weathering stages. Furthermore, there is little evidence of pyrite in the unweathered material of Chengjiang fossil Lagerstätte. These iron oxide framboids are interpreted as a replacement of later diagenetic pyrite precipitates into voids of sediment, such as dissolved sponge spicules. The unweathered material suggests Burgess Shale-type preservation for the Chengjiang sponges. Iron oxide and hydroxide framboids, and globular crystal aggregates in the sponge spicules of Guanshan material, suggest a late diagenetic replacement of the sponge spicules by several minerals during different weathering stages. Two main taphonomic pathways are involved in the sponge preservation of the Chengjiang-type fossil Lagerstätten. The Sancha fossil deposits (Hunan Province) show evidence of recrystalization of the amorphous silica of the spicules into crystalline-type silica. EDX analyses of the sponge spicules indicate a Si and O composition. In the Guanshan sponges, the biogenic silica of the spicules was first recrystallized as opal-CT, later dissolved, and was replicated by pyrite framboids; the latter were later pseudomorphically replaced by iron oxides and hydroxides during late stage weathering. Some of these framboids underwent subsequent weathering and changed in micro-crystal morphology and chemistry. Chengjiang sponges underwent extensive weathering. The opal-CT was dissolved, leaving a cavity that was successively filled by different minerals; alternatively, it possibly underwent dissolution under acidic conditions combined with oxygenation. This resulted in clay and iron oxide replication of the sponge spicules. Furthermore, there is a disparity in sponge preservation between BGBs and EBs that is not related to taphonomic bias. Rather, it can be explained with a short-distance transportation of the fauna during EBs deposition.

Chapter 3.2 analyzes the brachiopods. Linguliform brachiopods are applied here as a critical model phylum to analyze the taphonomy of Yunnan fossil Lagerstätten, because the shell and tissue composition of modern brachiopods can be compared with exceptionally preserved Cambrian remains. Palaeozoic linguliform brachiopods were presumed to have developed organo-phosphatic shells. Due to the variety of pristine Palaeozoic fossil material and the uncertain influence of diagenetic phosphatization, however, the detailed primary shell construction in earliest Cambrian linguliform brachiopods long remained unresolved. Systematic elemental mapping and Energy dispersive X-ray analyses were carried out to study fossil brachiopods and their matrix from Cambrian Stages 3-4 and modern linguliform

brachiopods from several geographical regions. This was designed to evaluate the detailed structure of the shells and the biological and environmental influences on shell composition. Analyses of earliest Cambrian fossils encompassing the complete spectrum of weathering stages show a primary organo-phosphatic brachiopod shell, visible in unweathered specimens. This was followed by a successive dissolution and replacement of the shell during weathering, observable in specimens that underwent different stages of weathering. Taphonomic analyses of unweathered material confirmed that organo-phosphatic shells were developed at least in the earliest crown-group lingulids since Stage 3 of the Cambrian. Multilayered shells, documented in linguliform brachiopods of the Guanshan Biota, of the Chengjiang Biota, and the Sinsk Biota, together with the presence of organic carbon between the phosphatic layers, demonstrate that this material is an original biological component. The earliest shell architecture is in principle comparable with those of extant linguliform brachiopods. Critical analyses of the fossil material, compared with recent material, yielded a new model for the preservation of linguliform brachiopods in Chengjiang Lagerstätte: Burgess Shale-type preservation does not depend on early iron adsorption. Rather, early carbon and apatite preservation together with rapid deposition in claystone – instead of early iron adsorption – appears crucial for the preservation of delicate tissues. Primary calcium, phosphorus, organic carbon and a multilayered shell are present, by inference between Cambrian fossils and Recent specimens, throughout the Phanerozoic. Elements such as silicon, sulphur, calcium, phosphorus and iron were detected, impregnated with organic compounds, in some organs of modern *Lingula*. I relate this to the potential of fossilization of Cambrian linguliform brachiopods. New data on modern shell and tissue composition presented in this chapter are therefore important for understanding preservation in fossil Lagerstätten. This preservation may be due not only to the different resistances of organic biomolecules, but also to the in vivo binding of specific elements to tissues and shell parts as well as post-mortem processes.

Chapter 3.3 deals with the lithogeochemistry of the Chengjiang and Guanshan Lagerstätten. One of the main contributions of this work is its analysis of the effects of extensive subsurface weathering on the Early Cambrian Lagerstätten of Yunnan Province, the Chengjiang and Guanshan. It involves resolving an extensive late diagenetic history of oxidative (and possibly sub-oxic) weathering, and peeling that back to reveal the complex early diagenetic history of the deposits and their exceptional fossils. The novelty and strength of this study is that it examines the effects of weathering on the fossils in the context of the weathering on the host rocks themselves. This approach provides a much more dependable and complete picture.

In this context, three primary contributions were achieved:

1. Detailed compositional study of soft-bodied fossils across a weathering spectrum;
2. Geochemical and mineralogical study of the sedimentary rocks across a weathering spectrum;
3. Evaluation of geochemical paleoredox proxy data (and pyrite size/morphology data as a paleoredox proxy).

This study takes into account previous models of Burgess Shale-type preservation, based mainly on iron minerals as a key factor, or on clay minerals as a key factor, besides the carbon framework shared among all taxa. The dearth of information underlying all the previous models, due to weathering, is analyzed. This information gap is avoided by analyses based on unweathered material. Iron mineral precipitation onto organic carcasses of Chengjiang-type fossils is mostly confined to later diagenetic processes and thus is not crucial for the early fixation of highly decayable tissues in Burgess Shale-type faunas. This statement is based on several facts. Organic carbon is detected in all taxa, independently of their weathering/alteration stage, whereas pyrite is not. Energy dispersive X-ray (EDX) analyses and elemental mapping of fresh fossil material from a variety of facies settings indicate that pyrite crystals are located only surrounding the fossils. Instead of this particular type of preservation, carbon is detectable in almost all metazoan clades present in this fossil deposit. Interestingly, some elements such as S are lost during alteration, but the labile and delicate organic carbon is not. The systematic and detailed study of various fossil groups, including brachiopods, priapulids, arthropods and sponges, is based mainly on the geochemical screening of body fossils and entombing clay matrix. It indicates a more complex preservational history than hitherto expected. The presence of apatite in sclerites of palaeoscolecids, shells of brachiopods, and bradoriids in unweathered samples supports the conclusion that these organisms were primarily biomineralizers. The analyzed material demonstrates that pyrite does not replace the morphology of the fossils in unweathered material, as it does in the weathered material. This is one piece of evidence that any material replacing the altered fossils (in this case iron oxides) appeared successively, probably from the Cretaceous onward, and thus is unimportant for the early fixation of delicate tissues. Undoubtedly, pyrite was present in Chengjiang-type fossil Lagerstätten, but the timing of its appearance is the central point of investigation.

The role of anoxia and possible alternative explanations for the preservation of these exceptional faunas are also thoroughly investigated. The role of benthic anoxia in promoting exceptional preservation in Burgess Shale-type deposits has been and continues to be an issue

of debate. Although anoxic conditions alone are clearly insufficient to induce organic preservation of soft-bodied macrofossils, most authors have considered benthic anoxia as a prerequisite (Gaines et al., 2010 and references therein). Note that a recent study (Garson et al., 2012) on the Spence Shale suggests that Burgess Shale-type preservation is favoured by bottom water anoxia, but may not require it in all cases. Redox parameters for least weathered samples do not indicate deposition under anoxic conditions. Accordingly, bottom-water anoxia conditions were not permanently present during deposition.

The samples were analyzed and classified into three groups with different degrees of alteration/weathering based on X-ray analyses, geological observation, and geochemical data combined with statistical analyses. The specific clay mineral composition shows increasing chlorite and goethite, decreasing kaolinite, $2M_1$-mica, and dolomite, and a, increase in the chemical alteration of mudstones. It also indicates slight variations between the primary types of beds (EB, BGB). This hints at variations in the source of clastics or the hydrochemical environment during the deposition of strata.

This study reveals that late-stage chemical alteration/weathering plays a much more prominent role in the taphonomy of the Chengjiang and Guanshan Biotas than previously recognized. The chemistry of UW and SW+W groups is significantly different due to chemical alteration, most likely linked to intense faulting since the Cretaceous.

Finally, an updated taphonomic pathway is proposed for Burgess Shale-type preservation.

2. Material and methods

During the two field campaigns in South China in 2008 and 2009, I collected material in Yunnan Province. The first field campaign concentrated on the Kunming district and the region near the Dianchi Lake and Fuxian Lake: the counties of Chengjiang, Anning, Haikou-Kunming, Jinning and Yiliang were visited, and fossils of the Chengjiang Fauna (Cambrian Stage 3) and of the slightly younger Guanshan Fauna (Cambrian Stage 4) were collected from 11 outcrops. The second field campaign focused on the north area of Yunnan Province: the Counties of Qujing and Malong, with 6 new outcrops, were added to the previous working area, where I collected again in the Haikou-Kunming area and in Jinning County. During the second field work season, I also worked on the Xiaotan section, one of the most complete sections of the Precambrian/Cambrian boundary (Fig. 1). I collected more than 400 fossil samples during the 2008 field campaign and 385 during the second campaign; this is supplemented by the samples we took from every outcrop to conduct various geochemistry analyses.

Concerning brachiopods, I extended the material to also include recent specimens of linguliform brachiopods. This approach was designed to use modern linguliform brachiopods as a key to understanding the fossilization potential of the different organs and the taphonomic pathways of the earliest Cambrian linguliform brachiopods. Recent specimens of *Lingula anatina* come from Japan (Kasari Bay, Amami Island and Ariake Bay, Kyushu), China (intertidal sand of the Gulf of Tonkin), Thailand, and Australia. Specimens of *Lingula adamsi* come from China (intertidal mud of the Gulf of Tonkin); specimens of *Lingula rostrum* come from Sumatra and *Glottidia albida* specimens from California.

My PhD was also devoted to determining the influence of later diagenetic changes in the chemical composition of fossils, especially due to weathering and alteration processes (mineralogical study of crystal shapes and sizes of iron oxides replacing most soft-bodied weathered fossils). This approach was based on SEM images, EDX analyses and geochemical analyses. For this purpose, Chengjiang-type fossils from the classical and highly weathered sites were compared with those from less altered sites. Previous studies on the Early Cambrian Chengjiang Biota were based solely on completely weathered material. Here, for the first time, we used material embracing the complete spectrum of weathering stages, from unweathered to weathered grade (Fig. 2). This enabled developing a more complete and plausible taphonomic model for the Chengjiang and Guanshan fossil Lagerstätten.
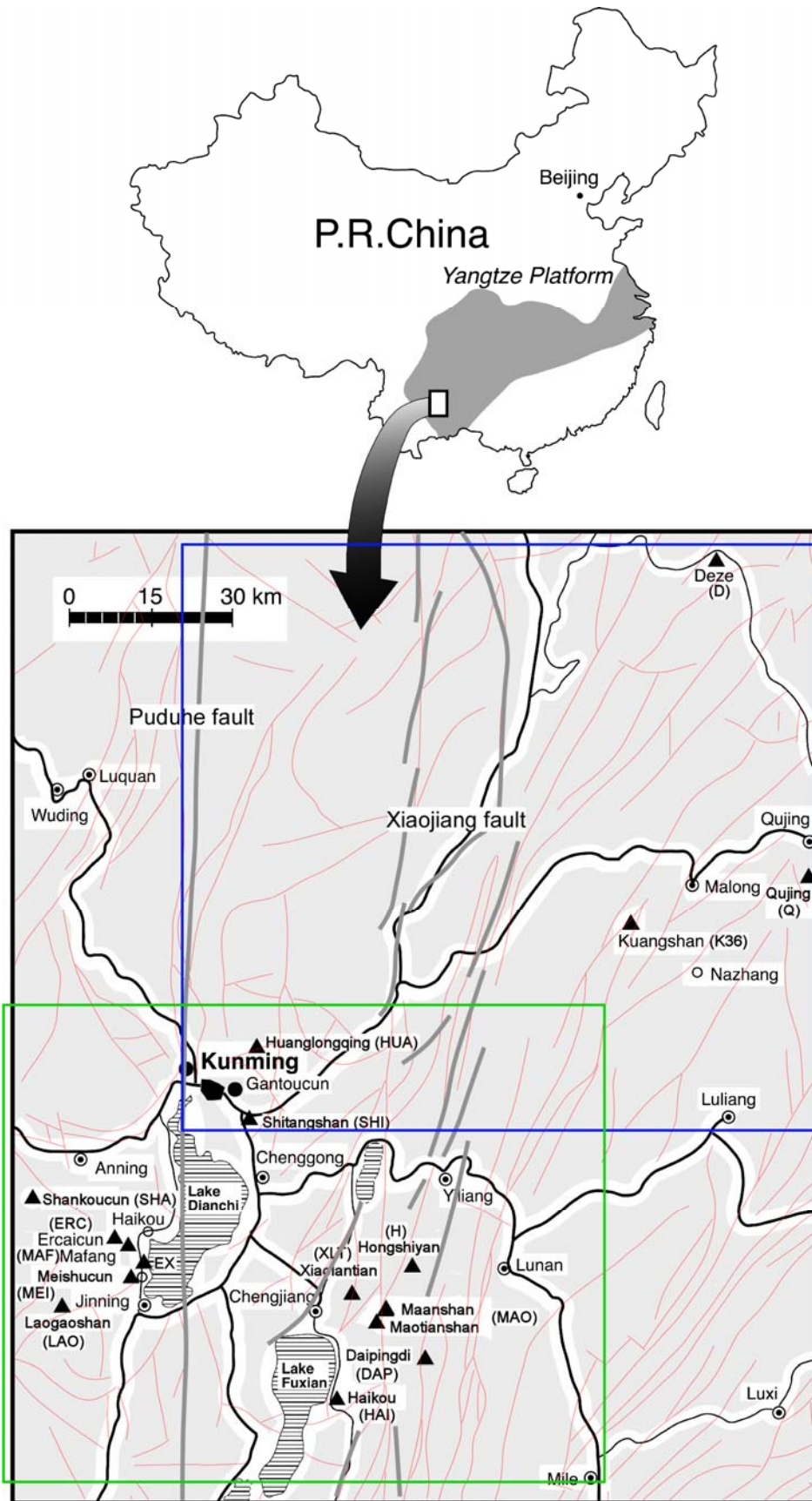
Figure 1- The sampling area: blue box for field campaign 2009; green box for field campaign 2008. Black triangles for fossil outcrops, red lines for faults. Modified after Forchielli et al., 2013 in press.

Figure 2- The whole alteration/weathering spectrum of the analyzed material. Note increase in alteration/weathering from right to left.
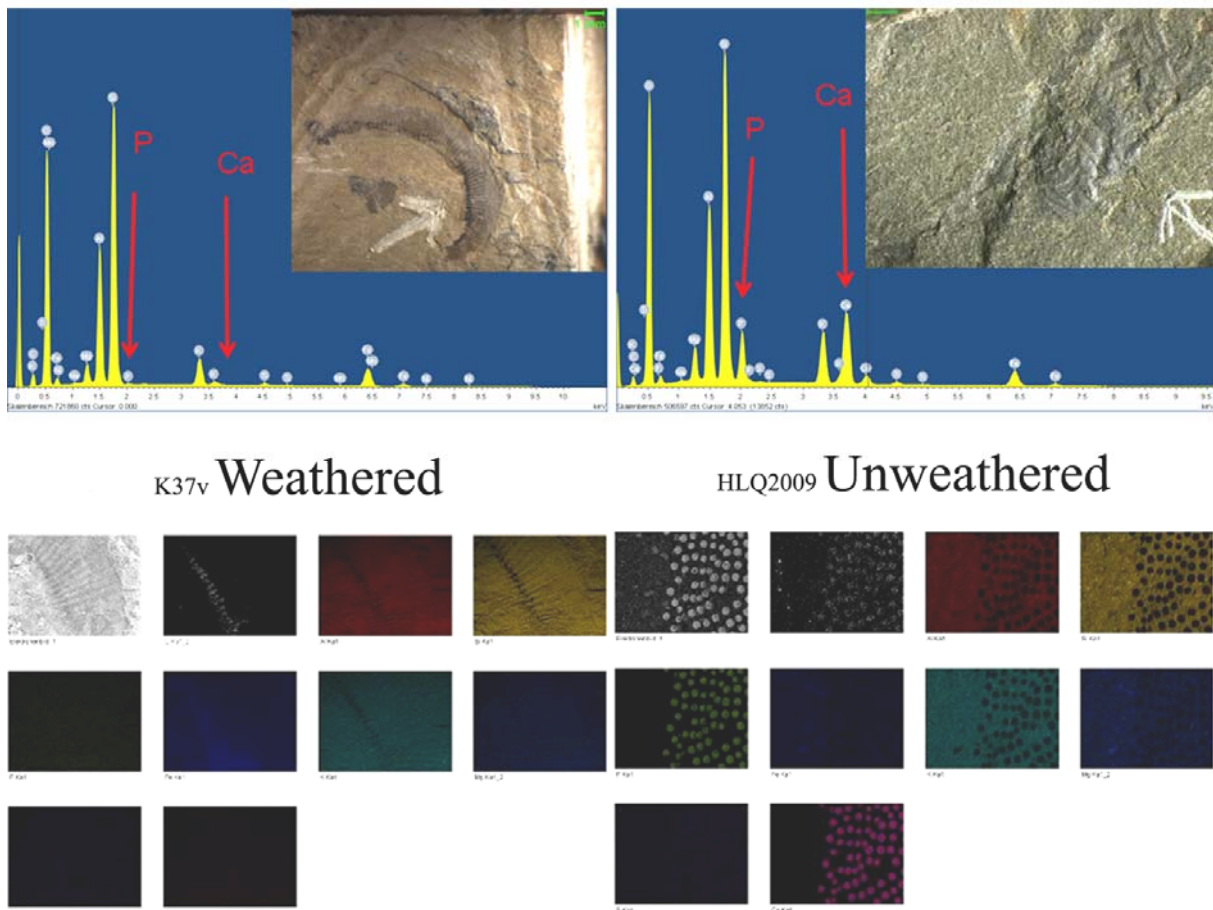
Figure 3- Differences in elemental mapping analyses of weathered and unweathered worms. On the right side of the image the spectrum (above) as well as the single element overview (below) show the presence of P and Ca (highlighted by arrows above and by light green and pink elements in the figure below) in unweathered material. Both elements are missing in the left side of the image, where a weathered worm in analyzed. These huge differences clearly undermine the reliability of the previous taphonomic pathways based solely on this type of material.

The results between unweathered and weathered material differed enormously (see Fig. 3 for an example on worms). Lithogeochemically, this study analyzes the geochemical and mineralogical features of the matrix in the different stages of alteration as well as the features of event beds (EB) and background beds (BGB) from outcrops covering a large area in the Yunnan Province.

2.1. Iron speciation

The sequential extraction procedure for iron is basically a further development of the degree-of-pyritization (DOP), a parameter which determines the extent to which iron minerals potentially reactive towards dissolved sulphide have been transformed into pyrite. It can therefore be used as a paleoredox proxy, indicating whether sediments have been deposited beneath oxic or anoxic bottom waters in both modern and ancient environments (Berner, 1970; Raiswell et al., 1988, see also Canfield, 1989; Raiswell et al., 1994; Raiswell and Canfield, 1998). The sequential extraction procedure for iron recognizes seven operationally derived iron pools (Poulton and Canfield, 2005): (1) carbonate associated Fe (Fe_{carb}), including siderite and ankerite; (2) easily reducible oxides (Fe_{ox1}), including ferrihydrite and lepidocrite; (3) reducible oxides (Fe_{ox2}), including goethite, hematite and akaganéite; (4) magnetite (Fe_{mag}); (5) poorly reactive sheet silicate Fe (Fe_{PRS}); (6) pyrite Fe (Fe_{py}); and (7) unreactive silicate Fe (Fe_U). The parameter used to demonstrate or infer deposition beneath an anoxic water column is the ratio of highly reactive FE (FeHR) to total Fe (FeT), whereby FeHR includes iron minerals that are likely to be 'highly reactive' towards dissolved sulphide (Canfield and Berner, 1987; Poulton et al., 2004).

The samples analyzed for this study are of Cambrian age: we can therefore rule out certain minerals that are not expected to be present in significant amounts in such ancient sediments, for example easily reducible oxides (Fe_{ox1}) (S. Poulton, personal communication). Therefore, the highly reactive portion of the iron pool included only Fe_{carb}, Fe_{ox2}, Fe_{mag} and Fe_{py}. Fe_{carb}, Fe_{ox2} and Fe_{mag} were extracted sequentially (following the methods evaluated by Poulton and Canfield, 2005) out of one unit of each powdered sample ranging from 50 to 100 mg. Fe_{carb} was extracted from the sediment by adding 10ml of 1M sodium acetate adjusted (with acetic acid) to pH 4.5 (see Tessier et al., 1979) into the test tube, which was then shaken for 48 h at 50°C. The resulting solution was carefully removed from the test tube and diluted 20 times in water in order to obtain a total dilution of 20,000 times. For extracting Fe_{ox2}, a sodium dithionite solution (50g l-1) buffered to pH 4.8 with 0.35M acetic acid/0.2M sodium citrate (Mehra and Jackson, 1960; Lord III, 1982) was used immediately after preparation in order to

prevent the solution from oxidizing. Ten milliters of the solution was then poured into the test tube and then shaken for 2 h at room temperature before being diluted again (total of 20,000 times). Fe_{mag} in the remaining sediment was extracted by adding 10 ml of a 0.2M ammonium oxalate/0.17M oxalic acid solution (pH 3.2; McKeague and Day, 1966; Phillips and Lovley, 1987), the resulting solution being diluted in the same way as for Fe_{carb} and Fe_{ox2}.

The extraction of pyrite Fe (Fe_{py}) was done separately by weighing about 4 g of sample powder (depending on extent to which the pyrite content can be estimated). During the procedure, two Fe sulphide phases were taken into consideration: acid volatile sulphide (AVS) and chromium reducible sulphide (CRS). AVS is rare in ancient sediments and basically corresponds to the FeS content in the sediment. AVS is collected by heating up the sample after adding a 50% HCl solution (Cornwell and Morse, 1987); the resulting H_2S gas is then led, supported by a flow of N_2 gas through the apparature, into a water-filled test tube with added silver nitrate (usually 0.25ml of 170g l-1 silver nitrate). This results in the precipitation of Ag_2S, which is then collected and should reflect the amount of FeS in the sediment. The extraction of AVS lasts about 15 min. CRS is subsequently extracted by adding chromous chloride (533g l-1, Canfield et al., 1986) to the sediment, keeping it boiling for 1 h. The escaping H_2S gas resulting from the dissolution of Fe_2S is then again precipitated as Ag_2S in the test tube with silver nitrate, which would have been replaced if the previous extraction with HCl yielded a significant amount of AVS.

To dissolve the total iron (FeT), about 100 mg of every powdered sample was weighed and first ashed overnight at 550°C in order to remove insoluble organic matter and sulphides. Five milliters of nitric was then added to the ashed powder, followed by 2 ml hydrofluoric acid (HF) and a few drops of $HClO_4$. The mixture was then dried on a hot plate at 130°C. Then, boric acid (50 g l-1) was added and dried up again. The remains of each sample were then again dissolved in 5 ml of 50% HCl and then heated up until total dissolution occurred. The resulting solution was diluted by first filling it up to 100 ml with water and then taking 0.1 ml of this solution and diluting it into 4.9 ml of water. This yielded an overall dilution of 5,000 times.

The concentrations of Fe_{carb}, Fe_{ox2}, Fe_{mag} and FeT in the prepared solutions were measured using an atomic absorption spectrometer (AAS). The collected Ag_2S precipitates were weighed and the corresponding FeS_2 concentration calculated; a slight loss of sulphide can occur using this method, especially in sulphide-poor samples.

2.2. Total digestion

INAAPortion

A 30 g aliquot of sample was encapsulated in a polyethylene vial and irradiated with flux wires and an internal standard (1 for 11 samples) at a thermal neutron flux of $7 \times 10^{12\,n\,cm^{-2}\,s^{-1}}$. After a 7-day decay to allow Na-24 to decay, the samples were counted on a high purity Ge detector with a resolution of better than 1.7 KeV for the 1332 KeV Co-60 photopeak. Using the flux wires, the decay-corrected activities were compared to a calibration developed from multiple certified international reference materials. The standard is only a check on accuracy and is not used for calibration purposes. One standard was run for every 11 samples.

ICP Portion

A 0.25 g aliquot of sample was digested in HClO 4-HNO3-HCl-HF at 260°C to fuming and was diluted with dilute HCl. This leach is partial for magnetite, chromite, barite, spinels, zircon and massive sulphides. The solutions were read on a Varian Vista or Varian 735ES ICP. Reported QC includes a blank analysis frequency of 2%, 1 for every 40 or fewer samples, a sample replicate frequency of 7%, 1 for every 15 or fewer samples, and 6% or more were analyzed international standards.

2.3. Lithium Metaborate/Tetraborate Fusion- ICP

Samples were prepared and analyzed in a batch system. Each batch contains a method reagent blank, certified reference material and 17% replicates. Samples were mixed with a flux of lithium metaborate and lithium tetraborate and fused in an induction furnace. The molten melt was immediately poured into a solution of 5% nitric acid containing an internal standard, and mixed continuously until completely dissolved (~30 min). The samples were run for major oxides and selected trace elements on a combination simultaneous/sequential Thermo Jarrell-Ash ENVIRO II ICP or a Varian Vista 735 ICP. Calibration was performed using 7 prepared USGS and CANMET certified reference materials. One of the 7 standards was used during the analysis for every group of ten samples.

Totals should be between 98.5% and 101%. If lower results were obtained, samples were scanned for base metals. Low totals may indicate sulphate being present or other elements such as Li, which normally will not be scanned for. Samples with low totals, however, were automatically refused and reanalyzed.

2.4. TOC and TS

Part of the samples was analyzed at Actlabs with the procedure:

Total carbon and sulphur were determined on an automated LECO CS-344 or an ELTRA CS 800 carbon sulphur analyzer. A weighed sample was mixed with iron chips and a tungsten accelerator and was then combusted in an oxygen atmosphere at 1370°C. The moisture and dust were removed and the CO_2 gas and SO_2 gas were measured by a solid-state infrared detector.

CO_2 was determined by placing a second sample in a ceramic crucible and adding 25% HCl drop-wise until no reaction was observed. The sample was dried on a hot plate at low temperature and C was re-determined on the dried residue. The difference was calculated as CO_2.

The sample was ignited at 600°C in order to drive off the CO_2 and the organic carbon. The remaining C is graphitic carbon, which was analyzed as above.

Organic carbon was determined as the difference after subtracting the above species.

Sulphide sulphur was determined by calculating remaining sulphur after sulphate sulphur was subtracted from total sulphur. Sulphate sulphur was determined by roasting at 250°C to drive off the sulphide sulphur; the sulphur was analyzed in the roast residue. This was converted to sulphate by calculation.

The rest of the samples were processed in Germany (Postdam-AWI or Berlin-TU) with a TOC Elementar Vario MAX EL III, CNS-analyzer Macro analyzer to determine carbon, nitrogen and sulphur; this approach used high temperature combustion at up to 1200°C with subsequent gas analysis. A second approach involved an Elementar LiquiTOC, using the Europe Standard procedure EN 1484 and the standard methods 5210A and B and also DIN 38409 H3, ISO 8245 and EPA 415.1.

2.5. Nanofocus-X-ray computed tomograph Phoenix Nanotom 180 kV.

Maximal tube voltage: 180 kV; maximal output: 15 W; Detail detectability: up to 200nm (0.2μm); Minimal focus-detector-distance: 0.4mm; Maximal voxel resolution (depending on object size): < 500 nm (0.5 μm); Geometric magnification (3D): 1.5 times up to 100 times; Maximal object size (height x diameter): 150mm x 120mm; Maximal object weight: 2 kg; 5-Megapixel fully digital image chain.

3D metrology with X-ray is the only technique allowing non-destructive measurement of the interior of complex objects. In contrast to conventional tactile coordinate measurement

techniques, a computed tomography scan of an object acquires all surface points simultaneously – including all hidden features such as undercuts, which are not accessible non-destructively using other methods of measurement.

Once scanned, the fully three-dimensional CT information allows non-destructive visualizations of slices or arbitrary sectional views. Since the whole geometry of the object is scanned, precise 3D measurements of complex objects are possible.

2.6. Resins

Recent specimens of *Lingula* and *Glottidia* were prepared with a four-component resin (Epon 812) suitable for SEM analyses. The resin was obtained with the following procedure: first, the samples preserved in alcohol (A) were switched to propylene (P) with the formula A 2: P 1, then 1:1, 1:2 to arrive at 100% propylene in 2.45 h. The resin was obtained by mixing 50 g of Epon 812 with 25 g of DBA and 25 g of MNA for 90 mins, then adding 2 ml of DMP and mixing again for 30 min. The obtained resin (R) was added in increasing proportion to the propylene: P 2: R1 for 1 h, 1:1 for an additional 1 h, P1:R2 for 15 h. Finally, the 100% resin obtained was dried for 48 h at 60°C.

2.7. T.E.M.

Phase analytical characterization of 16 selected samples was carried out by X-ray diffraction (XRD), measured by Labor für Prüfung mineralischer Roh- und Reststoffe, Gleichen-Weißenborn, and transmission electron microscopy (TEM), at the University of Greisfald, Institute of Geography and Geology.

Bulk samples were grinded at < 32 μm for the XRD-investigation. Randomly oriented powder samples and the oriented mounts of fraction < 2 μm of selected samples were studied using a Philips PW1710-BASIS X-ray diffractometer equipped with a Cu tube (Kα1,2 radiation) as well as a secondary monochromator. It operated at a current of 30 mA and a voltage of 30 kV (fixed divergence slit: 1°; collimator: 0.2; measured interval: 2.0 … 68.0° 2θ; measurement step: 0.02° 2θ; measurement time per step: 2 s; continuous scan). XRD analyses were conducted on oriented mounts, including measurement of air-dried and ethylene-glycol saturated specimens. The WinFit program (Krumm, 1994) was used to analyze the line-profile of clay minerals; broad and strongly overlapping XRD peaks and coherent scatter domains were used as an approximation for the particle thickness distribution. The BGMN program,

which is based on Rietveld methodology, was used to quantify and further characterize each identified phase (Bergmann et al., 1998; Ufer et al., 2004; Kleeberg et al., 2005; Ufer et al., 2008a+b; Dohrmann et al., 2009; Ufer et al., 2010). The refinement of XRD-diagrams by BGMN-Rietveld-software enables a quantification of selected phases and additional characterization of each phase by a refined data set for atom coordinates and other parameters concerning order/disorder. Pre-sedimentary processes and diagenesis affect the composition of mineral matter and also the chemical composition of the different phases. XRD is a typical main tool to identify the composition of mineral matter. Rietveld is a mathematical principle to evaluate XRD-diagrams, quantifying and characterizing each phase separately. BGMN-software represents a special type of Rietveld technique used to quantify the mineral composition in bulk samples. TEM allows a particle-wise characterization of a particle's morphology, chemical composition (calculation of mineral formula by EDX analysis) and stack order by electron diffraction (ED). TEM investigations were conducted on the <2 µm fraction using a Jeol JEM−1210 microscope, operated at 120 kV and equipped with a LaB6− cathode. Attached to the microscope are an ISIS LINKOXFORD energy dispersive X-ray (EDX) system and a GATAN MULTISCAN camera. These allow characterizing the morphology, crystal habit, and stack order (by electron diffraction) of the particles. They also yield element distribution images. Selected particles were analyzed chemically (semi-quantitative data) by EDX, which enabled calculating mineral formulae using the software toolkit of Kasbohm et al. (2002). The fraction < 2 µm was separated by sedimentation. Oriented mounts of the samples MAF 4 081 EB and MAF 4 081 BGB were prepared and measured under air-dried conditions and also under ethylene-glycol saturation in order to detect possible swelling phases.

2.8. S.E.M.

Chengjiang-type fossils were routinely analyzed for their elemental distribution and mineralogy. Elemental mapping was performed using two energy-dispersive X-ray (EDX) analyzers: a kevex delta V energy-dispersive elemental analyzer with a quantex light element detector coupled to an S-2700 SEM HITACHI and an Inca analyzer X-max 50 mm^2 coupled to a SEM ZEISS- SUPRA 40VP; fossils were analyzed uncoated and unpolished using 20 KV, 15 KV and 10 KV voltages.

2.9. Histological sections

Histological sections were used to identify the different organic components/tissues of the internal organs using longitudinal serial sections of a whole subadult specimen from Magnetic Island, Australia, fixed in Bouin's fluid. The organo-phosphatic shell was softened using diaphanol (3 days, room temperature). After dehydration through an alcohol series, butanol and methyl benzoate, the specimen was embedded in paraffin and subsequently sectioned (10 μm) with a Reichert Histo-Microtome. Serial sections were mounted on glass slides and stained with the Azan method (Geidies 1954).

Taphonomy of Cambrian (Stage 3/ 4) sponges from Yunnan (South China)

http://www.geology.cz/bulletin/contents/art1225

Taphonomy of the earliest Cambrian linguliform brachiopods

http://www.app.pan.pl/article/item/app20110182.html

73

Taphonomic traits of clay-hosted early Cambrian Burgess Shale-type fossil *Lagerstätten* in South China

Abstract

The Chengjiang and Guanshan fossil *Lagerstätten* of Yunnan represent key fossil deposits to understand and reconstruct early metazoan evolution. Despite extensive studies on the systematics of taxa from these *Lagerstätten*, the major mechanisms of exceptional soft-tissue preservation at these fossil *Lagerstätten* have remained controversial. The Chengjiang and Guanshan fossil *Lagerstätten* represent typical Burgess Shale-type deposits, influenced by late alteration and weathering that led to some major transformations in clay and iron minerals, as well as dissolution of dolomite and skeletal biominerals. The detailed geochemical screening of various fossil groups, such as brachiopods, priapulids, arthropods, and sponges, indicates a more complex preservational history than hitherto supposed. Besides oxidation processes during sub-recent/recent weathering, clay mineral formation and/or alteration, carbonization, phosphatization, and pyritization played key roles in the preservation of various metazoans.

The Chengjiang fossil *Lagerstätte* is characterized by the existence of clay-dominated background beds (BGBs) and event beds (EBs). Fossil preservation varies considerably in the two different depositional settings, with soft-tissue preservation occurring preferentially in EBs, whereas skeletal accumulations are typical of BGBs. The samples were analyzed and classified into three groups with different degrees of alteration and fundamentally different chemistries. The specific clay mineral composition shows increasing chlorite and goethite, decreasing kaolinite, $2M_1$-mica, and dolomite, and a rise in the chemical alteration of mudstones. It also indicates slight variations between the primary types of beds (EB, BGB), hinting at variations in the source of clastics or the hydrochemical environment during the deposition of strata. Furthermore, the geochemical paleoredox proxy data indicate that dysoxic or anoxic conditions were not permanently present during the deposition of EBs and BGBs in the Chengjiang and Guanshan fossil *Lagerstätten*.

We consider that rapid deposition in finest claystones had a greater influence on the preservation of highly volatile tissues than the presence of bottom-water anoxia, even though bottom-water anoxia and microbial sealing may further increase the probability of soft-tissue preservation. Using different geochemical proxies such as various redox indicators and iron speciation, statistics on framboid sizes, classical geological observation, and clay mineralogy, we show that iron mineral precipitation onto organic carcasses of the Chengjiang-type fossils is mostly confined to later diagenetic processes and thus is not crucial for the early fixation of easily decayable tissues in Burgess Shale-type faunas.

1. Introduction

Fossil deposits with exceptional soft-tissue preservation are rare in Earth history and are important not simply for understanding the taphonomic pathways of different taxa but also for understanding the Cambrian bioradiation (e.g., Aronson, 1992; Marshall, 2006; Hu et al., 2010). The Chengjiang and Guanshan fossil *Lagerstätten* are two of the oldest soft-bodied fossil deposits and yield a rich and highly diversified fauna that include many of the earliest known representatives of modern phyla, and play a pivotal role in understanding and reconstructing the metazoan bauplans at the very beginning of life evolution.

The processes by which delicate tissues are preserved can be various (e.g., pyritization, carbonization, phosphatization) and depend on a number of factors, including the type of tissues, organisms, the availability of ions, the amount of decay, the length of time between death and permineralization, and the geochemical conditions of the surrounding environment. The primary fossil preservation in the Chengjiang and Guanshan fossil *Lagerstätten* as carbonaceous compressions was originally the same as in the Burgess Shale and other Burgess Shale-type fossil *Lagerstätten* worldwide, representing a widespread and remarkable taphonomic window of Cambrian times. All post-Cambrian fossil *Lagerstätten* except the Ordovician Fezouata Biota (e.g. Van Roy et al., 2010) followed different taphonomic pathways (pyritization: Hunsrück-type; siderite nodules: Mazon-Creek-type; phosphatization in platy limestones: Solnhofen-type).

Despite extensive weathering of the early Cambrian Konservat *Lagerstätte* of Chengjiang, carbonaceous preservation is still recognizable in Chengjiang and in Guanshan material at most weathering/alteration stages. Although post-depositional alteration and weathering of most of the Chengjiang and Guanshan outcrops have been noted, the chemical alteration/weathering impact on the preservation of exceptional fossils has not yet been closely characterized. Analysis of the effects of extensive subsurface chemical alteration and near-surface weathering on Chengjiang and Guanshan material is pivotal to resolve the extensive late diagenetic history of alteration and to understand the complexity of early diagenetic history of these deposits and their exceptional fossils.

The preservation of these early Cambrian fossils has been particularly controversial, and several models have been proposed to account for the exceptional preservation of Burgess Shale-type fossils. Under present-day conditions, labile tissues and skeletal material of the Burgess Shale-type fossils from Chengjiang and Guanshan deposits are replaced by iron minerals. An early iron adsorption onto surfaces of organic carcasses was considered to be a key factor for the preservation of soft-tissued fossils (Petrovic, 2001). This model has also been applied to the Chengjiang fossil *Lagerstätte*, where extensive replacements of organic structures by iron oxides were interpreted as pseudomorphic alteration of early diagenetic framboidal pyrite stabilizing the labile organic tissues (e.g., Gabbott et al., 2004). Zhu et al. (2005) also emphasized the role of other authigenic minerals such as apatite and late diagenetic Fe-rich aluminosilicate in replacing parts of the exceptionally well-preserved Chengjiang fossils. Meanwhile, it has been variously discussed that the recorded mineral replacements may not be of an earliest diagenetic origin, but may even be a product of the weathering process itself (Hu, 2005; Gaines et al., 2008; Forchielli et al., 2012; in press). It was also proposed that clay minerals acted as templates to replicate labile tissues (Orr et al., 1998) or as binding substances for enzymes to inhibit autolytic decay (Butterfield, 1995). Recently, Gaines et al. (2012b) suggested that Burgess Shale-type deposits resulted from early inhibitions of microbial activity in the sediment by means of oxidant deprivation. Rapid entombment of fossils in fine-grained sediments and early sealing of sediments by pervasive carbonate cements of bed tops restricted oxidant flux into the sediments.

Framboidal pyrite is the most common pyrite texture in many sedimentary environments (Maclean et al., 2008), and pyritized organic carbon bioremains are common through geological time (e.g., the Jurassic crinoids, Szczepanik and Sawłowicz , 2005; Late Neoproterozoic Gaojishan Biota, Cai and Hua, 2007), but there are only two Paleozoic Faunas with common soft-tissue preservation: the Devonian Hunsrück Slate (Briggs et al., 1996) and the Lower Ordovician Beecher´s Trilobite Bed (e.g., Briggs et al., 1991).

The two most common morphologies of pyrite crystals (framboids and micro-sized single euhedral crystals) are thought to reflect the geochemical conditions of the depositional environment (e.g., Wilkin et al., 1996; Passier et al., 1997; Taylor and Macquaker, 2000). Framboidal pyrite in sedimentary rocks can be syngenetic, early diagenetic, or sometimes late diagenetic (Sawlowicz, 1993 and references therein). Framboidal morphologies are often related to pyrite, but other minerals have the same form, e.g., limonite (Taylor, 1982), hematite (Lougheed and Mancuso, 1973), magnetite (Suk et al., 1990), and chalcocite/ digenite (Sawlowicz, 1990).

Mechanisms of early diagenetic pyrite formation led to the development of geochemical paleoenvironmental indicators (Taylor and Macquaker, 2000). It has been suggested that the sizes and morphologies of these crystals can be used in addition to the degree of pyritization (DOP) and iron speciation analyses to determine the geochemical conditions of the environment (e.g., Wignall and Newton, 1998). Previous authors applied these methods to explore the geochemistry of both modern and ancient environments (e.g., Wignall and Newton, 1998; Wilkin and Barnes, 1997). Scott et al. (2009) suggested that no obvious morphological differences were recognizable between framboidal pyrite of syngenetic-early diagenetic origin and those interpreted to have formed during later burial, deformation or hydrothermal alteration. This suggests that crystallization paths were either independent of the geologic environment in which the framboids formed, or that different crystallization paths produce a similar range of framboid morphologies.

The main purpose of this study is to understand the effects of diagenetic alteration and weathering on early Cambrian fossil deposits of Yunnan Province, both on fossils and on sediments, using geochemical and mineralogical approaches. This study aims to characterize the sediments of Chengjiang-type *Lagerstätten* in Yunnan Province (South China) based on mineralogical investigations, geological observations, and geochemical data combined with statistical analyses. By using the sediments in concert with the fossils, it is possible to achieve a clearer picture of the effects of weathering on the original composition of the fossils. A new classification scheme of weathering intensity is developed here. Geochemical data were also used to determine the paleoredox setting of the deposits and the effects of weathering on these geochemical indices. These analytical methods will allow the evaluation of the impact on sediments by early diagenesis at the seawater/sediment interface, burial diagenesis, post-sedimentary fault-related hydrological activities, and potential late-stage chemical alteration during weathering and influence of microbes. Another focus of this paper is to shed light on the controversial issue of the preservation of the early Cambrian fossils by investigating the early or late diagenetic nature of the pyrite minerals, later pseudomorphed by iron oxide in the Chengjiang Fauna. To achieve this, we combine sizes and morphologies of the iron oxide minerals with other geochemical, mineralogical, and geological analyses, besides elemental mapping and energy dispersive X- ray (EDX) analyses. Finally, this paper aims to clarify the nature and role of the clay minerals in the preservation of the Chengjiang Biota for a better understanding of its taphonomic pathways, in order to develop a model for taphonomic pathways of the Burgess Shale-type *Lagerstätten* in South China.

2. Material and methods

The material described here was collected from a number of localities covering a large area of Yunnan Province and exposing the Yuanshan Formation (Chengjiang Fauna): Xiaolantian (XLT), Shankoucun (SHA, SHANK), Deze (D), Daipingdi (DAP), Laogaoshan (LAO), Meishucun (MEI), Ercaicun (ERC), Ma'anshan (MAO), Mafang (MAF), Dabaidi south of Qujing (Q), Kuangshan (near Malong) (MAL and K36), EX (Expressway site near Xiaotuanshan, near Mafang), and Haikou of Chengjiang County (HAI) sections, and the Wulongqing Formation (Guanshan Fauna): Shitangshan (SHI M, UP and SHI 41) and Huanglongqing (HUA) (see Fig. 1). A sample from Hongshiyan (H), belonging to the Black Shale Member of the Yuanshan Formation, underlying the Chengjinag fossil-bearing Maotianshan Shale Member, was used for comparison.

Elemental mapping was performed using two energy dispersive X-ray (EDX) analyzers: a Kevex delta V energy-dispersive elemental analyzer with a Quantex light element detector coupled to an S-2700 SEM HITACHI and an Inca analyzer X-max 50mm^2, with a Moxtex polycarbonate window (Oxford Instruments), coupled to a SEM ZEISS- SUPRA 40VP. Fossils were analyzed uncoated using 20KV, 15KV and 10 KV voltages. For this study, we analyzed fossils embracing the complete spectrum of alteration stages, from unaltered to heavily altered (Fig. 2), which is indicated by different rock coloration, bulk chemistry, and preservation of fossils. For the analyses, samples were separated according to two major sedimentological features, background beds (BGBs) and event beds (EBs) (see Hu, 2005 for a complete overview on sedimentological differences between BGBs and EBs).

Main and trace element analyses were carried out at Actlabs, Canada, using four-acid digestion-inductively coupled plasma (ICP), instrumental neutron activation analysis (INAA) and lithium metaborate/tetraborate fusion-ICP. Samples were analyzed for nitrogen, sulfur, and total carbon (TC) by a CNS-Analyser (Elementar Vario EL III) and for total organic carbon (TOC) using an Elementar Vario Max at AWI Potsdam and an Elementar LiquiTOC at TU Berlin. Iron speciation was performed at the Civil Engineering and Geosciences Department, Newcastle University, according to Poulton´s sequential extraction procedure for iron (Poulton et al., 2004; Poulton and Canfield, 2005).
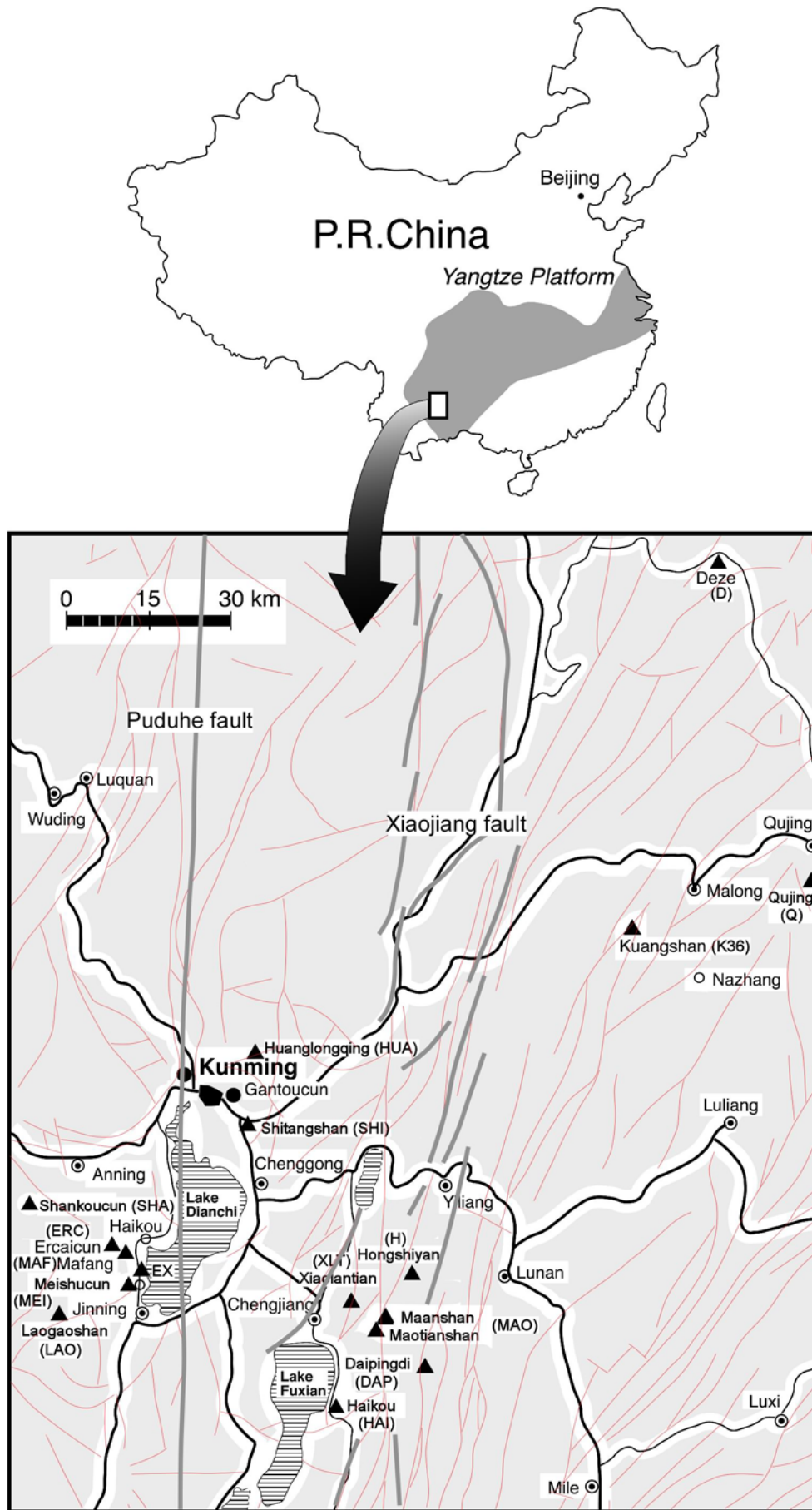
Fig. 1. Geographic distribution of the outcrops in Yunnan Province. Black triangles for fossil outcrops, red lines for faults.

Basic calculations and plots of geochemical data were carried out in Microsoft EXCEL, while the program package SPSS for Windows, Release 16.0.1, was used for canonical discriminatory analyses. SPSS analyses were performed using the row data from the iron speciation (pyrite iron, carbonate associated iron, magnetite iron, reducible oxide iron, highly reactive iron) besides geochemical proxies (DOP, Fe HR/FeT, U_{auth}, FeT/Al, Fe_{py}/FeHR, V/Cr, Ni/Co and V/V+Ni). Principal component analyses were carried out using the program package R, version 2.15.2 (2012-10-26). R analyses were performed using the geochemical data of main and trace elements, S and TOC/ TC (see matrix in the appendix).

Phase analytical characterization of 16 selected samples was carried out by X-ray diffraction (XRD), measured by the Labor für Prüfung mineralischer Roh- und Reststoffe (Gleichen-Weißenborn, Germany) and by transmission electron microscopy (TEM), measured at the University of Greifswald, Institute of Geography and Geology. XRD was the main method to identify the mineralogical composition in the investigated sediments. Selected samples were studied using a Philips PW1710-BASIS X-ray diffractometer equipped with a Cu tube (Kα1,2 radiation) as well as a secondary monochromator (current: 30 mA; voltage: 30 kV; fixed divergence slit: 1°; collimator: 0.2; measured interval: 2.0 - 68.0° 2θ; step: 0.02° 2θ; time per step: 2 s; continuous scan).

Bulk samples were ground at < 32 μm and measured as randomly oriented powder samples. The BGMN program, which is based on the Rietveld methodology, was used to quantify and further characterize each identified phase (Bergmann et al., 1998; Ufer et al., 2004; Kleeberg et al., 2005; Ufer et al., 2008a, b; Dohrmann et al., 2009; Ufer et al., 2010). To identify the impact of different geological processes, BGMN was applied especially to characterize such phases as $2M_1$ muscovite (concerning polytype and Fe amount) and chlorite in detail. Chlorite showed all five (00l) interferences in all samples. By applying the BGMN refinement procedures, it was possible to distinguish the composition of the two different octahedral sheets in chlorite. XRD analyses were also carried out on oriented mounts of the < 2 μm fraction and included measurement of air-dried and ethylene-glycol-saturated specimens. The WinFit program (Krumm, 1994) was used to analyze the line profile of clay minerals with broad and strongly overlapping XRD peaks and coherent scatter domains as an approximation to the particle thickness distribution. The refinement of XRD diagrams by BGMN-Rietveld software offers a quantification of selected phases and additional characterization for each phase by a refined data set for atom coordinates and other parameters concerning order/disorder.
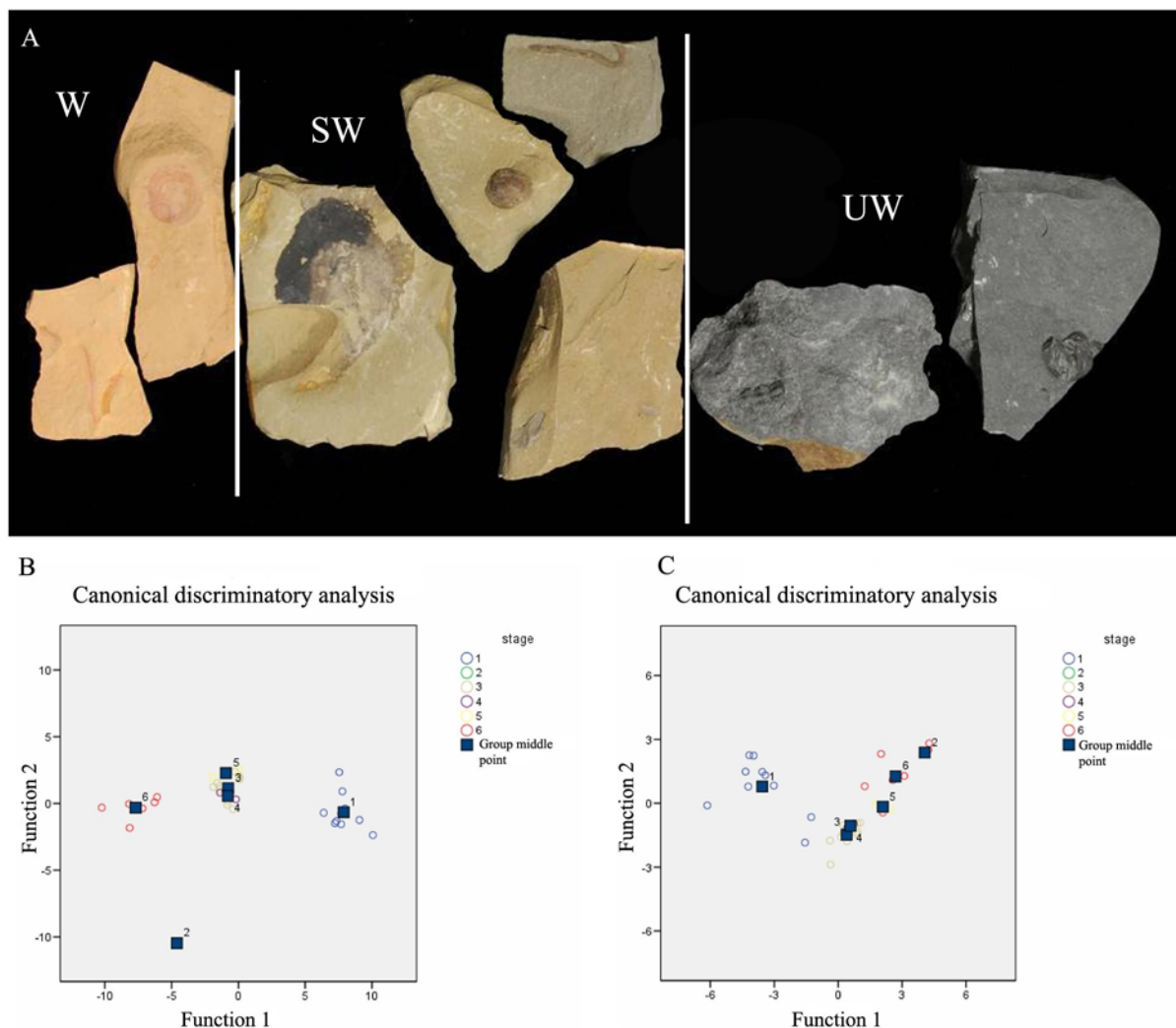
Fig. 2. Weathering stages. A- Weathering groups UW, SW and W. B and C, Canonical discriminatory analyses show three distinct groups. These analyses are based on data shown in Table 2.

TEM investigations were carried out on the <2μm fraction using a Jeol JEM-1210 TEM, operated at 120 kV and equipped with a LaB_6-cathode. Attached to the microscope are an ISIS LINKOXFORD energy-dispersive X-ray (EDX) system and a GATAN MULTISCAN camera, which allowed us to characterize morphology, crystal habit, and stack order (by electron diffraction) of the particles as well as to obtain element distribution images. Selected particles have been analyzed chemically (semi-quantitative data) by EDX, which allowed the calculation of mineral formulae using the software toolkit by Kasbohm et al. (2002).

The identification of the 2M1-polytype and 1M-polytype for 2:1 sheet silicates was described by Zöller (1993). Occurrence of 2M1-Mica in sediments is an indicator of the detrital origin of this mica species. The presence of the 1M-polytype indicates authigenic transformation or

neoformation of illite during sedimentary or diagenetic processes. In this contribution, the illite recognized during the TEM investigation is referred to as illite in accordance with Środoń et al. (1992), i.e., conforming to the following structural formula of illite sensu stricto with $FIX_{0.89}$ ($Al_{1.85}$ $Fe_{0.05}$ $Mg_{0.10}$) ($Si_{3.20}$ $Al_{0.80}$) O_{10} $(OH)_2$, where FIX represents fixed K+Na cations in the interlayer space. Furthermore, K- and/or charge-deficient dioctahedral micas, with tetrahedral Si ranging from 2.8 to 3.3 per $O_{10}(OH)_2$, are referred to as dioctahedral vermiculite. The acronyms "IS-ml" and "diVS-ml" refer to the illite/smectite mixed layer and the dioctahedral vermiculite/smectite mixed layer, respectively.

3. Results

3.1 Observations on fossil material

In the Chengjiang-type fossil *Lagerstätten* of Yunnan Province, the fossils are oriented parallel or sub-parallel to the bedding planes; they are flattened normal to the bedding planes. The fossils usually split along bed planes into parts and counterparts in weathered and dry samples. Unaltered, grey samples or wet samples split with a more irregular fracture and oblique to the bedding planes. Besides the common kerogen residues of fossils (Fig. 3), the minerals detected in Chengjiang-type fossils were iron oxides/-hydroxides, pyrite, calcite, apatite, Fe-Mg-rich aluminosilicate, barite and gypsum (the last two are both rare). Iron minerals and clay minerals are further described below (3.4 and 3.5, respectively) because they are crucial for understanding the taphonomic pathways of Burgess Shale-type *Lagerstätten*. Altered/weathered fossil material, the only material normally analyzed in earlier taphonomic studies, shows iron oxide minerals with framboidal and micro-sized single euhedral crystal morphologies. Altered/weathered fossils mostly revealed complete dissolution of original skeletal biominerals, such as apatite, opal, or calcite, but often still retained a carbon frame on which iron phases were precipitated. Iron minerals have been found in weathered sponge spicules, in the shells, pedicles and lophophora of linguliform brachiopods, in the sclerites of paleoscolecides (Fig. 4A; see Forchielli et al., 2012, in press), and in sclerites of the lobopodian *Microdictyon*. The iron phases in altered/weathered samples occurred as framboids, single octahedral crystals, or spherical aggregates. The least-altered fossils in grey shales lack evidence of pyrite or any other iron minerals that completely replace tissues or skeletal material.
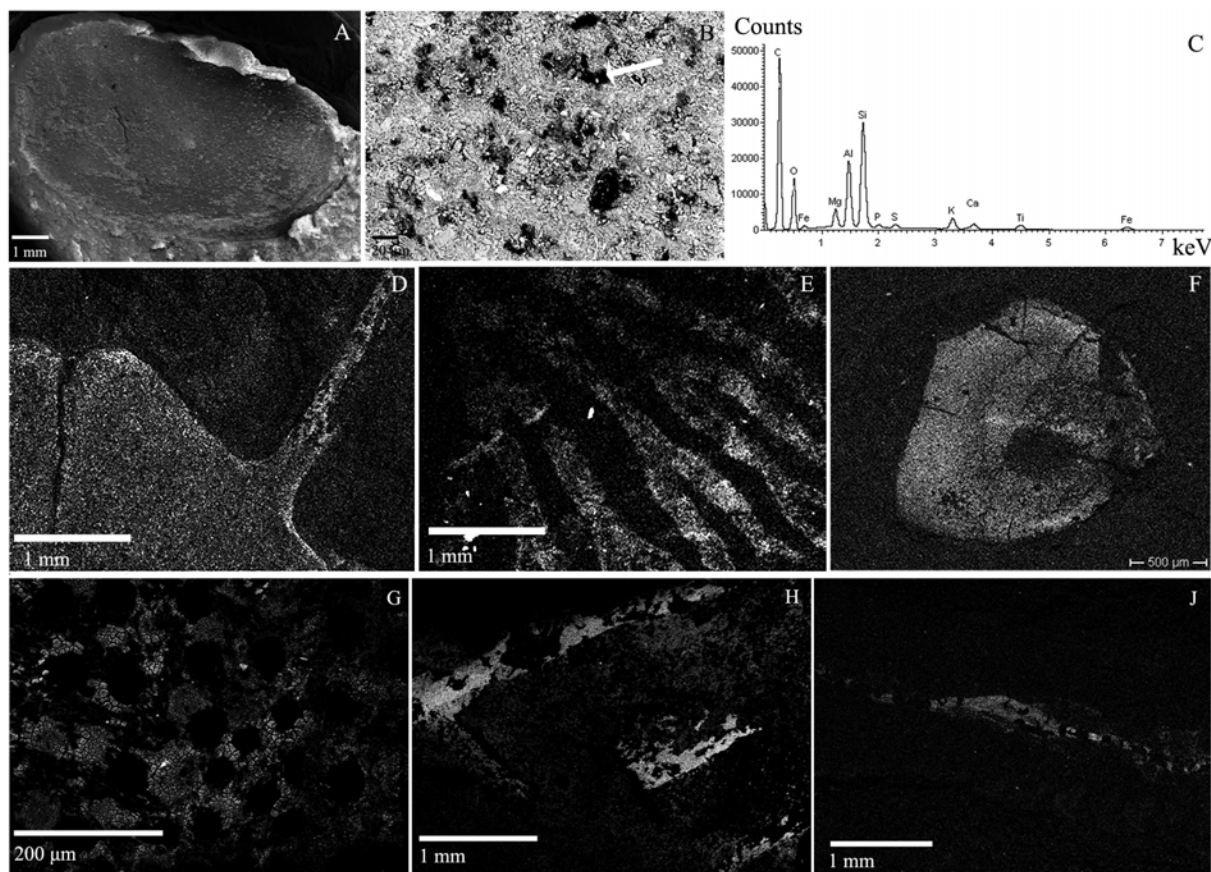
Fig. 3. Kerogen residues in fossils: A-C Bivalved arthropod from EX. UW Group; D *Kunmingella*, Malong-Qujing area (K36, W group); E- Gut caeca of *Naraoia*, Malong-Qujing area (Q, W group) ; F- Linguliform brachiopod from Haikou Chengjiang (HAI, SW group); G- Detail of *Guandoscolex* cuticle, from Guanshan Fauna (SHI, SW group); H and J- Worm guts, Chengjiang Fauna (ERC, W group).

In some cases, when pyrite is present in grey shales, pyrite may line shell fractures; in linguliform brachiopods from the Guanshan Fauna, for example, both crystal (octahedrons and icosahedrons) and framboidal morphologies are present (Fig. 4B). In one other case, pyrite was present in the matrix and in the fossil (a linguliform brachiopod of the Guanshan Fauna). In this latter case, the morphology of the pyrite inside the shell was tabular (Fig. 4C), whilst both framboids and octahedral crystals have been found in the matrix (Fig. 4D). Octahedral crystals of iron oxides have been found inside the shell of a linguliform brachiopod of the Guanshan Biota (Fig. 4N), but more often elemental mapping showed only a low percentage presence of iron inside the shell of unweathered material, and in the case of linguliform brachiopods the mapping of the shell revealed calcium, phosphorus, and carbon. The presence of iron minerals is more diffuse in the Guanshan Fauna than in the Chengjiang Fauna (but located mainly along the sides of shells, or in/along shell fractures, and generally sparse, often as single occurrences or small aggregates not covering whole cuticles or tissues).
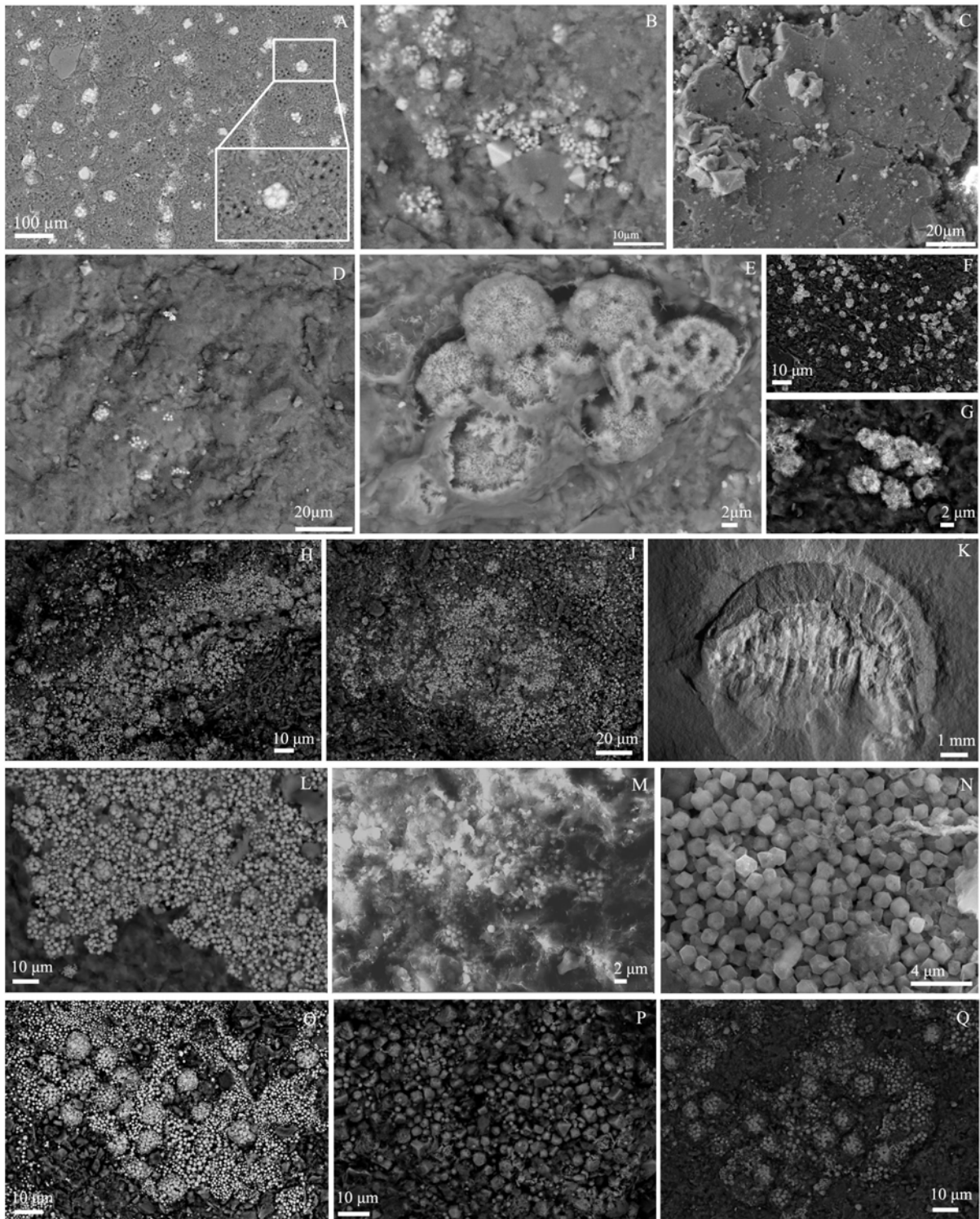
Fig. 4. Iron mineral morphologies. A- Iron in the worm (China-hu 56) plates. B- Linguliform brachiopod (Shi 4-0818) from Guanshan Fauna: crystals and framboids morphologies coexist. C- Guanshan brachiopod (Shi-hu-A): tabular pyrite in UW material. D- Pyrite in the matrix of Guanshan material UW (Shi-hu-A): both crystals and framboids are observed. E- Guanshan sponge *Paraleptomitella* (Shi up-2010) spherical aggregates. F, G- worm (Lao1-081): dissolution of the spherical aggregates. H-K- ERC arthropod (Erc-08): whole exemplar (K); iron minerals inside the shield (H) and in soft part (J). The latter are smaller in size. See also Fig. 11A for size histograms. L- UW group arthropod (Mei2-0822a) pyrite morphologies. M- Chengjiang matrix (Hai 4-082), UW group. N- Iron oxides octahedral crystals inside the shell of a linguliform brachiopod (Shi 0813) of the Guanshan Biota. O- Guanshan Fauna (SHI M-L 091) W group: iron oxide framboids and crystals in a specimen of *Panlongia*. P- Worm (ERC-0814) W group iron oxides with dissolution signs. Q- Worm from Mafang (Mafang-V): iron oxide framboids are visible.

3.2 Classification of alteration/weathering stages

The investigated mudstones were initially subdivided into six categories based on their sediment coloration (Fig. 2A) from unaltered to altered as grey (1), light grey (2), green (3), greenish (4), greenish yellow (5) and yellow (6). Coloration changes are common among the investigated outcrops; sometimes they can be seen in different rock packages in the same outcrops or even in single samples, where lighter colored (e.g., yellowish) outer rims line a darker colored (e.g., greenish) inner core. In addition to the changes in rock coloration, the different mudstone alteration is displayed by different fossil composition (mostly Fe oxyhydroxides in the most-altered samples; preservation of organic material in almost all fossils of least-altered samples), sclerite dissolution (no phosphates, carbonates, silica in skeletal remains of most strongly altered samples), bulk chemistry, and occurrence of color bandings in many altered, yellow mudstones (Fig. 5). Discriminatory analyses using iron speciation data and geochemical proxies show that the alteration/weathering stages fall into four different groups with alteration stage 2 rather distant from the others (Fig. 2B). This analysis covers 84% of the variance for the factor 1, and 10% for the factor 2. A further discriminatory analysis performed using DOP and geochemical proxies (without the iron speciation data) shows that alteration stage 2 is somehow related to alteration stage 6, and that alteration stage 5 can also be related to stage 6 (Fig. 2C). This analysis has 75% of the variance for the factor 1, and 19% for the factor 2. XRF analyses and geochemical data (values of the proxies and iron speciation data) show that the light grey to whitish sample 2 does not indicate features comparable with a low grade of alteration/weathering.
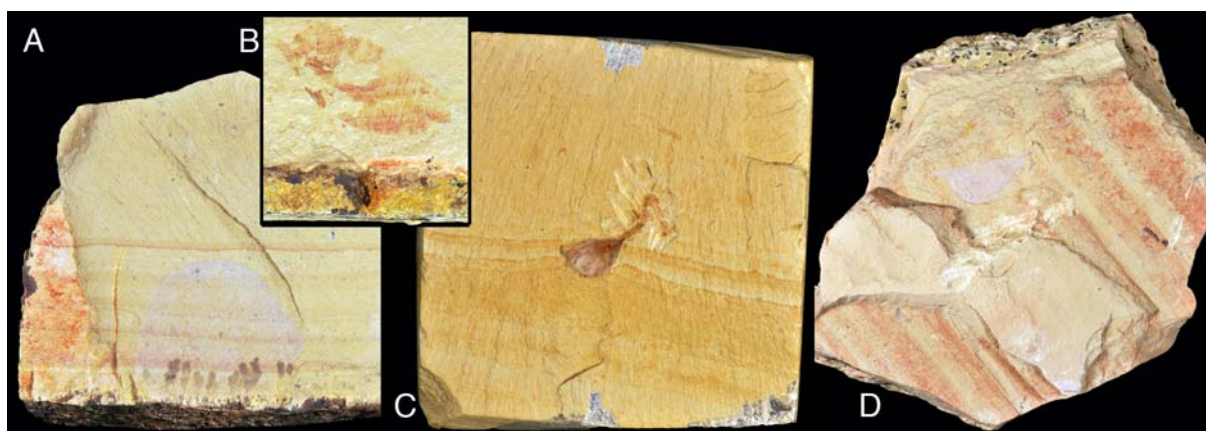
Fig. 5. Color banding during weathering processes. A (*Naraoia* Xlt-a-246 shield), C (linguliform brachiopod Xlt with soft-tissued pedicle): the band goes through fossil and matrix. The banding is mostly parallel to rock fractures that are often heavily impregnated with manganese oxides. B- (indet. arthropod fragment Xlt-211a): the banding is visible only in the fossil. D- (*Isoxys* Xlt210) figure D shows that banding sometimes does not affect all beds: here, for instance, it occurs only in the BGB but not in EB. The band runs through *Isoxys*. All samples are from the Xiaolantian outcrop.

The ranges of values shown are related to those of extremely altered/weathered material, and therefore can be considered to represent the strongest grade of alteration. Geochemical data also show that the values of group 5 agree better with group 6 than with those of groups 3 and 4. The results show three distinctive alteration/weathering groups classified as a least-altered/weathered group corresponding to alteration stage 1 with dark grey colored samples (here named UW), a second group of slightly altered/weathered samples corresponding to alteration stages 3 and 4 (here named SW), and a third group of intensively altered/weathered samples comprising alteration stages 6, 5 and 2 (here named W). The different alteration stages (UW; SW; W) also show changes in the main and minor mineral compositions. Mica of 2M1-polytype and IS-ml, quartz, and chlorite are present as major phases in all samples covering 75 to 90 % of rock composition (Fig. 6). Partially, and here especially in the least-altered samples, kaolinite may represent a major component of the mudstones (up to about 12 % in UW group; table 1). The main trends corresponding to the alteration intensity are discussed below and mostly contain an increasing amount of chlorite at the expense of kaolinite.

Fig. 6. Graphic visualization of quantitative mineral analysis by BGMN-Rietveld refinement (XRD of bulk samples); dashed line for Background Bed samples; solid lines for Event Bed samples.

86

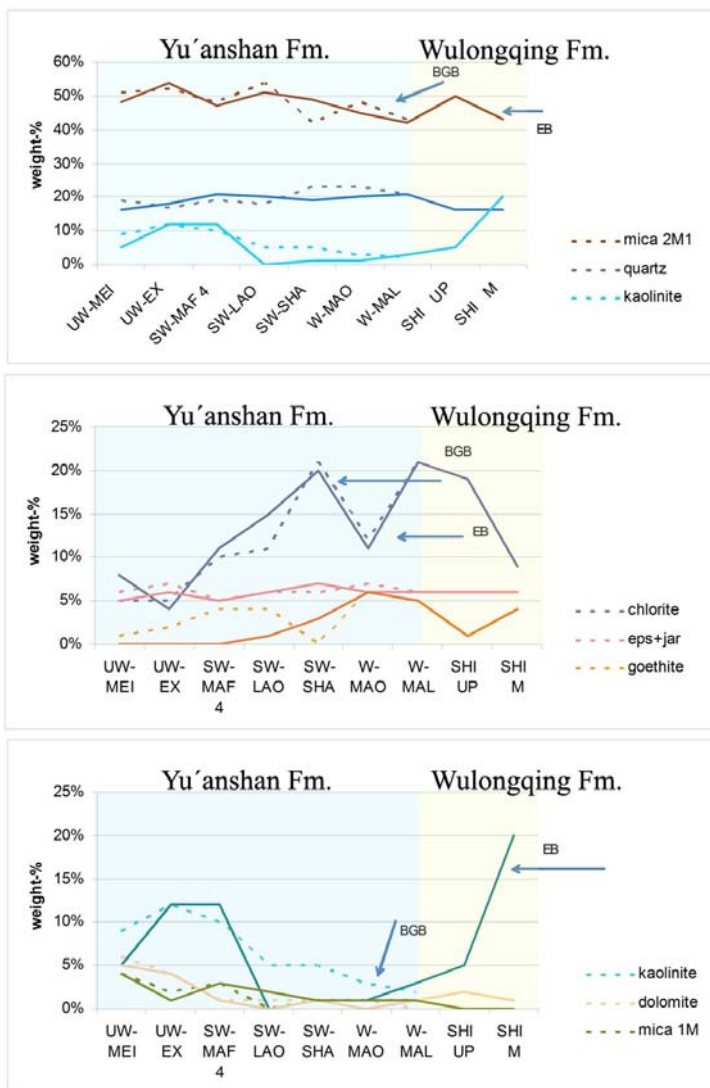| Sample	Weathering stage	quartz	muscovite (2M1)	illite (1M)	chlorite	kaolinite	goethite	dolomite	jarosite	epsomite	anatase	pyrite	K in mica (2M1)	K in illite (1M)
EX EB	UW	17,9%	54,2%	1,1%	4,5%	12,1%	0,2%	4,3%	1,1%	4,5%	0,3%	0,1%	0,6%	0,1%
EX BGB	UW	16,9%	51,5%	1,8%	5,4%	11,6%	1,9%	4,1%	1,4%	5,2%	0,3%	0,4%	0,6%	0,2%
MEI EB	UW	16,3%	47,8%	3,7%	8,4%	12,2%	0,5%	5,4%	1,0%	4,4%	0,4%	0,2%	0,6%	0,1%
MEI BGB	UW	18,7%	50,9%	3,9%	4,8%	8,7%	1,2%	5,8%	0,9%	4,9%	0,3%	0,7%	0,6%	0,1%
SHI UP EB	SW	16,1%	50,3%	0,0%	19,2%	4,6%	0,9%	2,0%	0,6%	5,5%	0,8%		0,9%	0,1%
MAF 4 EB	SW	21,5%	46,6%	2,7%	11,5%	11,6%	0,0%	0,6%	1,0%	4,1%	0,5%		0,6%	0,1%
MAF 4 BGB	SW	19,3%	47,9%	2,6%	10,3%	10,1%	4,3%	0,6%	1,5%	3,1%	0,3%		0,6%	0,1%
LAO EB	SW	19,7%	51,3%	1,7%	14,6%	4,7%	0,8%	0,4%	1,1%	5,0%	0,6%		0,7%	0,1%
LAO BGB	SW	17,8%	54,0%	0,4%	11,0%	5,4%	4,1%	0,7%	1,9%	4,2%	0,4%		0,6%	0,1%
SHA EB	SW	18,5%	48,8%	0,6%	20,2%	1,0%	2,5%	0,8%	2,0%	5,0%	0,4%		0,6%	0,1%
SHA BGB	SW	22,6%	41,9%	1,4%	21,0%	5,2%	0,0%	0,7%	1,2%	5,2%	0,8%		0,8%	0,1%
MAL EB	W	20,9%	41,7%	1,2%	20,8%	2,9%	4,9%	0,6%	1,7%	4,6%	0,8%		0,7%	0,1%
MAL BGB	W	21,1%	42,7%	0,9%	21,3%	1,8%	4,6%	0,5%	1,8%	4,5%	0,9%		0,7%	0,1%
MAO EB	W	19,7%	54,7%	1,4%	10,8%	0,8%	6,0%	0,4%	1,4%	4,1%	0,6%		0,6%	0,3%
MAO BGB	W	22,5%	47,8%	1,4%	11,5%	2,8%	6,5%	0,6%	1,4%	5,1%	0,4%		0,6%	0,1%
SHI M EB	W	16,1%	43,4%	0,2%	8,9%	19,6%	4,3%	0,6%	1,3%	5,2%	0,5%		0,8%	0,1%

Table1- Overview of semi-quantitative mineral analysis by BGMN-Rietveld refinement (XRD of bulk samples).

3.3 Geochemical data

Pyrite iron (Fe$_{py}$) concentrations in the shales of the Yuanshan Formation in Yunnan Province range from <0.001% to 0.61%; the average value is 0.09%. Total iron (FeT) and HCl-extractable iron (FeHR) abundances are between 1.53% and 5.74% and between 0.68% and 3.79%, respectively, whilst the average respective values are 4.2% and 1.71%. The highly reactive portion of the iron pool (Fe$_{HR}$) according to (Poulton and Canfield, 2005) includes: (1) carbonate-associated Fe (Fe$_{carb}$), including siderite and ankerite; (2) easily reducible oxides (Fe$_{ox1}$), including ferrihydrite and lepidocrite; (3) reducible oxides (Fe$_{ox2}$), including goethite, hematite, and akaganéite; (4) magnetite (Fe$_{mag}$); (5) pyrite Fe (Fe$_{py}$). The degree of pyritization (DOP) ranges from <0.001 to 0.3, and the average is 0.06 (Fig. 7C). The Fe$_{HR}$/Fe$_T$ ratios are between 0.08 and 0.85, and the average is 0.40 even if most values do not exceed 0.38 (Fig. 7A). Fe$_T$/Al ratios range from 0.27 to 0.52, except for the 1.02 value in Deze BGB sample, and have an average value of 0.42 (Fig. 7B). Authigenic uranium (U$_{autigenic}$) values range from < 0.01 to 2.8 (the average value is 0.64) (Fig. 7E). The vanadium to chromium ratios (V/Cr) are between 1.00 and 2.09 (the average value is 1.49) (Fig. 7F). The nickel to cobalt (Ni/Co) ratios range from 1.9 to 15.8; the average is 4.44, and most do not exceed 5 (Fig. 7H). Fe$_{py}$ / Fe$_{HR}$ values range from 9E^{-5} to 0.4; the average value is 0.07 (Fig. 7D). The

V/ V+Ni proxy shows values between 0.6 and 0.92, with an average value of 0.76 (Fig. 7G; see Table 2).
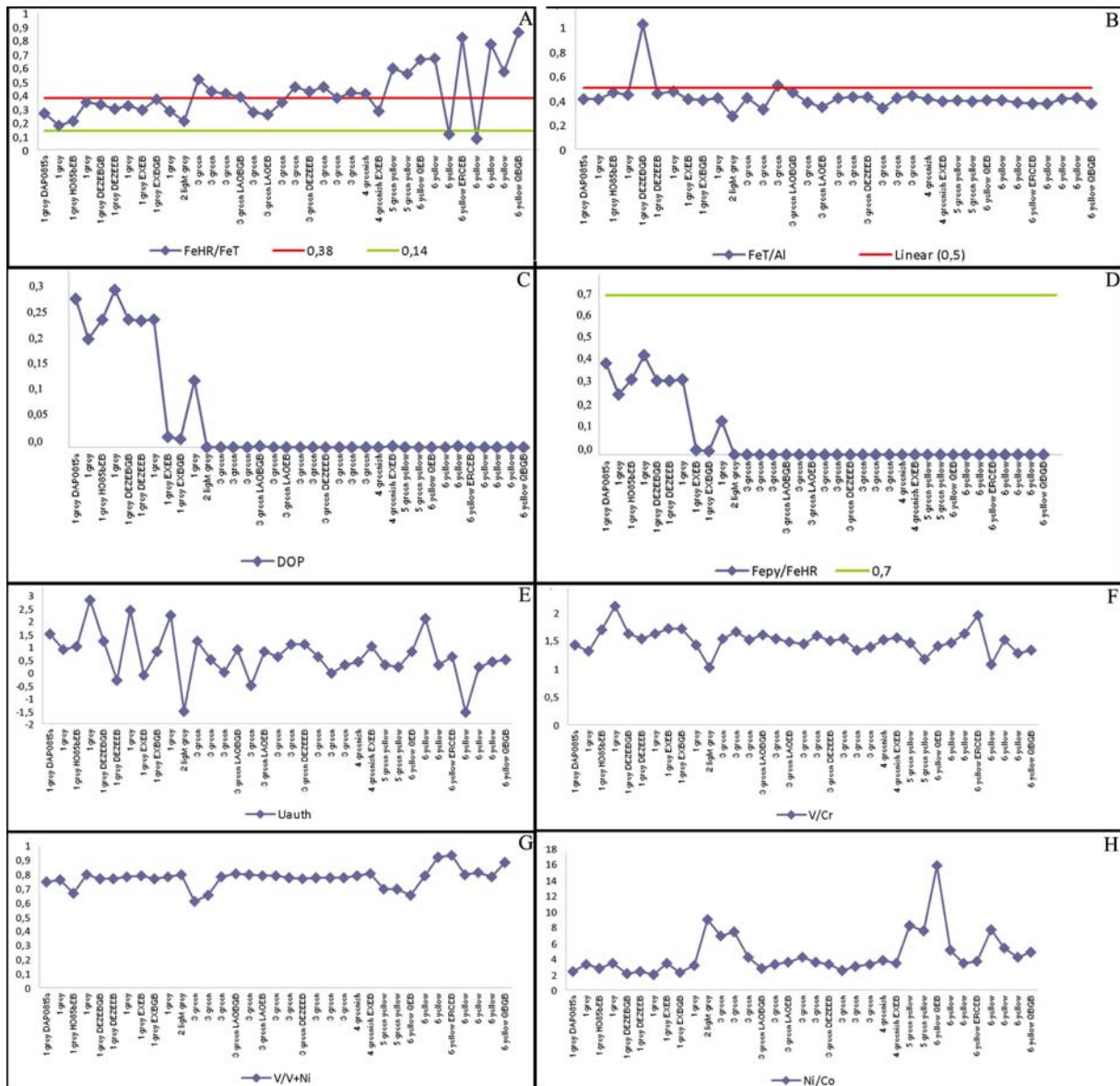
Fig. 7. Paleoredox proxies graphs.

Statistical discriminatory analyses performed with SPSS for all proxies and all samples show the V/ V+Ni proxy to be the only unreliable proxy. The results for the main and trace elements are shown in the appendix. The total organic carbon (TOC) values in the material analyzed for this paper range from 0.10% to 0.48%, with some samples below the detection limit of 0.1 % (mostly of the strongly altered group of samples-W; here, about 40% of samples).

	Fe py (wt%)	Fe carb (wt%)	Fe ox (wt%)	Fe mag (wt%)	Fe T (wt%)	FeHR/FeT	Fepy/FeHR	DOP	FeHR	Uauth	V/Cr	V/V+Ni	Ni/Co	FeT/Al
1 grey DAP0815a	0,41552	0,38972	0,04987	0,18895	3,97331	0,26277	0,39799	0,28469	1,04406	1,50000	1,41228	0,73853	2,37500	0,41004
1 grey DAP0815bEB	0,18035	0,29231	0,03718	0,17724	3,98446	0,17244	0,26249	0,20791	0,68708	0,90000	1,30075	0,75877	3,23529	0,40878
1 grey DEZEBGB	0,47356	0,64382	0,04551	0,29354	4,44103	0,32795	0,32515	0,24537	1,45643	1,20000	1,60952	0,76471	2,08000	1,02142
1 grey DEZEEB	0,37683	0,51718	0,03556	0,24153	3,95055	0,29644	0,32178	0,24344	1,17111	-0,30000	1,51648	0,76243	2,38889	0,45670
1 grey MEI20829BGB	0,46193	0,63494	0,07340	0,24103	4,36000	0,32369	0,32731	0,24660	1,41129	2,40000	1,60526	0,77872	1,92593	0,47301
1 grey EXEB	0,02322	0,40474	0,07259	0,59911	3,78627	0,29043	0,02111	0,02068	1,09966	-0,10000	1,69524	0,78070	3,33333	0,40627
1 grey EXBGB	0,01823	0,61742	0,05661	0,48025	3,18086	0,36861	0,01555	0,01531	1,17251	0,80000	1,70175	0,76378	2,14286	0,40338
1 grey MEI20829EB	0,16920	0,62578	0,05590	0,28571	4,05229	0,28048	0,14887	0,12958	1,13659	2,20000	1,41935	0,77876	3,12500	0,42179
2 light grey SHI 41EB	0,00000	0,01192	0,29147	0,01063	1,53582	0,20446	0,00000	0,00000	0,31401	-1,50000	1,00752	0,78824	9,00000	0,27214
3 green MAF4081BGB	0,00028	0,44969	1,79780	0,24654	4,84004	0,51535	0,00011	0,00011	2,49431	1,20000	1,51613	0,60256	6,88889	0,42001
3 green MAF4081EB	0,00000	0,35113	1,13822	0,24607	4,12289	0,42092	0,00000	0,00000	1,73543	0,50000	1,65714	0,64444	7,38462	0,32837
3 green SHANK2082EB	0,00029	0,23726	1,13397	0,41781	4,39024	0,40757	0,00016	0,00016	1,78933	0,00000	1,50000	0,77500	4,15385	0,52212
3 green LAOBGB	0,00232	0,30591	0,98076	0,32260	4,15515	0,38785	0,00144	0,00144	1,61159	0,90000	1,58871	0,79757	2,77778	0,46745
3 green HAI3081EB	0,00029	0,14763	0,69379	0,30710	4,22513	0,27190	0,00025	0,00025	1,14881	-0,52000	1,52632	0,78988	3,17647	0,38205
3 green LAOEB	0,00000	0,34432	0,46998	0,37138	4,57645	0,25909	0,00000	0,00000	1,18569	0,80000	1,47368	0,78715	3,53333	0,34253
3 green MEI20827EB	0,00026	0,37119	0,61391	0,30861	3,71945	0,34789	0,00020	0,00020	1,29397	0,60000	1,42742	0,78319	4,08333	0,41649
3 green DEZEBGB	0,00000	0,66581	0,92097	0,36323	4,30049	0,45344	0,00000	0,00000	1,95000	1,10000	1,58095	0,77209	3,50000	0,42908
3 green DEZEEB	0,00027	0,52262	0,96245	0,37212	4,34185	0,42780	0,00015	0,00015	1,85745	1,10000	1,48571	0,76098	3,26667	0,43048
3 green SHANK2082BGB	0,00181	0,23265	1,63703	0,28921	4,71087	0,45866	0,00084	0,00084	2,16070	0,60000	1,52632	0,77333	2,42857	0,33389
3 green HAI3085BGB	0,00000	0,20914	1,15822	0,29619	4,46734	0,37238	0,00000	0,00000	1,66355	-0,02000	1,33083	0,76957	2,94444	0,41475
3 green MEI20830BGB	0,00164	0,21675	1,31264	0,31888	4,48330	0,41262	0,00089	0,00089	1,84992	0,30000	1,36842	0,77119	3,17647	0,44001
4 greenish EXBGB	0,00085	0,21575	1,19181	0,30614	4,23423	0,40493	0,00050	0,00050	1,71455	0,40000	1,50000	0,78151	3,71429	0,40752
4 greenish EXEB	0,00136	0,40390	0,37121	0,33193	3,93775	0,28148	0,00123	0,00122	1,10841	1,00000	1,53226	0,80169	3,35714	0,38954
5 green yellow K36BGB	0,00026	0,32332	2,10447	0,42236	4,80340	0,59342	0,00009	0,00009	2,85042	0,30000	1,45614	0,69167	8,22222	0,40134
5 green yellow K36EB	0,00000	0,17919	1,97091	0,33524	4,52770	0,54892	0,00000	0,00000	2,48535	0,20000	1,16783	0,69008	7,50000	0,39340
6 yellow QEB	0,00000	0,06710	2,60129	0,07661	4,18933	0,65523	0,00000	0,00000	2,74499	0,80000	1,38710	0,64419	15,83333	0,39773
6 yellow MAF1082EB	0,00000	0,11467	2,50100	0,12900	4,12463	0,66543	0,00000	0,00000	2,74467	2,10000	1,44355	0,78166	5,00000	0,39773
6 yellow ERCBGB	0,00058	0,04401	0,37320	0,07320	4,53927	0,10816	0,00117	0,00117	0,49099	0,30000	1,61654	0,91489	3,33333	0,38576
6 yellow ERCEB	0,00000	0,03519	2,87720	0,04632	3,60902	0,81981	0,00000	0,00000	2,95871	0,60000	1,94737	0,92500	3,60000	0,37134
6 yellow SHI MEB	0,00000	0,02692	0,28397	0,03739	4,18548	0,08321	0,00000	0,00000	0,34829	-1,56000	1,06767	0,78889	7,60000	0,37134
6 yellow MAF1082BGB	0,00058	0,20711	3,22597	0,09675	4,60262	0,76692	0,00000	0,00000	3,52983	0,20000	1,49624	0,80567	5,33333	0,41132
6 yellow DAP0824BGB	0,00000	0,08854	2,28924	0,12381	4,43238	0,56439	0,00000	0,00000	2,50159	0,40000	1,26613	0,77723	4,09091	0,42224
6 yellow QBGB	0,00000	0,11648	3,65977	0,01379	4,41423	0,85860	0,00000	0,00000	3,79004	0,50000	1,32331	0,88000	4,80000	0,36790

Table 2- Overview of iron speciation data and proxy values. This table served as a matrix for the canonical discriminatory analyses we used to subdivide the samples into three weathering groups; for this reason, sample names are listed with the original subdivision into six groups.

The mean value of TOC of unaltered samples lies at 0.18 %, and at 0.15% for slightly altered samples, while the most-altered samples just retained an average of 0.08 %. Similarly, the TC shows average contents of 0.71 % in the UW group samples, 0.37% of SW group samples, and 0.15% of W group samples. The sulfur values analyzed with a CNS analyzer are generally low (between 0.6 to 0.05%), while they can reach a level of several % in the underlying Black Shale Member of Yuanshan Fm. Whereas the mean value for S of UW group samples is at 0.37 %, it only ranges from 0.04 to 0.05 % for the altered and slightly altered samples. The Mo proxy could not be applied because the Mo content was under the detection limit (1ppm) for almost all the samples. The only exceptions are the values from unaltered material in Deze (Zhanyi County, North Yunnan Province) and in the extremely altered light grey (group 2- SHI 41) material (both 1ppm), besides the samples of the Black Shale Member (H) with values of 10ppm (EB) and 3ppm (BGB).

A principal component analysis (PCA) was performed on a data matrix of main and trace elements of all samples (appendix) and separately for UW group and SW+W group matrixes. The PCA based on all samples has shown six factors which together cover 70.59% of the variance. The first factor (PC1) alone covers 31.3% of the variance, and the second (PC2) 12.1%. The other factors have very little variance coverage and very low loadings. The PCA carried out on the UW group has shown four factors, which together cover 76.33% of the variance. The first factor (PC1) has 33.8% of the variance, and the second (PC2) 19.9%. Also in this analysis, the other factors have very little variance coverage and also very low loadings. The PCA of SW+W groups has shown six factors, together covering 71.07% of the variance. The first factor (PC1) has 28.1% of the variance, and the second (PC2) 15%. In the biplot of the PCA based on all samples, a regional difference of the Malong-Qujing area is clearly observed (Fig. 8A). Also the samples of the Wulongqing Fm. are clearly separated from the Yuanshan Fm. Within this latter formation, a clear difference is observed between the strata yielding the Chengjiang Fauna, and the stratigraphically slightly older Black Shale Mb. The mean differentiation using all data of different alteration stages (Fig. 8A) is along the principal component one (PC1) between the carbonate phase with its related elements (Mg, Mn, Co) and clay minerals and heavy minerals. Different elemental relationships are visible if PCA is based only on the UW group data or on the SW+W group. In the UW group (Fig. 8B), iron is related to S, Mo, Ni and As along with TOC. In the SW+W group (Fig. 8C), iron is unrelated to all other elements. The main elements present in dolomite (Ca, Mg, C, Mn) show a close relationship in both UW and SW+W groups, and it is worth noting that the contrasting

principal relationships of elements enriched in dolomite and those related to heavy minerals and clay minerals are observable in both unaltered and altered samples. However, the relationship of Fe with other elements changes between the UW and the W+SW alteration groups. The UW alteration group samples, and here in particular the Black Shale Mb. (sample H085B), indicate a strong relationship of Fe with S (corr. coefficient 0.84943), As (corr. coefficient 0.78960), Ni (corr. coefficient 0.74501), and Mo (corr. coefficient 0.71782) and a similar biplot trend in the main principal components including other elements, such as TOC and Ag. By contrast, Fe does not indicate a specifically strong correlation with other elements in the SW+W alteration group samples except for a negative correlation with Mo (corr. Coefficient -0.84341). This indicates a fundamental change in the binding of Fe in the different alteration types of beds.

A comparison of the element distribution between BGB and EB samples by average values indicates that Fe, As, V, and Co have a trend to slightly lower values and that Eu, Y, Al, Nd, Mn, Cu, Zn, Ni, and Rb have a trend to slightly higher values in EBs. Some elements such as Fe, As, V, Co and LOI possess an EB/BGB ratio < 1; Ti, Eu, Y, Yb and partially also Al and Mg show an EB/BGB ratio of > 1. Other elements such as Cu, Zn, Ni and Rb do not follow a clear enrichment/depletion trend for EB samples (Fig. 9).

3.4 Crystal size statistics of iron minerals

Crystal size measurements of iron minerals have been carried out for several groups of metazoans of the Chengjiang-type fauna of Yunnan Province: sponges, arthropods, brachiopods, and worms. The measurements were divided according to the alteration stages, but it was not always possible to obtain statistically reliable data on the complete spectrum of alteration/weathering stages (at least with a significant number of measurements), as the unaltered material contains less common crystals of iron minerals. Altered material (alteration group SW and W) shows the most abundant presence of crystals and framboids of iron minerals (Fig. 10). In the Guanshan material, spherical aggregates are quite abundant (Fig. 4E), whereas these are absent in Chengjiang fossils, with few exceptions such as a worm specimen (group SW) from Laogaoshan (Jinning County). In this case, iron mineral crystals show dissolution of the external euhedral habitus, revealing a morphology similar to a spherical aggregate (Fig. 4 F and G). An average size of spherical aggregates of 8.66 μm (n=166) with values between 3.77 μm and 16.11 μm and an average size of 6.04 μm (n=339)

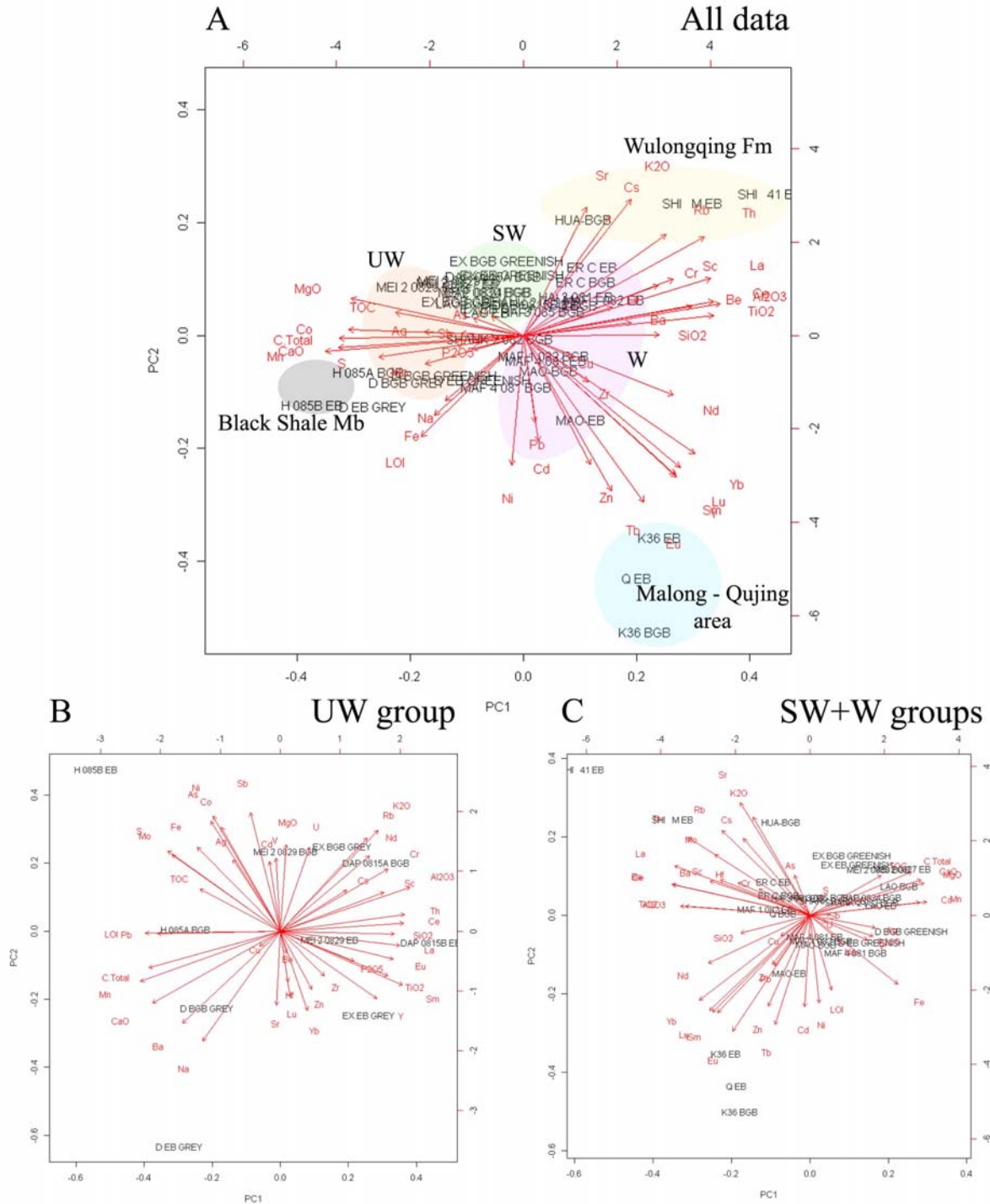μm for single crystals with values between 2.89 μm and 11.74 μm have been measured for sponges (Fig. 10).

Fig. 8. R-Principal component analyses. A- PCA for the entire data matrix has given 30 factors with the variance percentage >1, but only factor 1 (PC1: 31.3%) and factor 2 (PC2: 12.1%) show values > 10 % of variance. The main differentiation in Yuanshan Fm is along PC1: it means carbonate content versus clay minerals and heavy metals. B- PCA for the UW group matrix has given 9 factors with the variance >1. Factor 1 (PC1) has 33.8% of the variance and factor 2 (PC2) has 19.9%. The same trend (carbonate elements/clay minerals and heavy metals) observed in Fig. 8A is also observed here. Interesting to note are the iron relationships in UW and SW+W groups. C- PCA for the SW+W groups matrix has given 25 factors with the variance >1, but only factor 1 and 2 are >10. PC1 has 28.1% of the variance, and factor 2 (PC2) has 15% of the variance.
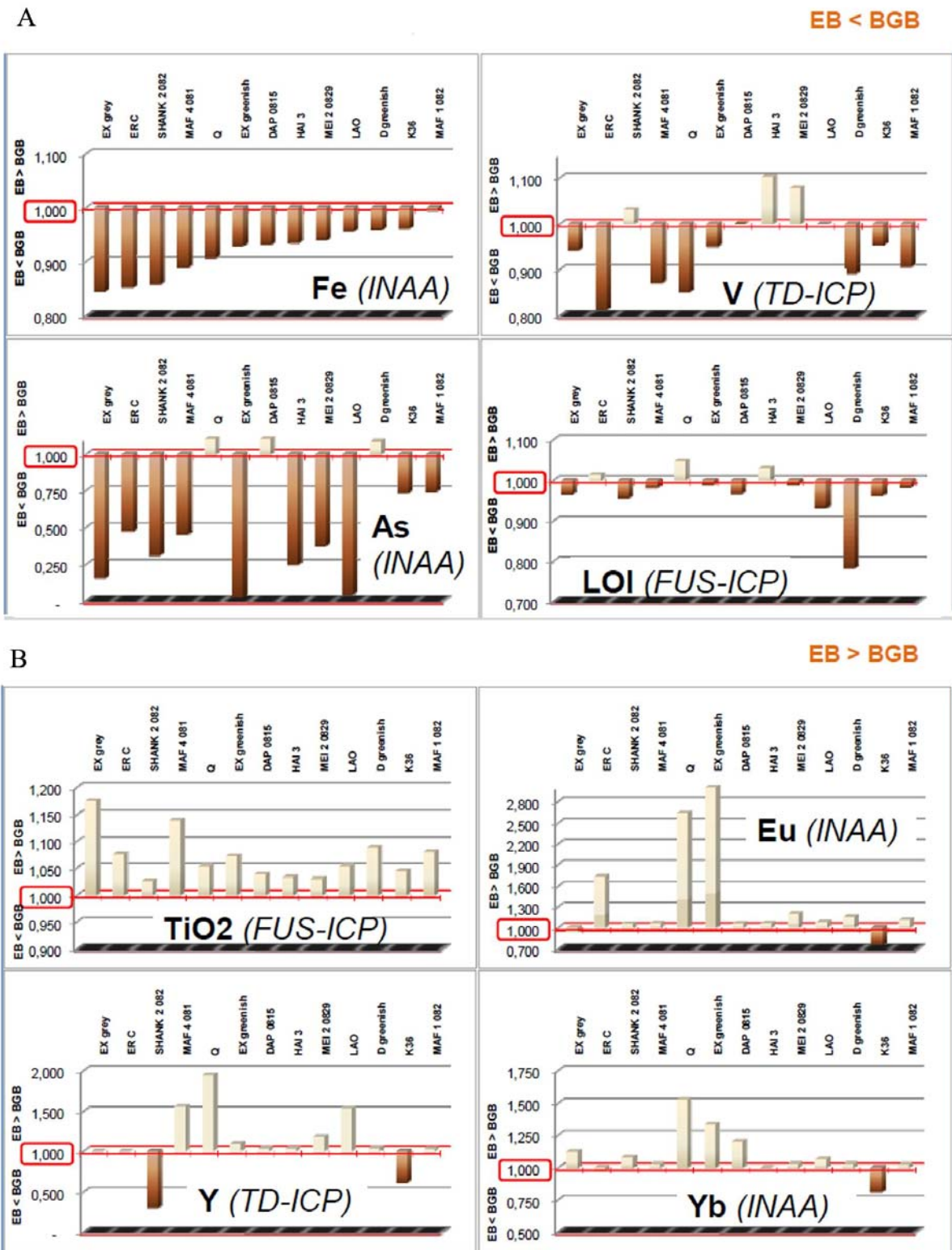
Fig. 9. Bulk sample chemistry: differences between EBs and BGBs. A- Differences in chemical composition between BGBs and EBs. y-axis: element EB: element BGB: there is a trend to reduced element distribution in EBs. B- Differences in chemical composition between BGBs and EBs. y-axis: element EB: element BGB: there is a trend to increased element distribution in EBs.

Sponge material from Guanshan shows only spherical aggregates (Fig. 4E).

Framboid size measurements of a worm from Malong indicate a size range from 2.9 μm to 12.5 μm (n= 32) with an average of 8.29 μm for the framboids (Fig. 4Q; the average framboid microcrystal size is 1.57 μm). Euhedral crystals are the most frequent crystal morphology (Fig. 10) with values between 0.53 and 14.72 μm (n=919, mean=3.97 μm); some crystals show dissolution at different stages (Fig. 4P). In the Laogaoshan sample, only spherical aggregates are visible, and their sizes range between 1.67 μm and 7.69 μm (n=295, mean=3.97 μm, Fig. 10).

The iron mineral crystal sizes of the brachiopods range from 0.27 μm to 11.1 μm. Iron euhedral crystals are the most common morphology in this group, with an average size of 1.67 μm (n=1666). Iron mineral framboids have been measured in brachiopod material, too; their sizes range between 1.2 μm and 9.7 μm (n= 120, mean=5.19 μm; Fig. 10).

The measurements of iron minerals of arthropods show values between 4.06 μm and 11.07 μm for framboids (Fig. 4O), with an average size of 8.25 μm (n=96). Furthermore, iron mineral crystals have a size range between 0.49 μm and 8.01 μm (mean=1.50 μm; n= 500; Fig. 10).

In a sample from Xiaolantian (Chengjiang County), a reduction in size for crystals in the pedicle was observed in respect of those inside the shell (Forchielli et al., in press; Fig. 5C). The iron mineral crystal sizes inside the shell show values between 0.6 μm and 11.1 μm (average value is 4.26 μm; n=266), whilst the crystal sizes in the soft parts show values between 0.27 μm and 5.93 μm (average size is 1.12 μm; n=1188; Fig. 11B). As for the brachiopods, a size reduction of the crystals has also been observed for arthropods in a sample from Ercaicun (Haikou Town), in iron mineral crystals of lightly cuticularized body parts (here the legs of an arthropod, likely *Leanchoilia*) and the iron mineral crystals in the shield (Fig. 4K and 11A).

In this case, the morphologies of iron minerals were different depending on the different grades of sclerotization: inside the shield (Fig. 4H) both framboids (average size 7.89 μm; range between 4.9 μm and 10.29 μm; n=53) and single euhedral crystals (average size 2.41 μm; range of size included between 1 μm and 8.01 μm; n= 104) have been observed. Measurements of iron mineral sizes inside weakly sclerotized parts (Fig. 4J) show only single euhedral crystals, with an average size of 1.26 μm (n= 208) and a size range between 0.49 μm and 2.5 μm (Fig. 11A). Statistical analyses of iron mineral crystal sizes of unaltered material (alteration group UW) were possible only on brachiopods, arthropods and worms.
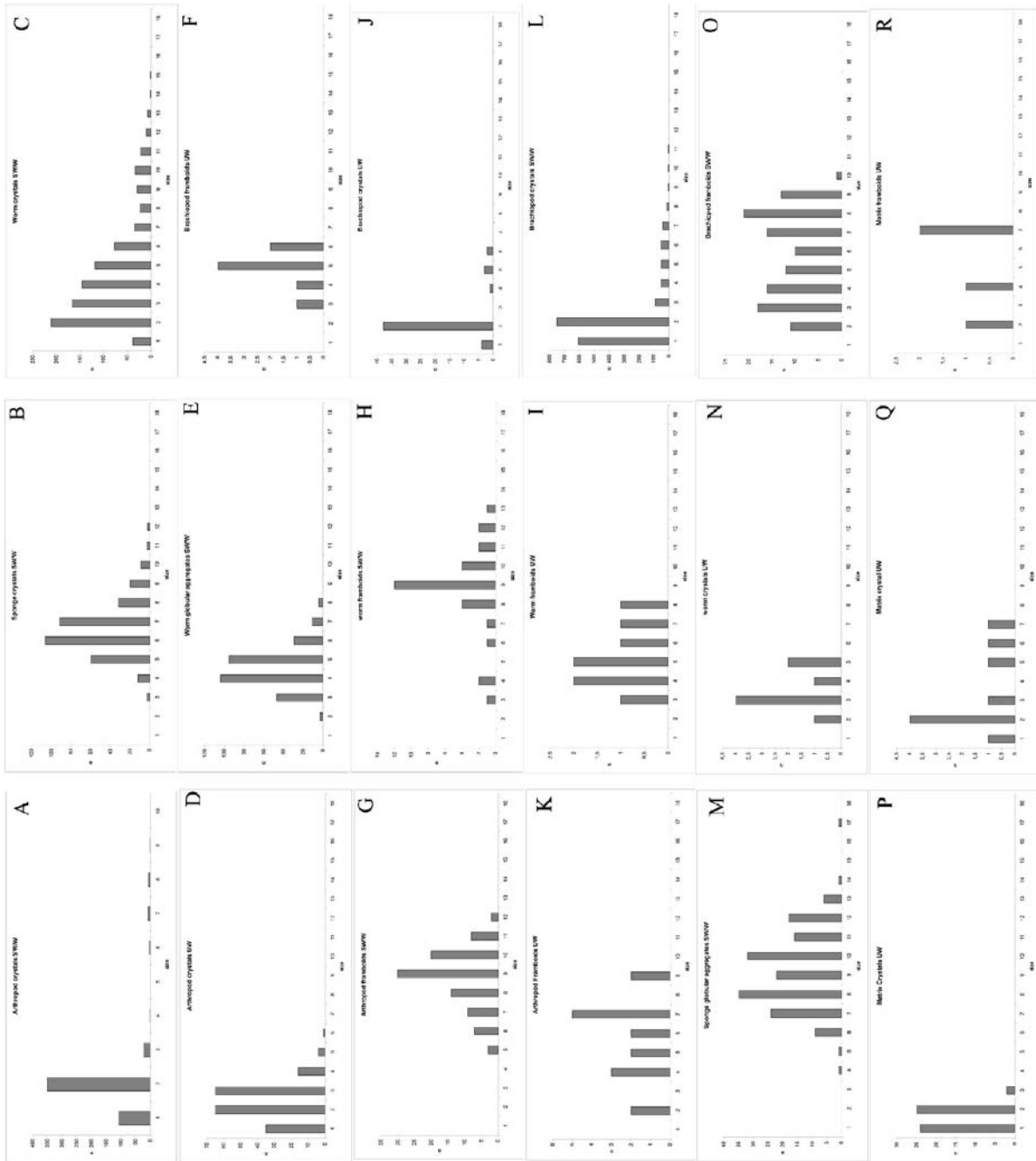
Fig. 10. Iron mineral data: crystal size histograms of several groups of metazoans in the three weathering stages. y-axis: n; x-axis: sizes. Measurements were based on specimens Xlt; Shi 0813; Maf2 081; Shi4 0818; Shi-hu-A; Shi 3 089b; Lao 082a; BM; Shi up 0924 for brachiopods and the Guanshan matrix. Measurements were based on specimens Shi up 2010; Xlt-a-262 and Y24-065B for sponges; on specimens Erc 0814; Lao1 081; Mafang V; hu China- 56; Mei 2008 and Erc 0830 for worms, and on specimens Erc 08; Shi M-L 091; K4-3-04; Mei2 0822; Hai1 085; Hai4 082 and Mei2 0819 for arthropods and the Chengjiang matrix.

The rare single crystals and framboids of this alteration group are mainly irregularly scattered along outer shell/shield sides and more regularly located along fractures. Point analyses of crystals and framboids show a composition of iron and sulfur.

Fig. 11. Iron mineral data: differences in crystal sizes in shell/shield and soft parts (W group).
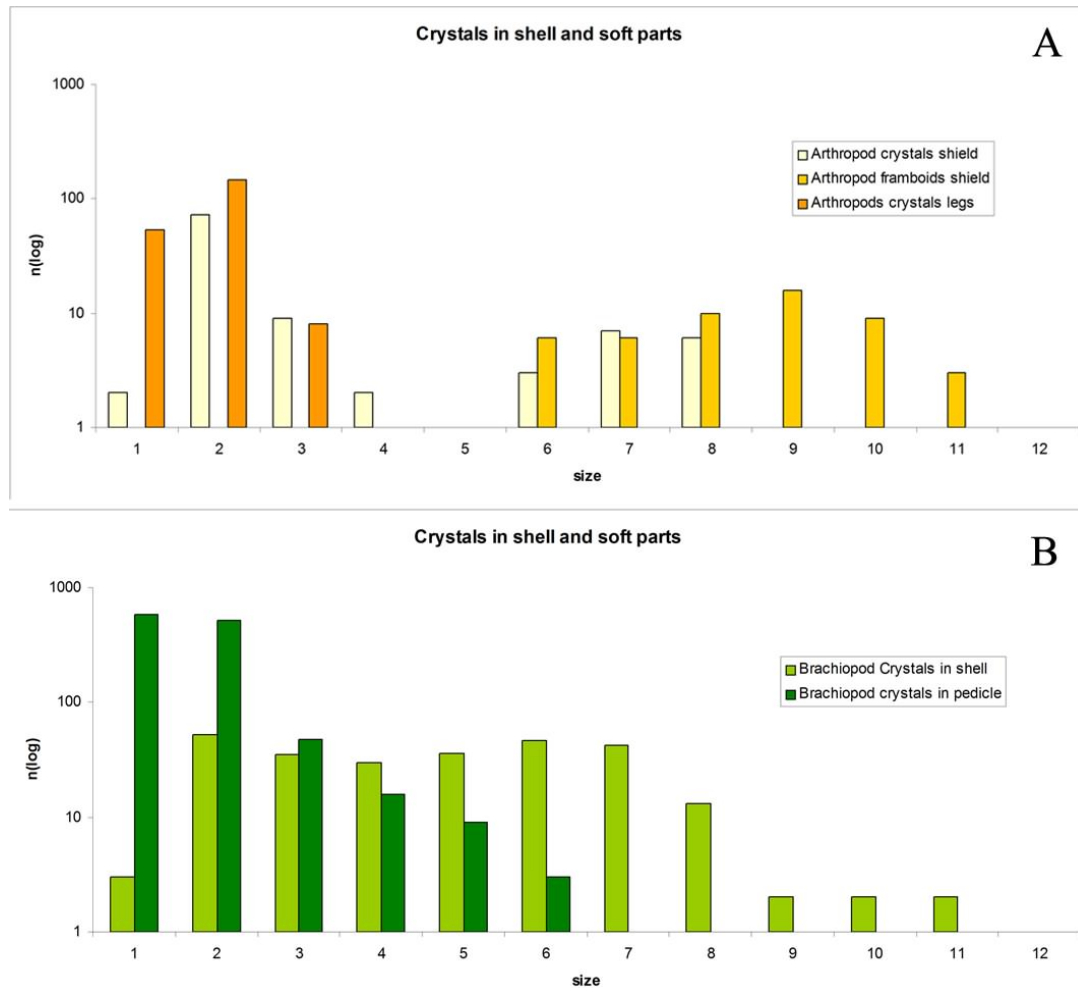
The measurements of iron mineral sizes in worms show values between 2.18 µm and 7.57 µm for framboids (average size: 4.65; n=10) and values between 1.34 µm and 4.07 µm for crystals (average size is 2.83 µm; n=10). The measurements of iron mineral sizes in brachiopods show an average size of 1.90 µm (n=50) for crystals (size ranges from 0.73 µm to 5.98 µm), and an average size of 4.33 µm (n=10) for framboids (size values between 2.48 µm and 5.64 µm). The measurements of iron mineral sizes of arthropods show framboids with a size range of 1.65 µm to 8.68 µm (average size is 5.23 µm; n=18) and crystals with sizes between 0.1 µm and 5.63 µm (average size is 1.91 µm; n= 188; Fig. 4L). Crystal size measurements of iron minerals have been carried out for the matrix of unaltered material, too: pyrite crystals and framboids are also rare in the matrix.

In the Chengjiang matrix, crystals range between 0.61 µm and 2.58 µm (the average size is 1.06 µm; n= 53; Fig. 4M and Fig. 10), and in the Guanshan matrix both crystals and framboids are present, with framboids ranging from 1.9 µm to 6.55 µm (the average size is

4.5 µm; n=4) and single crystals having a range of sizes between 0.87 µm and 6.9 µm with an average size of 2.76 µm (n= 11; Fig. 4D; Fig. 10).

3.5 Clay matrix analyses of Chengjiang and Guanshan fossil Lagerstätten

Clay matrix analyses have been carried out to identify the mineralogical composition of EBs and BGBs and to characterize UW and SW/W samples. These analyses make it possible to discriminate between primary mineral composition and secondary diagenetic or late stage alteration/weathering and potential primary environmental changes.

Pre-sedimentary processes and diagenesis affect the composition of mineral matter and also the chemical composition of the different phases.

3.5.1 Clay mineral analyses by XRD with BGMN-Rietveld refinement

Mica of $2M_1$-polytype (illite), quartz and kaolinite as well as chlorite are the major phases in the bulk samples (Tables 1 and 3; Fig. 6). Mica of 1M-polytype (illite), goethite, epsomite, jarosite, anatase, and in part dolomite represent minor phases. Occurrence of $2M1$-mica in sediments is an indicator of the detrital origin of this mica species.

Phase	Origin	Ratio (in weight-%)	Notes
Illite-smectite mixed layer structure ($2M1$-polytype)	detrital	40 ... 55%	dominated by illitic layers
Quartz	detrital	15 ... 25%	
Chlorite	detrital	4 ... 20%	Mg: 1.49 ... 2.84 per $(OH)_8 O_{10}$
Kaolinite		0 ... 20%	
Illite-smectite mixed layer structure ($1M$-polytype)	diagenetic	0 ... 5%	dominated by illitic layers
Goethite	diagenetic	0 ... 6%	
Jarosite (K Fe-Sulfate), Epsomite (Mg-Sulfate)	diagenetic	< 3%	
Dolomite		0 ... 6%	normally < 0.5%; MEI with 6%
Pyrite	diagenetic	< 1%	

Table3- Overview of XRD results of mineral matter in bulk samples (quantification by BGMN-Rietveld).

Comparison of the mineralogical composition of mudstones of different alteration/weathering stages reveals some systematic trends. For instance, the mudstones belonging to the UW

alteration group (MEI, EX) have the lowest amounts of goethite and chlorite (Fig. 6), but higher values for $2M_1$-mica, kaolinite (Fig. 6) and dolomite (Table 1).

There are also some differences in the composition of the EB and BGB samples (Table 3), but it is not possible to recognize any systematic depletion/enrichment pattern between BGB sediment and its EB counterpart (Fig. 6) connected to these semi-quantitative XRD analyses. Goethite shows a higher concentration in EB than in BGB sediments in UW material and most of SW material, although it appears equally distributed in EBs and BGBs in the most-altered material (group W; Fig. 6). The BGMN-Rietveld refinement allowed a detailed characterization of $2M_1$-mica in the sediments.

The identified octahedral Fe-content exceeded the typical concentration of Fe in $2M_1$-mica especially in EB sediments (Table 4). BGB sediments show a trend to a higher Fe concentration in $2M_1$-mica with increasing alteration/weathering. The lowest Fe amount occurs in the UW samples (such as MEI and EX, but also in the SW-MAF 4).

Sample	Weathering stage	Potassium	octahedral Fe	octahedral Al	b-axis (in nm)	EB/BGB: Fe	EB/BGB: b-axis
MEI 2 0829 EB	UW	0,61	0,12	1,88	0,903	0,92	0,997
MEI 2 0829 BGB	UW	0,60	0,13	1,87	0,906		
EX grey EB	UW	0,60	0,00	2,00	0,902	0,01	1,002
EX grey BGB	UW	0,60	0,18	1,81	0,900		
MAF 4 081 EB	SW	0,60	0,04	1,96	0,905	0,10	1,002
MAF 4 081 BGB	SW	0,60	0,40	1,60	0,903		
LAO 0913 EB	SW	0,68	0,15	1,85	0,901	0,28	0,993
LAO 0913 BGB	SW	0,60	0,54	1,46	0,907		
SHA EB	SW	0,60	0,30	1,70	0,903	7,50	1,003
SHA BGB	SW	0,82	0,04	1,96	0,900		
MAO EB	W	0,60	0,67	1,33	0,905	1,12	1,001
MAO BGB	W	0,60	0,60	1,40	0,904		
MAL 025 EB	W	0,67	0,55	1,45	0,901	0,93	1,000
MAL 025 BGB	W	0,69	0,59	1,41	0,901		
SHI UP EB	SW	0,89	0,40	1,60	0,909		
SHI M EB	W	0,84	0,70	1,30	0,904		

Table 4- Composition of 2M1-mica (per half unit cell, $(OH)_2 O_{10}$) in bulk samples as a result of BGMN-Rietveld refinement.

The values for octahedral Fe of these samples are increased in the EB horizons in comparison to the BGB sediments. The BGMN-Rietveld refinement also offers options to calculate the octahedral composition of chlorite from XRD data of bulk samples. Octahedral cations such as Mg^{2+}, Fe^{2+}, Fe^{3+} and Al^{3+} show a variable chlorite composition (Table 5). This variability is also mirrored by the total Fe amount of chlorite (Y-values in Table 5) and the number of total octahedral cations (n^{VI} values in Table 5). The total Fe concentration in chlorite shows a similar enrichment trend to that in $2M_1$-mica concerning the relationship between BGBs and EBs. The total Fe amount is higher in EBs compared to BGBs for UW and SW alteration group samples, but slightly lower or equal in strongly altered samples (W group; Fig. 12A, B). However, the enrichment/depletion is much lower in chlorite (Fig. 12B) than in $2M_1$-mica (Fig. 12A).

It is more remarkable that the mudstones show a general change in the Fe content in $2M_1$-mica and chlorite from the least and slightly altered samples (UW, SW group) toward the most-altered samples (W group), although in a reversed manner. $2M_1$-mica indicates a trend toward higher Fe content, whereas chlorite reveals a distinct depletion in Fe. Chlorite, indicated by the D value (Table 5) and a higher total octahedral Fe concentration (see UW material), promotes an incorporation of Fe partially also in the HYDR octahedra. Otherwise, Fe is located only in the SIL octahedra represented by D-value = +3 (Table 5).

Sample	SIL-Octahedra Mg	Fe2+	Fe3+	Fetot/(Fetot+Mg)	R2+/(R2+ + R3+)	HYDR-Octahedra Mg	Fe2+	Fe3+	Al3+	Fetot/(Fetot+Mg)	R2+/(R2+ + R3+)	D	Y	Fetot/(Fetot+AlVI)	R2+/(R2+ + R3+)	n^{VI}
MEI 2 0829 EB	1,20	1,02	0,78	0,60	0,74	0,76	0,23	0,40	0,94	0,46	0,43	2,21	2,44	0,72	0,60	5,34
MEI 2 0829 BGB	1,10	1,50	0,40	0,63	0,87	0,85	0,25	0,40	1,00	0,44	0,44	2,23	2,55	0,72	0,67	5,50
EX grey EB	0,83	1,50	0,67	0,72	0,78	0,62	0,23	0,55	0,93	0,56	0,36	2,21	2,95	0,76	0,60	5,33
EX grey BGB	1,02	1,50	0,48	0,66	0,84	0,76	0,24	0,46	0,98	0,48	0,41	2,21	2,69	0,73	0,65	5,44
MAF 4 081 EB	1,25	1,50	0,25	0,58	0,92	1,31	0,00	0,00	1,31	0,00	0,50	3,00	1,75	0,57	0,72	5,62
MAF 4 081 BGB	1,50	1,50	0,00	0,50	1,00	1,37	0,07	0,00	1,30	0,05	0,53	2,86	1,57	0,55	0,77	5,75
LAO 0913 EB	1,29	1,50	0,21	0,57	0,93	1,32	0,00	0,00	1,32	0,00	0,50	3,00	1,71	0,56	0,73	5,64
LAO 0913 BGB	1,57	0,67	0,76	0,48	0,75	1,21	0,00	0,00	1,21	0,00	0,50	3,00	1,43	0,54	0,64	5,42
SHA EB	1,33	1,50	0,17	0,56	0,94	1,33	0,00	0,00	1,33	0,00	0,50	3,00	1,67	0,56	0,73	5,65
SHA BGB	1,25	1,50	0,25	0,58	0,92	1,31	0,00	0,00	1,31	0,00	0,50	3,00	1,75	0,57	0,72	5,62
MAO EB	1,39	1,50	0,11	0,54	0,96	1,34	0,00	0,00	1,34	0,00	0,50	3,00	1,61	0,55	0,74	5,68
MAO BGB	1,31	1,50	0,19	0,56	0,94	1,32	0,00	0,00	1,32	0,00	0,50	3,00	1,69	0,56	0,73	5,65
MAL 025 EB	1,15	1,50	0,35	0,62	0,88	1,29	0,00	0,00	1,29	0,00	0,50	3,00	1,85	0,59	0,71	5,58
MAL 025 BGB	1,16	1,50	0,34	0,61	0,89	1,29	0,00	0,00	1,29	0,00	0,50	3,00	1,84	0,59	0,71	5,59
SHI UP EB	1,50	0,00	1,50	0,50	0,50	1,06	0,00	0,00	1,06	0,00	0,50	3,00	1,50	0,59	0,50	5,12
SHI M EB	0,90	1,50	0,60	0,70	0,80	1,29	0,26	0,00	1,03	0,17	0,60	2,67	2,36	0,70	0,71	5,58

Table 5- Chlorite: Composition of both octahedral sheets ([SIL], [HYD]) as a result of BGMN refinement of XRD diagrams (bulk samples). Legend: SIL – octahedral layer between the two tetrahedral layers forming the 2:1 component; HYDR – octahedral layer between two 2:1 sheet silicate units; D – Localization of Fe (value +3 means all Fe is located in SIL-octahedral layer; value -3 means all Fe is located in HYDR-octahedral layer); Y – total Fe; n^{VI} – numbers of cations in the two octahedral layers.

An opposite behavior to the total Fe-amount may be observed for the number of total octahedral cations (n^{VI} values). UW samples are characterized by a lower octahedral occupation in EB sediments than in BGB sediments (Fig. 12C). The total octahedral Fe-amount shows a strict inverse relation to the number of total octahedral cations and to the ratio R^{2+} / (R^{2+} + R^{3+}). That means that an increasing Fe-amount (as in UW material) is incorporated in a higher ratio as Fe^{3+}-cations (Table 5). XRD investigations have shown only slight differences in the quantitative distribution of BGB and EB sediments. Besides the content of dolomite, few Fe-related parameters from $2M_1$-mica, chlorite, and goethite indicate notable differences between EB and BGB sediments, especially for UW samples.
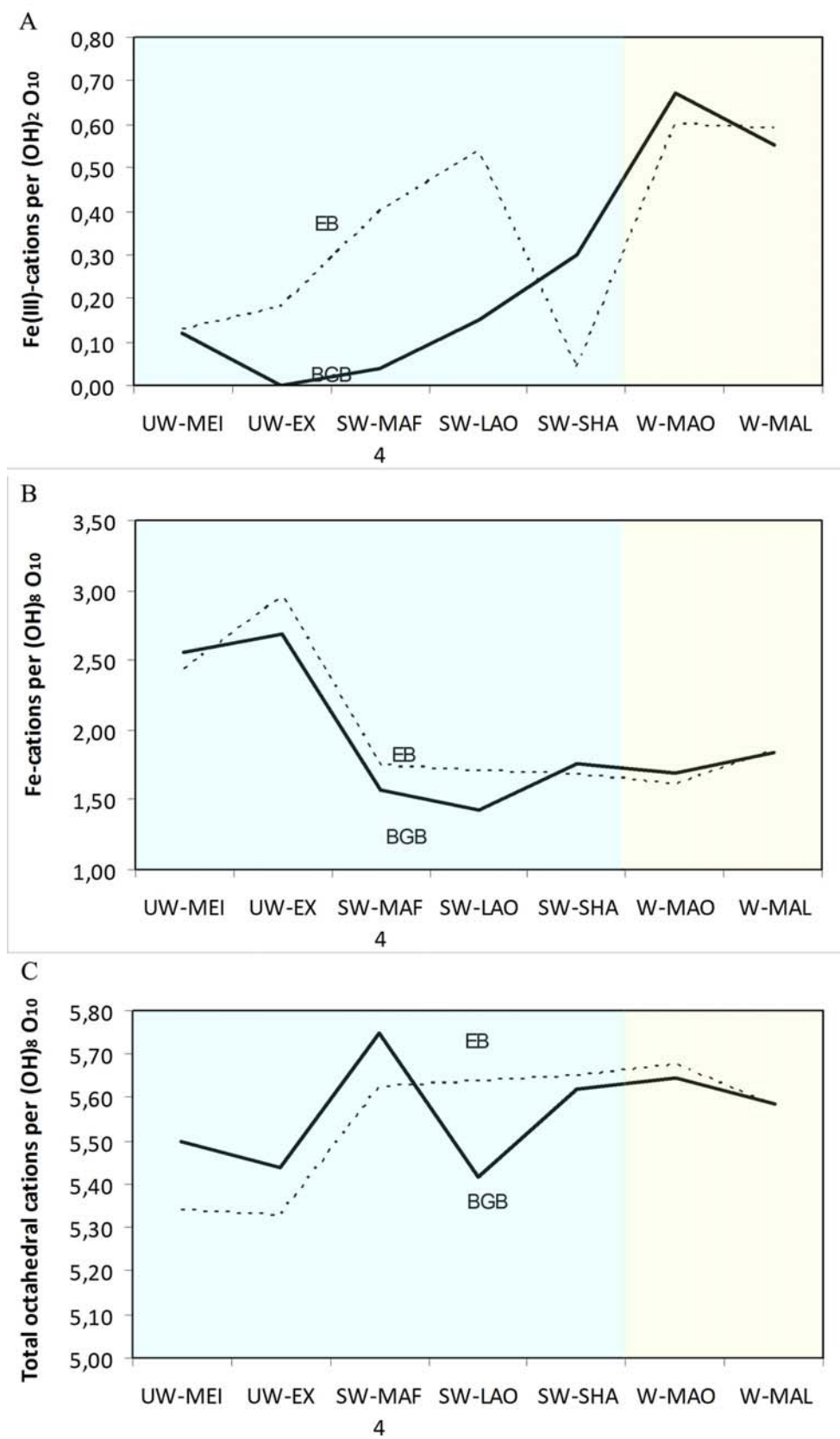
Fig. 12. BGMN-Rietveld refinement. A- Different distribution of octahedral Fe (III) in $2M_1$ –mica from BGB and EB sediments. B- Different distribution of total octahedral Fe in chlorite from BGB and EB sediments. C- Different distribution of total octahedral cations in chlorite from BGB and EB sediments. Pale blue for UW+SW groups and pale yellow for W group.

The EB sediments of UW alteration grade are characterized by higher octahedral Fe amounts in $2M_1$-mica, chlorite, and goethite than in BGB sediments. The reduction of total Fe in chlorite leads to a higher ratio of divalent octahedral cations and to a higher occupation of octahedral sheets.

3.5.2 Clay mineral data from the < 2 µm fraction (TEM)

The mineral < 2 µm fraction of samples MEI, EX grey (unaltered UW group), MAO and MAF B (altered W group) was investigated by TEM. These samples are composed of illite-montmorillonite mixed layer phases (IS-ml), dioctahedral vermiculite-montmorillonite mixed layer phases (diVS-ml; a K- and charge deficient type of IS-ml), kaolinite-smectite-vermiculite mixed layer phases (KSV-ml) and partially also by chlorite-saponite-trioctahedral vermiculite mixed layer structures (CSV-ml) (Fig. 13A). Quartz and opaque Fe-bearing particles (goethite?) were further phases identified by TEM in the < 2 µm fraction (Table 6).

Sample	Weathering stage	frequency-%				
		IS-ml	diVS-ml	KSV-ml	CSV-ml	others
MEI 2 0829 EB	UW	44%	43%	1%	10%	
MEI 2 0829 BGB	UW	42%	44%	4%	9%	
EX grey EB	UW	49%	40%	0%	11%	
EX grey BGB	UW	44%	47%	0%	8%	
MAF 4 081 EB	SW	25%	55%	20%	0%	
MAF 4 081 BGB	SW	10%	85%	5%	0%	
MAO EB	W	21%	58%	4%	7%	10%
MAO BGB	W	24%	62%	4%	4%	6%

Table 6- Mineralogical composition of the < 2 µm fraction investigated by TEM.

The different types of mixed layer structures formed mainly aggregates composed of small particles. These particles showed xeno- or hypidiomorphic shapes (Fig. 13C). Especially compact particles in EB samples were characterized by partial dissolution impacts (Fig. 13C).

The semi-quantitative distribution of mixed layer phases indicates the highest amount for IS-ml and CSV-ml as well as the lowest values for diVS-ml and KSV-ml in least-altered UW sediments (MEI, EX) (Fig. 14 A and B). It is important to note that the trend of decrease of CSV- and increase of KSV-ml toward more strongly altered samples is reverse to the distribution pattern of their end members kaolinite and chlorite. Event bed samples have shown commonly similar or higher concentrations for IS-ml, CSV-ml and KSV-ml as well as lower values for diVS-ml than in BGB sediments (Fig. 14 A and B). The chemical composition of IS-ml and diVS-ml in the TEM-investigated samples indicated that the composition of octahedral sheets of IS-ml and diVS-ml follows a slight trend of Al-

enrichment from least-altered samples MEI, EX toward most altered samples MAF or MAO (Fig. 15 A and C, Fig. 13B).
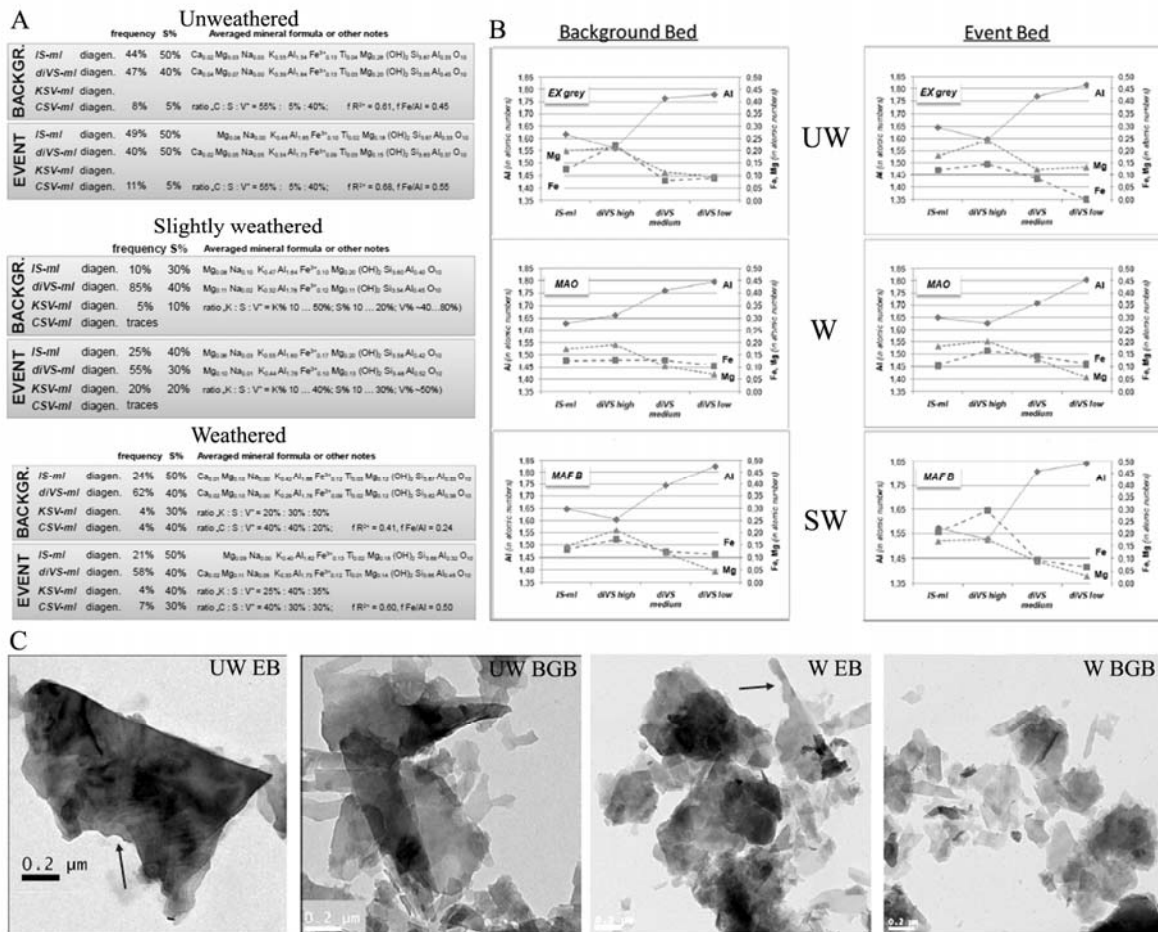

Fig. 13. TEM analyses. A- Results of < 2 μm fraction (S% -ratio of smectite layers in mixed layer phases). Legend: IS-ml = illite-smectite mixed layer phases; diVS-ml = dioctahedral vermiculite-smectite mixed layer phases (a K and charge deficient version of IS-ml); KSV-ml = kaolinite-smectite-dioctahedral vermiculite mixed layer phases; CSV-ml = chlorite-smectite-trioctahedral vermiculite mixed layer phases. B- Distribution of different cations in octahedral layers of dioctahedral mixed layer phases (series "IS-ml –diVS-ml high charged-diVS-ml medium charged-diVS-ml low charged" form the order of alteration from IS-ml finally into low charged diVS-ml and vice versa) for the three weathering groups on < 2 μm fraction. C-Micrographs of selected EBs and BGBs. Left sample is from UW group; right sample is from W group. Dissolution signs are present in both weathering stages; this means they are not weathering-dependent.

The role of Mg- and Fe-loss was comparable in BGB samples (for IS-ml: Mg > Fe; for low diVS-ml: Mg < Fe) and was different in the investigated EB samples. The abundance of iron rises continuously in the EB samples from least- to most-altered samples (Fig. 13B). The decreasing development of tetrahedral Si in IS-ml and diVS-ml represents an illitization process (Fig. 15 B and D).

4. Discussion

4.1 Alteration/weathering stages

Late alteration/weathering and the loss of information that it causes is common in the Burgess Shale-type *Lagerstätten* of Chengjiang and Guanshan. The alteration processes change the physical, chemical, mineralogical, petrographical, and mechanical properties of the rocks, affecting taphonomic analyses performed on them. This study provides evidence for major differences between alteration/weathering stages along with slightly differences between the Yuanshan Fm. and the Wulongqing Fm., as well as some regional impacts in the chemical composition of the matrix.

All data show that there is a distinct difference between the UW and the SW/W groups. Higher TC and TOC contents and the presence of S characterize the UW group. Pyrite is present in the matrix only in the UW alteration group. By contrast, goethite increases from 0-4 % in UW group mudstones to 5-6 % in W group mudstones. Some clay minerals also show distinct enrichment/depletion patterns with increasing alteration. Kaolinite (9-12%), IS-ml (40-49 % of < 2 μm), and CSV-ml (8-12 % of < 2 μm) are more enriched in the least-altered sediments of the UW group compared with the most strongly altered samples [W group: kaolinite (1-3 %), IS-ml (10-25 % of < 2 μm), CSV-ml (0-7 % of < 2 μm)]. Chlorite (4-8 %), diVS-ml (40-47 % of < 2 μm), and KSV-ml (0-4% of < 2 μm) increase, on the other hand, toward the more strongly altered samples of W group
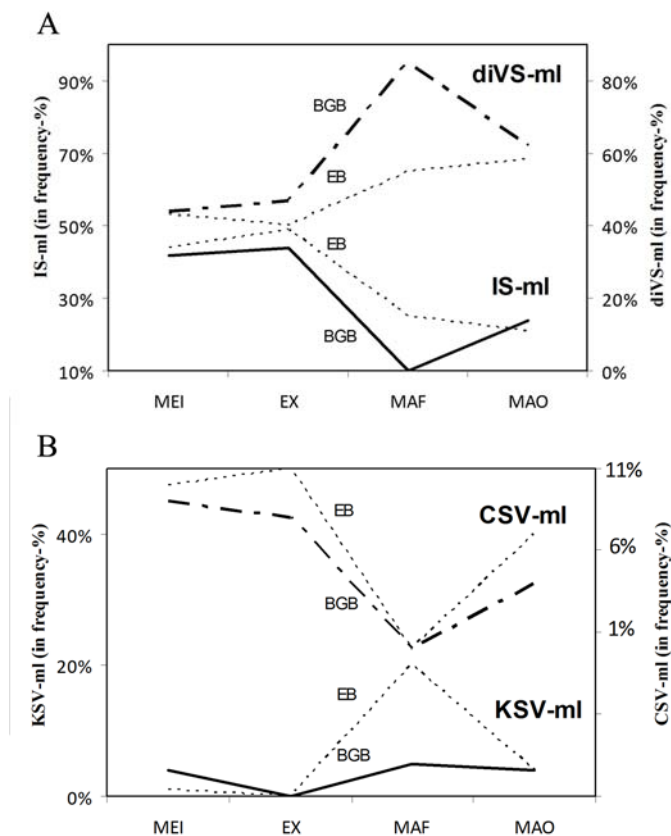

Fig. 14. TEM analyses in < 2 μm fraction of BGB and EB samples ordered by weathering grade (from UW to W). A- Distribution of illite-smectite mixed layer phases (IS-ml) and dioctahedral vermiculite-smectite mixed layer phases (diVS-ml) B- Distribution of CSV-ml (chlorite-saponite-trioctahedral vermiculite mixed layer structure) and KSV-ml (kaolinite-smectite-dioctahedral vermiculite mixed layer structure).

sediments (chlorite 11-21%, diVS-ml 55-85 % of < 2 μm, and KSV-ml 4-20 % of < 2 μm, Table 3).

The unaltered samples (UW group) also retain the highest dolomite (identified by XRD analyses; Table 3) contents (4-6 %), which are reduced to about 0-1 % in the most-altered/weathered mudstones (W group). Major trends are recognized among several elements in the UW group: the main differentiation is along factor 1 (Fig. 8B) of the principal component analysis, between carbonate content with CaO, C total, Mn, Ba and Na versus elements mainly bound to clay minerals and heavy minerals.

The trend of iron is also interesting, since it is related to S, Mo, Ni, As, and TOC only in the UW group, revealing sulfide formation that is even more strongly expressed in the underlying Black Shale Mb. of Yuanshan Fm. Surprisingly, the sulfides in the least-altered mudstones (W group; TOC = 0.1-0.21 %) are mostly dispersed in the rock matrix and not enriched on the fossil remains of the Chengjiang or Guanshan faunas. It is remarkable that most of the preserved fossils in UW group samples show strong carbon signals, but Fe and S do not cover most of the tissues and carcasses. The strongest enrichments of pyrite are seen along linear linings at folds or along cracks, indicating a slightly later diagenetic origin.

In the most-altered samples, Fe is not related to S or the other trace elements, possibly because iron follows another enrichment trait during alteration/weathering, which is different from the UW group samples (where Fe is bound to sulfides). Earlier taphonomic analyses carried out on weathered material from Chengjiang show completely different results from those of the material of the UW group, which were not subjected to stronger weathering and the consequent loss of information. The UW material is, therefore, the most reliable material to carry out such analyses. Similar observations were made by Marynowsky et al. (2011) for the Lower Carboniferous, where they noticed that paleoweathering resulted in a 97% decrease in TOC and total loss of sulfur and that pyrite framboids decreased considerably in the partially weathered zone and vanished totally in the weathered zone.

The samples from the Wulongqing Fm. (SHI M, SHI UP and HUA) (Fig. 8) show a slightly different trait than those of Yuanshan Fm., with a prevalence of elements such as Sr, Cs, Rb, Th, and some REEs. Also the samples of Yuanshan Fm. from the Malong-Qujing area show a slightly different elemental incorporation, with a stronger influence of Pb, Zn, and REEs that may be due to a local hydrothermal overprint.
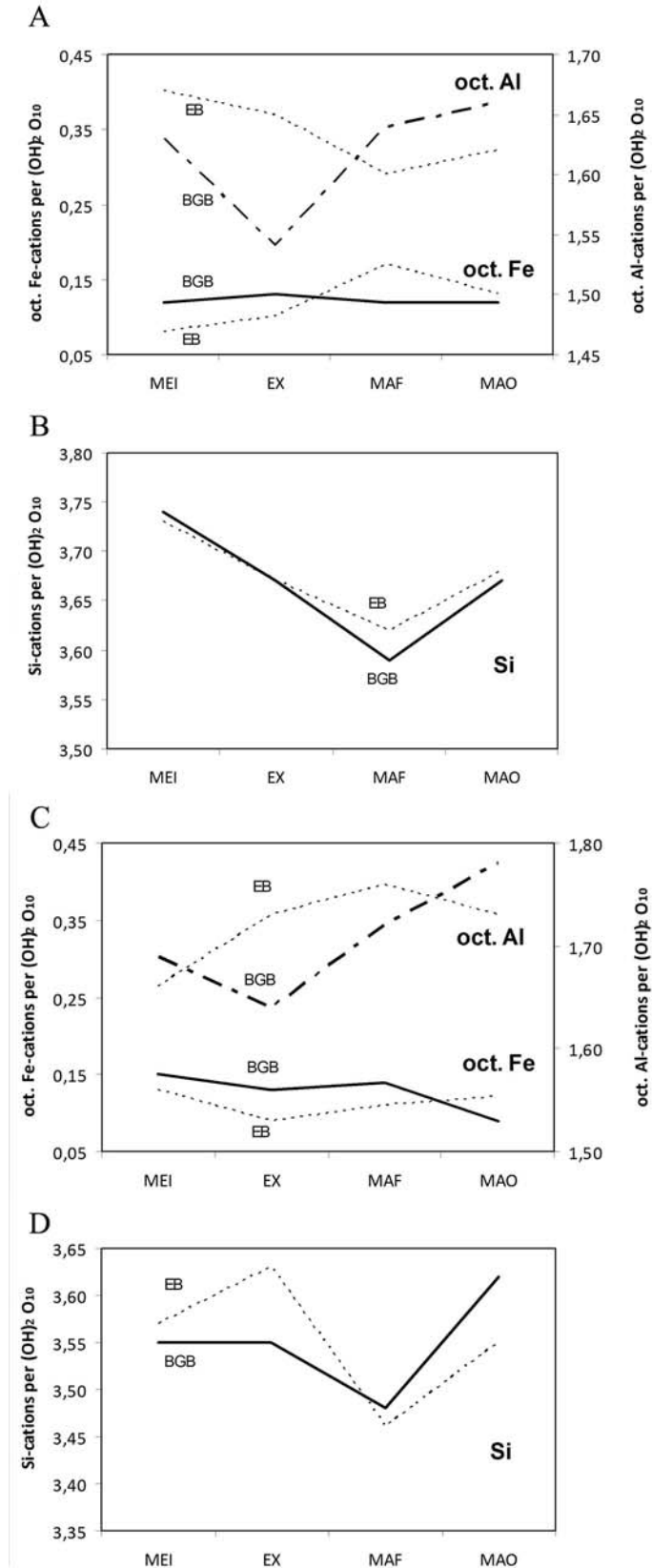
4.2 Paleoredox proxies

Fig. 15. TEM analyses. A- Distribution of octahedral Fe and Al cations in IS-ml from BGB and EB sediments. B- Distribution of tetrahedral Si in IS-ml from BGB and EB sediments. C- Distribution of octahedral Fe and Al cations in diVS-ml from BGB and EB sediments. D- Distribution of tetrahedral Si in diVS-ml from BGB and EB sediments.

The role of benthic anoxia in promoting exceptional preservation in Burgess Shale-type deposits has been, and still is, a matter of debate. Anoxic conditions alone are insufficient to induce organic preservation of soft-bodied macrofossils (because preservation required protection of organic remains from the processes of decomposition, and, therefore, must have been mediated by mechanisms operating at the micron-scale and below). Nevertheless, most authors have considered benthic anoxia as a prerequisite (Conway Morris, 1986; Allison, 1988; Butterfield, 1995, 2003; Gaines et al., 2005; Gaines and Droser, 2010). A recent study (Garson et al., 2012) on the Spence Shale suggests that Burgess Shale-type preservation is favored by bottom water anoxia, but may not require it in all cases. Gaines and Droser (2010) argued that iron speciation and trace element proxies are useful tools for detecting well-developed water column anoxia, but are not capable of detecting

105

near bottom anoxia. They concluded, therefore, that the studied Burgess Shale-type assemblages were preserved under anoxic benthic conditions, requiring Burgess Shale-type fossils to have been transported from habitable benthic environments to a preservation site. According to this hypothesis, benthic anoxia was an important control over the preservation of Burgess Shale-type biotas worldwide. This hypothesis is not fully confirmed by sedimentological, paleobiological, and geochemical evidence in our study. One argument against the permanent presence of bottom-water anoxia is the relative abundance of sponges in BGB assemblages that indicates a benthic autochthonous life during their deposition. Zhao et al. (2012) also proposed that the fossil assemblages in the Chengjiang fossil *Lagerstätte* reflect the original biodiversity because most of the benthic animals (such as worms, brachiopods and epifaunal vagrant organisms) could not make a sufficiently quick response to escape from burial as a result of the rapid sediment deposition. More support for oxygenated bottom-water conditions is given by the lithological data of Zhu et al. (2001). They show typical current lineations, current marks, and cross bedding, not only at the top beds, but also within their lithofacies 3. This indicates the presence of currents and higher turbulence that would be inconsistent with the permanent presence of bottom-water anoxia. The Zr content of bulk rock analyses of EBs and BGBs of Maotianshan Shale Mb. (Yuanshan Formation) also ranges from 150 to 240 ppm (average 168 ppm); this is closer to the average shale composite value (PAAS; Zr = 210 ppm) and contrasts with lower values in the underlying Black Shale Mb. of Yuanshan Formation (Zr: 75- 135 ppm). This indicates that sediment influx and turbulence increased during the deposition of Yuanshan Fm. from the basal Black Shale Member, partially deposited under anoxic conditions, toward the upper Maotianshan Shale Member interpreted to reflect normal marine conditions (Steiner et al., 2001). Furthermore, Zhu et al. (2001), Hu (2005), and Zhang et al. (2007) demonstrated the presence of weak bioturbation, simple trace fossils, and diminutive trace fossils in close association with Burgess Shale-type preservation in the Yuanshan Formation. Although Burgess Shale-type preservation is commonly thought to occur in suboxic/anoxic conditions and in strata lacking bioturbation (e.g., Butterfield, 1990; Gaines and Droser, 2010; Gaines et al., 2012a), the fossiliferous beds of the Burgess Shale and Kinzers Formation were deposited beneath oxygenated bottom waters, whereas those beds deposited under anoxic conditions notably lack fossils of soft-bodied biota (Powell et al., 2003); deposition of the Burgess Shale beneath oxygenated bottom waters is reported also by Powell et al. (2003). Evidence of oxygenated bottom water conditions during deposition of the Burgess Shale, documented by minor burrows and in situ moults and sponges anchored to the substrate (at the time of burial), is

also reported from the Raimond Quarry (Powell et al., 2003). Wilson (2006), on the basis of Allison and Brett (1995) and Devereux (2001), reports the lack of appreciable quantities of pyritized organic matter, together with evidence of bioturbation and *in situ* fossils, concluding that, at least for the Raymond Quarry, conditions were locally oxic. Gaines et al. (2012a) showed that in many Burgess Shale-type *Lagerstätten* (e.g., Wheeler and Marjum Formation, Spence Shale, Kaili Formation, Pioche and Latham Formations, Stephan Formation and the Raimond Quarry Member) the most diverse Burgess Shale-type biotas occur predominantly in unbioturbated beds that are closely interbedded with weakly to moderately bioturbated intervals. By contrast, the Guanshan Fauna, with soft-tissue preservation, occurs in often strongly bioturbated interbeds with a diverse ichno-fauna (Weber et al., 2012). In contrast to this, the Chengjiang deposits show only a low grade of shallow bioturbation in some beds. However, it is remarkable that the lower Yuanshan Fm., where partially anoxic conditions were reconstructed by geochemical redox indicators (Steiner et al., 2001), only contains fossil shell remains, and not all of the Maotianshan Shale Member contains soft-tissued fossil remains. It appears likely that anoxic conditions may enhance the potential for exceptional fossil preservation, but may be not the crucial factor causing it.

Concerning the geochemical evidence of oxygenated bottom waters, several paleoredox proxies were applied in this study to investigate the depositional environment of the Chengjiang fossil *Lagerstätte*. Since the strata yielding the Chengjiang Biota were deposited in Cambrian Stage 3, special caution has to be taken for some proxies such as DOP (Raiswell and Berner, 1987) because the initial organic carbon content is thought to be low for pre-Devonian Shales, and also because changes in the oceanic burial of organic carbon strongly affect sedimentary pyrite formation (Berner, 1984; Raiswell and Berner, 1986, 1987). DOP analyses performed on our material show oxygenated bottom water values for the UW group, with values between 0.015 and 0.284 and an average value of 0.169. The W group has only one sample slightly above the detection limit (at Ercaicun section) with 0.0011. The SW group also shows values lower than those of the UW group, and just above the detection limit; they range between $1.440E^{-3}$ and $9.066E^{-5}$. Because the SW and W groups underwent different levels of alteration/weathering, we consider the values of the UW group to be more reliable. Our values reach a maximum of 0.284 and are, therefore, below the 0.42 threshold of oxic/dysoxic boundary conditions proposed by Raiswell et al. (1988).

The iron proxy FeHR/FeT shows that at least bottom water anoxia conditions were not permanently present during deposition of the strata yielding the Chengjiang Fauna. FeHR consists of mineral phases that have the potential to react with dissolved H_2S when exposed

on short timescales within the water column or during earliest diagenesis, plus the Fe that has already reacted and is present as FeS_2 (Raiswell and Canfield, 1998). This proxy has been widely used as a paleoenvironmental indicator of bottom-water oxygenation (e.g., Canfield et al., 1996; Raiswell and Canfield, 1998; Raiswell et al., 2001; Poulton and Raiswell, 2002; Anderson and Raiswell, 2004; Poulton and Canfield, 2005; Lyons and Severmann, 2006). Ratios of FeHR/FeT exceeding values of 0.38 point to anoxic deposition (Raiswell and Canfield, 1998), and the FePY/FeHR ratios define whether the system was ferruginous (i.e., <0.8) or euxinic (i.e., >0.8) (Poulton et al., 2004). Our data of the UW group show ferruginous, oxygenated bottom water values (Fig. 7 A and D).

Since V may occur adsorbed onto clay minerals, an association that probably results after burial, and Cr is thought to be associated only with the detrital fraction (and is not influenced by redox conditions), high V/Cr values (i.e., >2) are thought to indicate anoxic conditions (Rimmer, 2004 and references therein). High Ni/Co ratios are also thought to be associated with anoxic conditions (Rimmer, 2004 and references therein). The V/Cr ratio with values <2 suggests completely oxic conditions (Jones and Manning, 1994), and the Ni/Co ratio is also mostly below the threshold of 5 that indicates oxic conditions (Jones and Manning, 1994). In contrast to the Ni/Co and V/Cr proxies, V/(V + Ni) with values ≥ 0.7 for the UW group indicates anoxic redox conditions (0.54-0.82 is the threshold based on Hatch and Leventhal, 1992). However, because the canonical discriminatory analyses that we performed on all the proxies showed that the V/(V+Ni) proxy was not a reliable indicator for redox conditions, we here consider its values not solid enough. The poor agreement between these three proxies was already observed by Rimmer (2004), who noticed that V/(V+Ni) ratios tend to indicate consistently lower oxygen regimes than the other two paleoredox indicators. Furthermore, V/(V+Ni) is the only proxy that does not show a sharp difference between the UW and the SW+W groups.

$U_{authigen}$ was proposed by Wignall & Myers (1988) as an indicator of bottom water anoxia in ancient sedimentary sequences. We use the values of 5 proposed by Jones & Manning (1994) as discriminating between oxic and dysoxic bottom waters. Values of the Maotianshan Shale Mb. with Chengjiang-type fossils were always below the threshold, suggesting oxygenated bottom water during deposition of the fossiliferous interval of the Yuanshan Formation in Yunnan Province. This is in good accordance with earlier studies of the Yuanshan Fm. at Haikou (Chengjiang County), where anoxic conditions could be only reconstructed for the lower Black Shale Member (Steiner et al., 2001).

The ratio of total iron to aluminum (FeT/Al) is also an important indicator of ancient redox conditions. It is broadly used as paleoredox proxy in modern and ancient shales (e.g., Werne et al., 2002; Lyons et al., 2003; Anderson and Raiswell, 2004; Lyons and Severmann, 2006). This approach assumes that values of FeT/A1 higher than base-line values (i.e., the FeT/A1 ratio in lithogenous sediments deposited in shelf environments) are due solely to the addition of FeHR (Raiswell and Anderson, 2005); the FeT/Al ratio of average shale is 0.5 (Chang et al., 2010). Measured FeT/Al ratios for our samples are from 0.27 to 0.52, which is almost similar to average shale. Only one sample (BGB of the UW group in Deze) shows values >1. Since the FeT/Al ratios exceed 0.5 in anoxic basins, the results gained from our samples relate this material to oxygenated bottom water conditions.

The geochemical redox proxies involve metals that are accumulated at the seafloor. Therefore, EB samples may reflect considerably different settings from BGBs with respect to timing for element accumulation and origin of material. BGB sediments may reflect a stronger contribution of seawater signals and more local conditions for sediment composition. However, the difference of average values for the redox-sensitive metals (Th, V, U, Cr and Ni) for both types of beds is irrelevant; that is, there is no major systematic trend of major depletion. The only exception to this observation exists for As, where the values of the UW group show BGB values somewhat higher than EB values (e.g., 14ppm, 28ppm versus 5.2ppm and 4.3ppm, respectively). Since the bacterial activity was mostly confined to BGBs (with higher TOC than EBs), the somewhat higher values in As may also be related to bacterial enrichment during later diagenetic stages.

Several trace metals (Mo, Zn, Ni, Co, Cr, U and V) are also enriched in shales deposited under anoxic conditions. Molybdenum is considered a reliable paleoredox proxy (e.g., Algeo and Lyons, 2006). The average shale composition is 2 ppm Mo (Taylor and McLennan, 1985; Powell et al., 2003). The Black Shale Mb. considered to have been deposited under anoxic conditions (Steiner et al., 2001) shows indeed the only values higher than the average shale composition (sample H: 10 and 3 ppm for EB and BGB, respectively; 189 to 50 ppm Mo in the lowermost one meter at Haikou, Chengjiang County). Mo values in analyzed shales are below the detection limit (1 ppm) for almost all samples, (the only two exceptions show a value of 1 ppm: a BGB of the UW group in Deze, and the sample of group 2, belonging to the W group from the Guanshan material near Kunming City), indicating that the samples were not deposited in oxygen-depleted bottom water.

A key control on pyrite formation is the amount and reactivity of organic matter within the sediment, which controls the rate at which sulfide is produced by sulfate-reducing bacteria

(Taylor and Macquaker, 2000). Unaltered samples with contents in TOC of 0.1-0.48 wt% reveal that pyrite is not common. Our element mapping of fossils from the UW samples also reveals that pyrite is mostly dispersed within sediments (see Fig. 4), and usually not concentrated on soft tissues or skeletal parts. The mean TOC content of the fossiliferous Burgess Shale ranges from 0.11 % to 0.42% (more recent data show values from 0.17 to 0.32%) and from 0.11 to 2.42% for the Kinzers Formation (McKirdy et al., 2011). The TOC content of the Emu Bay Shale layers ranges from 0.25% to 0.55% and is thought to be insufficient to have accumulated under stable anoxic or suboxic conditions (McKirdy et al., 2011).

In our material, the TOC content was low, FeHR/FeT ratios mostly do not exceed 0.38, and FeP/FeHR values suggest that the water column was not stratified with sulfidic bottom waters. Redox parameters for least-altered samples of Chengjiang-type fossils from Yunnan Province do not indicate deposition under anoxic conditions (e.g., $U_{authigen} \leq 2.4$; V/Cr = 1.9-1.0; Fe HR/ Fe TOT = 0.36-0.27).

4.3 Crystal size statistics of iron minerals

Sedimentary pyrite occurs in ancient and modern environments as single or clustered framboids, single or clustered euhedral crystals, and replacements of organic matter (Wilkin et al., 1996). Kaplan et al. (1963) suggested that the relative proportion of the different textural types of pyrite is variable in specific sediments, but all forms develop early during anoxic diagenesis, usually within the top few centimeters of the sediment column, owing to interaction between bacterially produced H_2S and detrital iron minerals in the sediment (e.g., Love, 1967; Berner, 1970, 1984; Canfield et al., 1992; Wilkin et al., 1996; Raiswell and Canfield, 1998). Framboids precipitate in waters highly supersaturated with both Fe monosulfides and pyrite via iron monosulfide intermediates (Sweeney and Kaplan, 1973; Wilkin et al., 1996). Euhedral pyrite forms more slowly at saturation levels below those of Fe monosulfides and with porewater oversaturated only with respect to pyrite (Taylor and Macquaker, 2000). Thus, framboids are the first formed generation of sulfides within sediments, with euhedral pyrite becoming progressively more important in later diagenesis (Wignall et al., 2010). However, framboids can also form during late diagenesis, e.g., by the pyritization of biotite (Menon, 1967) or magnetite (Canfield and Berner, 1987), in hydrothermal veins, and along dissolution surfaces (Scott et al., 2009).

110

Framboidal pyrite is common in recent marine sediments and in black shales (Sawlowicz, 1993), but it has also been reported from many other environments such as magmatic rocks (Steinike, 1963; Kanehira and Bachinski, 1967; Love and Amstutz, 1969), carbonate deposits (Menon, 1967), coals (Wiese and Fyfe, 1986), tills (Stene, 1979), coastal acid sulfate soil (Poch et al., 2009), mangrove swamp soils, non-tidal marsh soils and mine-spoil soils (Fitzpatrick and Self, 1997), estuarine sediments (Bush and Sullivan, 1999), and beach sands (Hossain, 1975) .

Different genetic origins have been proposed for framboids, ranging from a purely inorganic origin, based on laboratory synthesis (e.g., Berner, 1969; Farrand, 1970; Sunagawa et al., 1971; Sweeney and Kaplan, 1973; Wang and Morse, 1996), occurrences in magmatic rocks, through indirect biogenic formation (e.g., Vallentyne, 1963; Kalliokoski and Cathles, 1969; Lougheed and Mancuso, 1973), to a direct biogenic origin (e.g., Schneiderhoehn, 1923; Fabricius, 1961; Skripchenko, 1968; Locquin and Weber, 1978).

The size distribution of pyrite framboids has been proposed as a paleoredox proxy by several authors such as Wilkin et al. (1996), Wignall and Newton (1998), Taylor and Macquaker (2000) and Wignall et al. (2005). The crystal size distribution theory (sensu Wilkin et al., 1996) relates framboid size to growth time and rate. The smaller sizes of framboids in sediments of modern euxinic basins reflect shorter average growth times relative to oxic or dysoxic environments. A mean framboid diameter < 5 μm has been interpreted by these authors as the signal of prevalently anoxic bottom waters. Wilkin and Barnes (1997), Lyons et al. (2009), and Alvarez-Iglesia & Rubio (2012) suggested that syngenetic pyrite formation in anoxic bottom waters may be reflected by the presence of small, very uniformly sized framboids that precipitated out of suspension upon reaching a critical size, whereas diagenetically formed pyrites typically appear as more variously sized framboids or as euhedral crystals. Our material shown in the Guanshan matrix (UW group) presents both morphologies (framboids and euhedral crystals), with a size range varying between 1.9 μm and 6.55 μm for framboids, and between 0.87 μm and 6.9 μm for euhedral crystals. In the Chengjiang matrix (UW group), only pyrite euhedral crystals are present, ranging in size between 0.6 μm and 2.5 μm. According to Alvarez-Iglesia & Rubio (2012), our material points to diagenetically formed pyrites. On the basis of size, the Guanshan material (the only material showing framboids) has values that could be related to both oxygen-depleted and non-oxygen-depleted bottom conditions, but the presence of crystals and the scarcity of material suggest that conditions of bottom water were not oxygen-depleted. Pyrite formation was not possible at the time of burial. Conditions may only have become anoxic or dysoxic

after burial or during late diagenesis. Pyrite was observed also in a few samples belonging to group UW, but pyrite crystals and framboids were located only along fractures, folds, or lateral rims, and did not replace the main soft tissue; in addition, pyrite within fossils of UW group samples was sparse and rare.

The UW group data referring to pyrite framboids on fossil material [arthropod (n=16), worm (n=8), and brachiopod (n=8) groups] show that they are rare. Crystals are the most frequent pyrite morphology in the UW group for arthropods (n=186) and brachiopods (n=48), whilst worms were equally frequent (n=8). The equivalent framboids in the altered/weathered mudstones that have an iron oxide/(?) hydroxide composition have a slightly bigger mean diameter (see Fig. 10). Previous authors used the size distribution of pyrite framboids as a paleoredox proxy to understand the geochemistry of both modern and ancient environments (e.g., Jurassic black shale, Wignall and Newton, 1998; Lower Jurassic, Taylor and Macquaker, 2000; and the Permian to Jurassic pelagic sediment succession of the Mino-Tamba terrane, SW Japan, Wignall et al., 2010; modern environments, Wilkin et al., 1996; Wilkin and Barnes, 1997). Pyrite in our UW group's matrix is rare, and only infrequent finds of pyrite framboids (and crystals) on fossil material have been recorded; they are more abundant in deeply weathered samples where the framboids have been pseudomorphed by iron oxides/hydroxides. This discrepancy of data can be explained by a much later formation of iron minerals during advanced stages of diagenesis. The Fe species data show average values for Fe_{tot} of 4.71% (UW), 4.95% (SW), and 5.02% (W). A slight but obvious enrichment of iron occurred during alteration/weathering because the SW and W groups have higher iron percentage values than the UW group. This may be due to the influence of sulfate-rich waters and clay mineral transformations during late alteration and weathering, as have also been reported in acidic soil environments (e.g., Poch et al., 2009). The Black Shale Mb. at the base of the Yuanshan Fm. is stratigraphically older than the horizon bearing the Chengjiang Fauna and the horizons bearing the Guanshan Fauna, and is rich in TOC and pyrite (Steiner et al., 2001). Exposure of these bedrocks and oxidation of sulfides during later weathering is a possible and plausible source of sulfate- and iron-enriched groundwater, leading to the enrichment of iron minerals on organic carcasses of these fossils. Tectonic uplifting and fracturing as well as enhanced groundwater and geothermal water circulation are well-known features in the Kunming and Chengjiang region, where the Xiaojiang and Puduhe fault zones (Fig. 1) with strike-slip rates of up to 9 mm/a have had a strong impact since the Cretaceous (Shen et al. 2003).

It is also possible that groundwater slightly enriched in Fe- and sulfate ions was only derived from oxidation of pyrite-bearing beds of the Maotianshan Shale Member of Yuanshan Fm. The widely distributed pseudomorphosed framboids in the most-altered mudstones indicate that sulfate-reducing and Fe-reducing bacteria were involved in the formation of late-stage pyrite during metabolic consumption of sulfate-rich groundwater veneering through the mudstones of Yuanshan Fm. in the weathering zone. Bacterial activity was mostly confined to BGBs (with slightly higher TOC than EBs) and organic carcasses in EBs that provided organic compounds for the metabolic processes and were largely consumed during these alteration processes and replaced by late-stage pyrite. This process may be comparable to pyrite framboid formation by sulfate-reducing bacteria in anaerobic environments in modern acidic soils. The acidic groundwater was also responsible for dissolving carbonate and apatite in lingulid brachiopods and chancelloriid spicules, for example. The dissolution of carbonate from the Yuanshan mudstones also led to a higher pH in deeper ground- and porewaters and provided further ions (e.g. Mg^{2+}) that, besides the mobilized iron, interacted with the clay mineral matrix (see discussion below).

Strongly altered fossiliferous samples often showed iron stain banding parallel to rock fractures that may run through the fossils into the clay matrix or are visible only within the fossils (Fig. 5). In some cases, iron banding of the rock matrix only affects BGBs, but not the adjacent EBs (Fig. 5D), supporting the interpretation that sulfate-reducing bacteria were mostly active in mudstone layers richer in TOC or on organic carcasses (Fig. 5B). The color banding confirmed the strong impact of alteration by circulating groundwater derived from rock fractures. The fracture zones of most-altered yellow mudstones are often heavily incrusted by manganese oxide (Fig. 5 A and B), which likely derives from the dissolution of dolomite by acidic groundwater and precipitation in oxygenated waters. The most-weathered mudstones are then significantly depleted in Mn (average 108 ppm), compared with the least-altered mudstones (average 462 ppm).

The iron minerals that occur in the Chengjiang and Guanshan samples (only in altered material) display evidence of several grades of alteration: spherical aggregates that were once framboids, and euhedral crystals that were partially oxidized, as shown by dissolution signs and oxide recrystallization in the individual crystals (see Fig. 4). Furthermore, iron mineral crystals of soft parts are smaller than those in the shells of brachiopods and arthropods. This is also probably due to different durations of deposition and different geochemical conditions. Data on the size distribution of pyrite framboids (and crystals) of the UW group with a size range of mostly ≥ 5 µm are in agreement with the majority of the other geochemical proxies,

generally suggesting the absence of oxygen-depleted conditions during the deposition of the strata yielding the Chengjiang and Guanshan organisms. Nevertheless, the statistical size of framboidal pyrite should be considered only in relation to other proxies, since in this case framboid sizes may have been influenced by the high sedimentation rate of the EBs, which limits residence time near the oxic-anoxic boundary. Another potential influence is the clay-rich matrix, which probably hinders the migration of raw material for framboid growth from ions in interstitial water, as suggested by Alvarez-Iglesia & Rubio (2012).

4.4 Clay mineral analyses

Hu (2005) proved the existence of sedimentological differences between BGB beds and EB beds in Chengjiang-type fossil *Lagerstätten* in Yunnan Province. In this study, we provide evidence of some mineralogical differences in the characterization of the clay minerals between the different alteration grades of UW and SW+W mudstones and to a minor extent between EBs and BGBs.

The main clay mineral transformations were observable between the least-altered mudstones of the UW group and those of the SW+W groups. Although most major and minor mineral components can be found in both least- and most-altered mudstones (except for dolomite, pyrite and goethite), their main differences are expressed in the proportions of some specific clay minerals and in their ion substitutions. Decreasing amounts of kaolinite (Fig. 6), IS-ml (Fig. 14A), CSV-ml (Fig. 14B), and increasing concentrations of chlorite (Fig. 6), diVS-ml (Fig. 14A), and KSV-ml (Fig. 14B) are associated with the shift from least-altered UW mudstones toward those of the W group. Weathering, burial diagenesis, microbial activity, and early diagenesis at the interface between seawater and sediment could be discussed as possible alteration processes.

2M1-mica represents a typical detrital mineral, which, like the continental weathering products kaolinite and IS-ml, is considered to have been primarily transported from the continent and deposited in the shallow marine basin. The increasing amount of diVS-ml and KSV-ml with increasing alteration/weathering is in good accord with a potential stronger neoformation of clay minerals during chemical alteration, weathering and/or increased microbial activity.

However, a decreasing amount of kaolinite (Fig. 6) coupled with an increasing concentration of chlorite (Fig. 6) and partial illitization of IS-ml (Fig. 15) usually indicates a stronger diagenetic impact of sediments during low-grade metamorphic processes. Burial diagenetic

formation of chlorite is often accompanied by temperatures >80°C (e.g., Hower et al. 1976; Hurst, 1985), represented by a burial depth of more than 1000–2000 m. Such high post-Cambrian sedimentary overburden is not recognized from this region of the shallow Yangtze Platform. However, there is no simple relationship between chlorite polytype and temperature, and thus all attempts to establish a universal chlorite geothermometer have failed. Low-temperature and near-surface formation of chlorite is also known: for example, in post-depositional early diagenesis in marine basins or evaporitic basins (Mg-rich chlorite). Odinite (a Fe (III)-rich 1:1 sheet silicate) and glauconite are typical authigenic minerals in the early diagenesis of marine sedimentary basins. Hillier (1995) described odinite as a possible precursor of the formation of chamosite under low temperature conditions. A tetrahedral Si-value of 3.2 per half unit cell determined by BGMN-Rietveld refinement and an occupation of octahedral sheets remarkably lower than 6 (Table 5) confirm low temperature conditions during authigenic formation of chlorite in the herein investigated samples. However, the near proximity of samples of different alteration types (in some cases even different alteration types in the same outcrops or the same rock samples) combined with specific changes in the elemental content and spatial distribution of minerals such as pyrite, goethite, and dolomite, and the dissolution of biominerals preclude the possibility that the increase of chlorite in W group mudstones of Yuanshan Fm. might be explained by higher burial diagenesis or different marine settings with different grades of early diagenesis in the Cambrian. However, during normal weathering, where oxidizing and acidic conditions prevail, chlorite is gradually destroyed and transferred to vermiculite and smectite (e.g., Wilson 2004; Arocena & Velde 2009; Uzarowicz et al. 2011). Numerous studies have provided evidence of microbial reduction of Fe (III) bearing phyllosilicates (e.g., Stucki et al., 1987; Kostka et al., 1996; Stucki and Kostka, 2006; Jaisi et al., 2007; Bishop et al., 2011; Wu et al., 2012) and the importance of Fe (III) bearing dioctahedral phyllosilicates as an electron acceptor for dissimilatory Fe (III) reducing bacteria in sediments (Wu et al., 2012). A variety of clay minerals contain high concentrations of structural ferric iron which may be used as an electron acceptor for both Fe-reducing and sulfate-reducing bacteria (e.g., Li et al., 2004; Liu et al., 2012; Wu et al., 2012). Among the clay minerals with structural Fe (III), the smectite to illite reaction is of special significance because it is normally related to hydrocarbon maturation, geopressuring of shales, formation of growth faults and a change in water chemistry. Kim et al. (2004), Jaisi et al. (2012), and Liu et al. (2012) demonstrated that the S-I reaction does not proceed only through IS-ml intermediates in which the percentage of illite layers in the mixed layer phases increases with increasing temperature, time, K-concentration,

and water/rock ratio, but is a reaction that can be microbially mediated at 30°C and ambient pressure. An illitization was recognized with increasing alteration in the herein investigated mudstones too; this illitization may have been microbially mediated (indicated by decreasing tetrahedral Si in IS-ml (Fig. 15 A and C) with increasing alteration). The trend to an increasing amount of octahedral Fe in $2M_1$-mica (Fig. 12A) also indicates the specific role of Fe^{3+} that may be derived from the influence of the slightly acidic and Fe- and sulfate-rich groundwater.

We therefore conclude that bacterial bioalteration by Fe-reducing and sulfate-reducing bacteria played a key role in the chemical and mineralogical alteration processes of the mudstones of Chengjiang and Guanshan fossil *Lagerstätten*. The activity of sulfate-reducing bacteria can explain the late diagenetically formed pyrite in most-altered samples (W group mudstones) and the loss of organic matter by metabolic assimilation. Chlorite formation at the expense of kaolinite occurs in near-surface conditions at slightly alkaline pH and slightly reducing Eh conditions (the stability field of chlorite has a pH of 7-9). The reaction of the slightly acidic and sulfate- and Fe-rich groundwater with the dolomite fraction of the mudstones resulted in a buffering and increase in pH that also allowed transformation of kaolinite under the influence of mobilized iron and magnesium. The sulfate-reducing and Fe-reducing bacterial activity resulted in the precipitation of framboidal pyrite and also reduced Eh conditions, so chlorite formed at the expense of kaolinite. Stronger incorporation of Mg^{2+} from the dissolved dolomites resulted in a different incorporation of Fe and Mg in the octahedral cations of lately formed chlorites in the most-altered mudstones (Table 5, Fig. 12 B and C). This interpretation is in accordance with the observed enrichment/depletion trends of goethite (high values exist only in the W group), pyrite (only UW group samples show
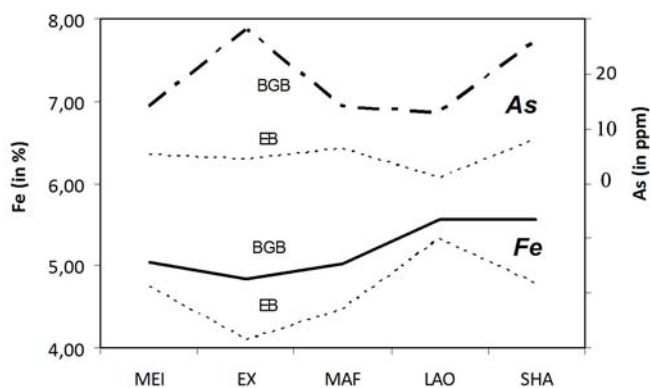

Fig. 16- Distribution of Fe and As in BGBs and EBs.

pyrite), and dolomite (the highest values in the UW group; Table 1). Concerning the differences between BGBs and EBs, the chemical analyses of bulk samples show enrichment trends of some elements in some of the beds. In the BGBs, the Fe and As content is systematically higher than in the EBs; this may be related to

higher TOC contents in BGBs (Fig. 16). A general enrichment trend of Fe with increasing alteration toward W group mudstones is also observable. This may be due to preferred microbial precipitation of Fe from Fe- and sulfate-rich groundwater in BGBs and along fossil concentrations of EBs that are primarily richer in organic matter. An increasing role of iron in dioctahedral ml phases in comparison to Mg is also present in EB samples of all groups. The mineralogy of bulk samples shows that in contrast to chlorite (higher values in EB) most other minerals (kaolinite, dolomite, mica 1M, goethite and epsomite + jarosite) have generally slightly lower values in EBs with respect to BGBs in the least-altered samples (Fig. 6), although this result requires better statistical support before being interpreted. TEM analyses on mineral matter <2 μm show that EB samples have in general less diVS-ml in comparison to IS-ml than in BGB samples and a slight smectization in diVS-ml (Fig. 13). The chemical analyses of bulk samples show also an enrichment trend of some REE, Ti, Mn and partially Al and Mg for EBs (Fig 9). This enrichment of REE can also be related to microbial activity (Takahashi et al., 2005; 2007), but might derive from the previously mentioned influence of slightly acidic groundwater in modern acidic soil environments.

Furthermore, there are indications of dissolution processes mostly in the EBs. Especially compact clay particles in EBs were characterized by partial dissolution impacts (Fig. 13C). The results of X-ray diffraction of oriented mounts effectuated on the EB-BGB couple of the SW group sample MAF indicated an Ostwald ripening: dissolution of smallest particles and zoned precipitation of solution at larger particles. This dissolution of smallest particles of diVS-ml was accompanied by precipitation of diVS-ml with more smectite layers of the EB, showing that Si is not removed in the event beds and can be related to an increased influence of biota. The partial etching of clay minerals likely occurred during the influence of slightly acidic groundwater.

An early diagenetic stabilization by pyrite replacement of organic tissues of Chengjiang and Guanshan fossil *Lagerstätten* was not crucial to the preservation of soft-bodied organisms. We consider that a rapid deposition in finest claystones had a greater influence on the preservation of highly "volatile" tissues. In a recent fossilization experiment, nauplia of *Artemia salina* were buried in finely dispersed non-saline aqueous suspensions of kaolinite and montmorillonite for 2-5 months at room temperature (Naimark et al., 2013). The experiment has confirmed that finest anatomical details and even gut structures of the nauplia can be preserved in a fine clay matrix over a long period of time. It was shown that the structural morphology of the matrix is of fundamental importance for rapid mineralization and further diagenesis in the organic/mineral system. The authors ascribe the observed inhibition

of nauplian decomposition to a rapid increase in local acidity caused by the decomposition-induced excretion of organic acids, as well as protein coagulation promoted by aluminum cations. The colloidal nature of the mineral matrix is important for the authors because of the large surface area available for the interactions with the organic mixture in the acidic media. They suggest that fossilization in the colloidal system can be considered as a surface-catalyzed process.

Wilson (2006) proposed that the clay mineral kaolinite enhances preservation, promoting cross-linkages in proteins that secondarily stabilize organic tissues. The discovery that preservation of proteins may be enhanced by burial in kaolinite led her to suggest that clay minerals played an important role in increasing the recalcitrance of proteinaceous matter during early diagenesis. She suggested that the organic preservation in the Burgess Shale is primarily a matter of protein preservation in a determinate environment: rapid burial in a suitable clay mineral assemblage, low oxygen levels, reduced permeability, and low porewater content. She also rejected the model of Burgess Shale-type preservation proposed by Orr et al. (1998) because she considered it did not account for the organic preservation of structures as highly reflective carbon films; furthermore, she stressed that some aluminosilicates replacing fossil tissues had a late diagenetic origin. The model proposed by Petrovic (2001) was also rejected based on the observation of relatively low levels of iron in the Burgess Shale (Powell, 2003), making an early diagenetic stabilization in the marine sedimentary environment unlikely.

Recently, Drouin et al. (2010) investigated the role of clay minerals in organic preservation in laboratory experiments that demonstrated that, under marine water column conditions, the organic fixation is only a sorption process, controlled by the surface properties of clays. These results support a previous model by Butterfield (1990; 1995), proposing that clay mineral availability at a presence of low TOC played a crucial role for exceptional fossil preservation by contributing physical packing material, by inhibiting decay due to adsorption of autolytic enzymes, and by stabilizing organic molecules by ion exchange between clay-mineral surfaces and organic compounds. For this, the existence of a high fraction of expandable clay minerals (e.g., mixed layer minerals with smectite) is very important (Keil et al., 1994), a factor that is also present in the investigated Chengjiang and Guanshan fossil *Lagerstätten.* The experiment by Naimark et al. (2013) also revealed that kaolinite suspensions enable the preservation of highly decayable arthropod tissues. It is evident that the UW samples of Chengjiang fossil *Lagerstätte* contain a high percentage of kaolinite, which is potentially a key factor for exceptional fossil preservation. Drouin et al. (2010) report that according to

Salmon et al. (2000) and Pichevin et al. (2004) the principal argument in favour of effective organic preservation by way of sorption on clay is the observation at the nanoscopic scale of an intimate relationship between organic matter and clay, as nanolayer alternations, in petroleum source rock and recent upwelling sediments. The role of event beds in the preservation of organic carbon in fine-grained sediment of source rocks was investigated by Ghadeer and Macquaker (2012). They suggest that the organic carbon in the Toarcian mudstones of England is likely to have been preferentially preserved because the frequency of depositional events was sufficiently high to minimize both oxidant diffusion into the sediment and organic carbon mineralization.

The importance of the presence of expandable clay minerals and kaolinite for the exceptional Burgess Shale-type preservation is also supported by the fact that all Cambrian fossil *Lagerstätten* of this type are located in the tropical realm, with its strong weathering processes and high flux of clay minerals into marine sedimentary basins.

Rapid entombment in a clay mineral matrix with a high content of kaolinite and expandable clay minerals deposited at a frequency sufficiently high to minimize both oxidant flux and permineralization might be a valid explanation for Burgess Shale-type preservation in the Chengjiang-type fossil *Lagerstätten* of Yunnan Province. While the clay composition was similar in EBs and BGBs, but did not guarantee an exceptional fossil preservation in most BGBs, the combination of bed composition and rapid deposition in a fine suspension appears to represent the important combination of parameters responsible for soft-tissue preservation.

5. Conclusions

Previous taphonomic studies of the Chengjiang Biota defined the fossil *Lagerstätte* as a taxonomically, temporally, and spatially specific case of a Burgess Shale-type fauna (e.g., Steiner et al., 2005). Albeit intensively studied, the conditions promoting Burgess Shale-type preservation have remained poorly understood. Organic preservation of fossil remains is widespread in the analyzed material presented here, whereas skeletal minerals were commonly dissolved. The presence of apatite in sclerites of paleoscolecids, brachiopod shells, and bradoriids in unaltered samples supports the conclusion that these organisms were primary biomineralizers.

The presence of bottom-water anoxia is not absolutely necessary to promote Burgess Shale-type preservation. However, bottom-water anoxia and microbial sealing may further increase

the probability of soft-tissue preservation because these factors support fast and undisturbed embedding in clastic sediments. The existence of persistent bottom-water anoxia and widespread early diagenetic pyrite formation can be largely ruled out for the Chengjiang and Guanshan fossil *Lagerstätten* according to the results we gained for the least-altered material and the paleobiological observations. On the contrary, the presence of rare pyrite in the matrix, the lack of significant quantities of pyritized organic matter in UW material, the geochemical proxies, and the paleobiological data suggest a possible fluctuating oxycline. Here we propose a classification of the alteration/weathering stages in the Burgess Shale-type fossil *Lagerstätten* of Yunnan Province (South China) based on X-ray analyses, geological observation, and geochemical data combined with statistical analyses. Our current studies reveal that late stage chemical alteration/weathering plays a much more prominent role in the taphonomy of the Chengjiang and Guanshan Biotas than previously recognized. The chemistry of UW and SW+W groups is significantly different owing to chemical alteration, likely linked to intense faulting since the Cretaceous. A new taphonomic model for the preservation of Chengjiang Biota based on five major stages has therefore been developed (Fig. 17).

(1) BGBs represent the normal sedimentary environment with slow rates of accumulation for aluminosilicates. Organic remains are mostly decayed, and disarticulated and skeletal remains and strong cuticles are preferentially preserved in the fossilization process. Sponge preservation is preferred (see Hu, 2005). TOC is low, but significantly higher than during deposition of EBs. The EBs result from storm-generated rapid deposition of fine suspensions mainly composed of detrital 2M1 mica, quartz, kaolinite, chlorite, and minor contents of illite-smectite mixed layer phases, of which especially kaolinite and IS-ml phases appear crucial for exceptional fossil preservation.

The strata yielding the Chengjiang Biota in Yunnan Province were mostly deposited under an oxic water column, and anoxia was not permanently present. Oxygen-depleted bottom water is not a prerequisite for Burgess Shale- type preservation (Fig. 17 A and B).
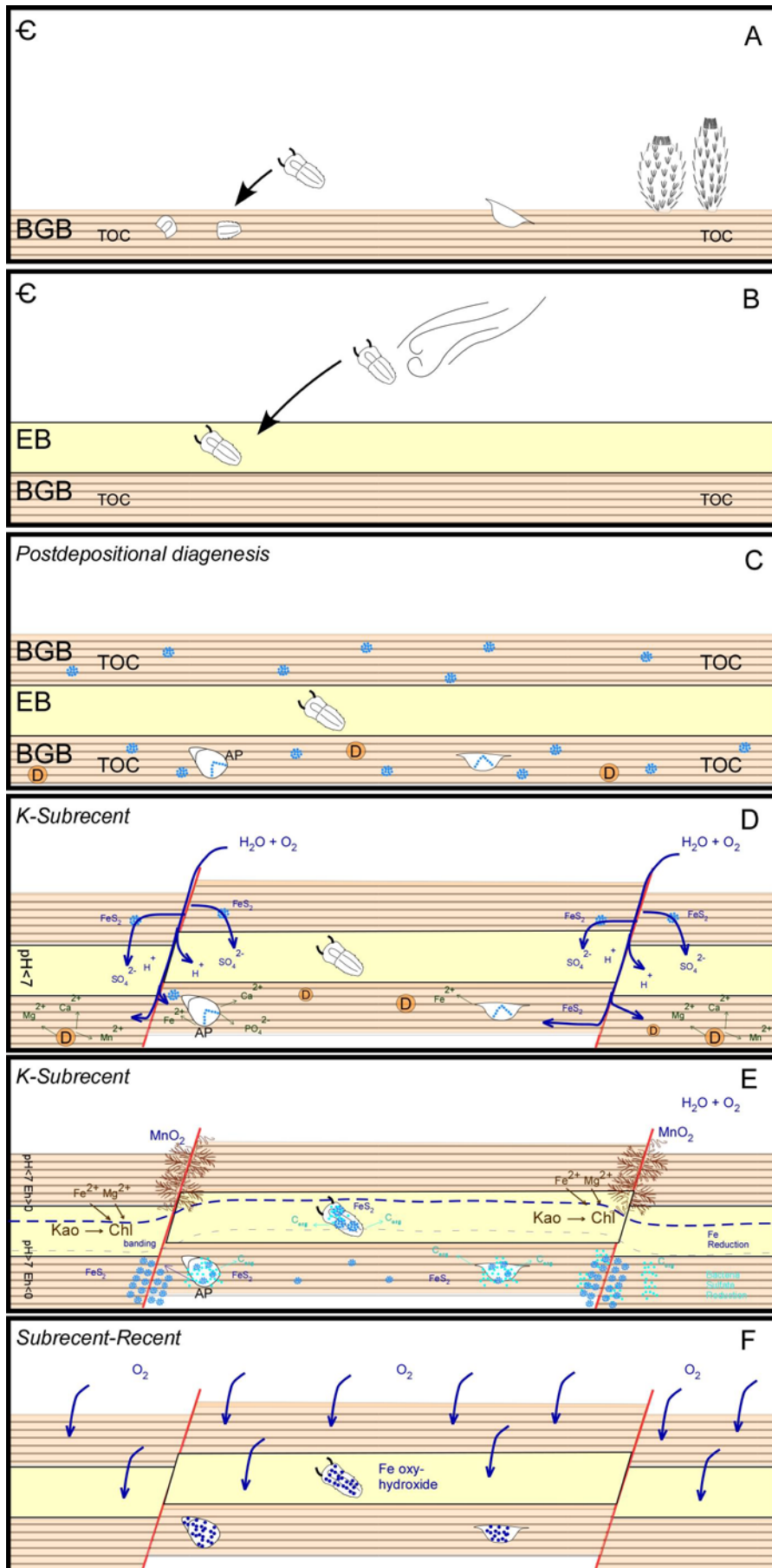
(2) During post-depositional early diagenesis, expandable clay minerals inactivate autolytic enzymes and stabilize organic molecules by means of cationic bonds. Mudstones are compacted, and entombed fossils partially crack and compact. Pyrite formation is very scattered in the organic-richer sediments, possibly also owing to migrating hydrogen sulfides. Organisms in EBs do not significantly pyritize, except for some later diagenetic fills along cracks and folds and sporadic patches (Fig. 17C).

(3) Owing to intense faulting from the Cretaceous onward, mudstones of Yuanshan Fm. are exposed to the surface, fractured, and exposed to intense groundwater circulation. Oxidation and weathering of the underlying Black Shale Member of Yuanshan Fm. and/or the Maotianshan Shale Mb. containing the exceptionally preserved fossils cause pyrite decomposition, and slightly acidic Fe- and sulfate-rich groundwater is formed. The weak sulfuric acid dissolves most skeletal biominerals (apatite, calcite) and sedimentary dolomite. Fe^{2+}, Mg^{2+}, Mn^{2+}, SO_4^{2-} are liberated and incorporated in the clay alteration. Some gypsum, epsomite, and jarosite may form (Fig. 17D).

(4) In the oxic zone, MnO_2 is precipitated along rock fractures. In deeper groundwater horizons where oxygen is mostly consumed, sulfate- and Fe-reducing bacteria settle in organic-richer BGBs and along organic carcasses of EBs, metabolizing organic compounds and reducing sulfate and Fe ions, respectively. This chemical alteration greatly reduces the TOC and results in widespread pyrite-framboid formation that partially replaces organic tissues. Iron mineral precipitation onto organic carcasses of the Chengjiang- type fossils is mostly confined to this later alteration process and thus is not crucial for the early fixation of highly decayable tissues in Burgess Shale-type faunas. In zones where bacterial activity has lowered the Eh to reducing conditions under slightly alkaline pH, the detrital kaolinite from continental weathering is transferred to chlorite, incorporating part of the mobilized Fe and Mg (Fig. 17E).

(5) During long weathering phases in recent to subrecent times, the lately formed pyrite replacing the organic fossils is oxidized and pseudomorphosed by Fe oxy-hydroxides (Fig. 17F).

Fig. 17 (Next page) - Taphonomic model for the preservation of Chengjiang Biota. A- Sedimentation in BGB; the TOC is comparatively higher than in EBs. Preservation of sponges, strong cuticles and mostly disaggregated shells is stratigraphically preferred. B- Rapid and chaotic entombment of whole organisms in fine clay matrix of EBs. C- Compaction of mudstones and fossils. Scattered pyrite formation, mostly in sediment, rarely on fossils, and here only along cracks. D- Intense groundwater circulation along faults and cracks. Pyrite is decomposed, and slightly acidic Fe- and sulfate-rich groundwater is formed. The weak sulfuric acid dissolves most skeletal biominerals (apatite, calcite) and sedimentary dolomite. Fe^{2+}, Mg^{2+}, Mn^{2+}, SO_4^{2-} are liberated and incorporated in the clay alteration. E- Precipitation of MnO_2 along rock fractures. In deeper groundwater horizons where oxygen is mostly consumed, sulfate- and Fe-reducing bacteria settled in organic-richer BGBs and along organic carcasses of EBs, metabolizing organic compounds and reducing sulfate or Fe ions. This chemical alteration greatly decreases the TOC and results in widespread pyrite-framboid formation that partially replaced organic tissues. Where bacterial activity had lowered the Eh to reducing conditions and where carbonate dissolution had buffered pH to slightly alkaline values, the detrital kaolinite from continental weathering is transferred to chlorite incorporating part of mobilized Fe and Mg. F- Latest weathering.

6. Acknowledgements

4. References

Algeo, T.J. & Lyons, T.W., 2006. Mo–total organic carbon covariation in modern anoxic marine environments: Implications for analysis of paleoredox and paleohydrographic conditions. *Paleoceanography* 21, PA1016, doi:10.1029/2004PA001112.

Allison, P.A., 1988. The role of anoxia in the decay and mineralization of proteinaceous macro-fossils. *Paleobiology* 14, 139–154.

Allison, P.A. & Briggs, D.E.G., 1993. Exceptional fossil record: Distribution of soft-tissue preservation through the Phanerozoic. *Geology* 21, 527-530.

Allison, P. A. & Brett, C. E., 1995. In situ benthos and paleo-oxygenation in the Middle Cambrian Burgess Shale, British Columbia, Canada. *Geology* 23, 1079-1082.

Álvarez-Iglesias, P.& Rubio, B., 2012. Early diagenesis of organic-matter-rich sediments in a ría environment: Organic matter sources, pyrites morphology and limitation of pyritization at depth. *Estuarine, Coastal and Shelf Science* 100, 113-123.

Anderson, T.F. & Raiswell, R., 2004. Sources and mechanisms for the enrichment of highly reactive iron in euxinic Black Sea sediments. *American Journal of Science* 304, 203–33.

Arocena, J.M. & Velde B., 2009. Transformation of Chlorites by Primary Biological Agents—A Synthesis of X-ray Diffraction Studies. *Geomicrobiology Journal* 26, 382-388.

Aronson, R.B., 1992. Decline of the Burgess Shale fauna: Ecologic or taphonomic restriction? *Lethaia* 25, 225–229.

Barthel K.W., Swinburne, N.H.M. & Conway Morris S., 1990. Solnhofen—A Study in Mesozoic Palaeontology. Cambridge, UK: Cambridge Univ. Press. 236 pp.

Bengston, S., 2005. Mineralized skeletons and early animal evolution. *In*: D.E.G. Briggs (ed.), *Evolving Form and Function: Fossils and Development*, pp. 101–124. Yale Peabody Museum, New Haven, CT.

Bergmann, J., Friedel, P. & Kleeberg, R., 1998. BGMN – a new fundamental parameters based Rietveld program for laboratory X-ray sources, its use in quantitative analysis and structure investigations. *CPD Newsletter* 20, 5-8.

Berner, R.A., 1969. The synthesis of framboidal pyrite. *Economic Geology* 64, 383-384.

Berner, R.A., 1970. Sedimentary pyrite formation. *American Journal of Science* 268, 1 –23.

Berner, R.A., 1984. Sedimentary pyrite formation: An update. *Geochimica et Cosmochimica Acta* 48, 605-615.

Bishop, M.E., Jaisi D.P., Dong H., Kukkadapu R.K. & Ji J., 2010. Bioavailability of Fe(III) in loess sediments; an important source of electron acceptors. *Clays and Clay Minerals* 58, 542-557.

Blochmann, F., 1900. Untersuchungen iiber den Bau der Brachiopoden Pt.2 Die Anatomie von Discinisca und Lingula. Gustav Verlag, Jena, 124pp.

Briggs, D.E.G., 2003. The role of decay and mineralization in the preservation of soft-bodied fossils. *Annual Review Earth Planetary Sciences* 31, 275–301

Briggs D. E. G., Crowther P. R., 2001. Palaeobiology 2. Oxford, UK: Blackwell.

Briggs, D.E.G. & Gall, J.C., 1990. The Continuum in Soft-Bodied Biotas from Transitional Environments: A Quantitative Comparison of Triassic and Carboniferous Konservat-Lagerstätten. *Paleobiology* 16, 204-216.

Briggs, D. E. G., Raiswell, R., Bottrell, S.H., Hatfield, D. & Bands, C., 1996. Controls on the pyritization of exceptionally preserved fossils: an analysis of the Lower Devonian Hunsrück Slate of Germany. *American Journal of Science* 296, 633-663.

Briggs, D.E.G., Bottrell, S.H., Raiswell, R., 1991. Pyritization of soft-bodied fossils: Beecher's Trilobite Bed, Upper Ordovician, New York State. *Geology* 19, 1221–1224.

Bruguière, J. G., 1797. Tableau Encyclopédique et Méthodique des trois Règnes de la Nature, Vol.2 : vers, coquilles, mollusques et polypes divers. Agasse, Paris, 96-314.

Bush, R.T, Sullivan, L.A., 1999. Pyrite micromorphology in three Australian Holocene sediments. *Australian Journal of Soil Research* 37, 637–654.

Butterfield, N.J., 1990. Organic preservation of non-mineralizing organisms and the taphonomy of the Burgess Shale. *Paleobiology* 16, 272-286.

Butterfield, N.J., 1995. Secular distribution of Burgess Shale-type preservation. *Lethaia 28*, 1–13.

Butterfield, N.J., 2002. *Leanchoilia* guts and the interpretation of three dimensional structures in Burgess Shale-type fossils. *Paleobiology* 28, 155–171.

Butterfield, N.J., 2003. Exceptional fossil preservation and the Cambrian explosion. *Integrative and Comparative Biology* 43, 166–177.

Cai, Y., Hua, H., 2007. Pyritization in the Gaojiashan Biota. *Chinese Science Bulletin* 52, 645–650.

Canfield, D.E., 1989. Reactive iron in marine sediments. *Geochimica et Cosmochimica Acta*, 53(3): 619-632.

Canfield, D.E., Raiswell, R., Westrich, J.T., Reaves, C.M. & Berner, R.A., 1986. The use of chromium reduction in the analysis of reduced inorganic sulfur in sediments and shales. *Chemical Geology*, 54(1-2), 149-155.

Canfield, D.E. & Berner, R.A., 1987. Dissolution and pyritization of magnetite in anoxic marine sediments. *Geochimica et Cosmochima Acta* 51, 645–659.

Canfield, D.E., Raiswell, R. & Bottrell, S.H., 1992. The reactivity of sedimentary iron minerals toward sulfide. *American Journal of Science* 292, 659–683.

Canfield, D.E., Lyons, T.W. & Raiswell, R., 1996. A model for iron deposition to euxinic Black Sea sediments. *American Journal of Science* 296, 818–34

Chang, H.J., Chu, X.L., Feng, L.J. & Huang J., 2010. Iron speciation in cherts from the Laobao Formation, South China: Implications for anoxic and ferruginous deep-water conditions. *Chinese Science Bulletin* 55, 3189−3196.

Chen, J.Y., 2004. The Dawn of the Animal World, Jiangsu Science and Technology Press, Nanjing, China, 366 pp.

Chen, J., Hou, X. & Lu, H., 1989. Lower Cambrian leptomitids (Demospongea), Chengjiang, Yunnan. *Acta Paleontologica Sinica 28*, 17–31.

Chen, J., Hou, X. & Li, G., 1990. New Lower Cambrian Demosponges *Quadrolaminella* gen. nov. from Chengjiang, Yunnan. *Acta Paleontologica Sinica 29*, 402–413.

Chen, Z., Hu, J., Zhou, C., Xiao, S. & Yuan, X., 2004. Sponge fossil assemblage from the Early Cambrian Hetang Formation in Southern Anhui. *Chinese Science Bulletin* 49(15), 1625-1628.

Comfort, A., 1951. Observation on the shell pigments of land pulmonates. *Malacological Society London, Proceedings* 29, 35-43.

Conway Morris, S., 1986. The community structure of the Middle Cambrian phyllopod bed (Burgess Shale). *Palaeontology* 29, 423-467.

Conway Morris, S., 1989. Burgess Shale Fauna and the Cambrian explosion. *Science* 246, 339-346.

Cornwell, J.C. and Morse, J.W., 1987. The characterization of iron sulfide minerals in anoxic marine sediments. *Marine Chemistry* 22(2-4), 193-206.

Cusack, M., Williams, A., & Buckman, J.O., 1999. Chemicostructural evolution of Linguloid brachiopod shells. *Palaeontology* 42, 799–840.

Dall, W.H., 1870. A revision of the Terebratulidae and Lingulidae. *American Journal of conchology* 6, 88-168.

Devereux, M.G., 2001. Palaeoecology of the Middle Cambrian Raymond Quarry Fauna, Burgess Shale, British Columbia. M.Sc., The University of Western Ontario.

Dohrmann, R., Rüping, K.B., Kleber, M., Ufer, K. & Jahn, R., 2009. Variation of preferred orientation in oriented clay mounts as a result of sample preparation and composition. *Clays and Clay Minerals* 57(6), 686–694.

Drouin S., Boussafir, M., Rober, J.L., Alberic, P. & Durand, A., 2010. Carboxylic acid sorption on synthetic clays in sea water: In vitro experiments and implications for organo-clay behaviour under marine conditions. *Organic Geochemistry* 41, 192-199.

Emig, C.C., 1990. Examples of post-mortality alteration in Recent brachiopod shells and (paleo) ecological consequences. *Marine Biology* 104, 233-238

Fabricius, F., 1961. Die Strukturen des „Rogenpyrits" (Koessener Schichten, Raet) als Beitrag zum Problem der „Vererzten Bakterien". *Geologische Rundschau* 51,647–657.

Farrand, M., 1970. Framboidal sulphides precipitated synthetically. *Mineralium Deposita* 5, 237–247.

Fitzpatrick, R.W. & Self, P.G., 1997. Iron oxyhydroxides, sulfides and oxyhydroxysulfates as indicators of acid sulfate weathering environments. *Advances in Geoecology* 30, 227–240.

Forchielli, A. & Pervesler, P., 2013. Phosphatic cuticle in thylacocephalans: a taphonomic case study of Austriocaris (Arthropoda, Thylacocephala) from the Fossillagerstätte Polzberg (Raingraben shales, Carnian, Upper Triassic, Lower Austria). *Austrian Journal of Earth Sciences* 106(1), 46-61.

Forchielli, A., Steiner, M., Hu, S. X., & Keupp, H., 2012. Taphonomy of Cambrian (Stage 3/ 4) sponges from Yunnan (South China). *Bulletin of Geosciences* 87, 133-142.

Forchielli, A., Steiner, M., Hu, S., Lüter, C. & Keupp, H., in press. Taphonomy of the earliest Cambrian linguliform brachiopods. *Acta Palaeontologica Polonica*, doi: http://dx.doi.org/10.4202/app.2011.0182.

Forchielli, A., Steiner, M., Hu, S.X. & Keupp, H., 2012. Taphonomy of Cambrian (Stage 3/ 4) sponges from Yunnan (South China). *Bulletin of Geosciences* 87, 133–142.

Forchielli, A., Steiner, M., Keupp, H., Hu, S. & Li, G. 2009. Taphonomy of Early Cambrian Chengjiang fossils and phosphatized organic tissues. in: Eynatten, Reitner and Wörner (Eds.), Abstracts (GV Annual Meeting 2009, Earth Control on Planetary Life and Environment, October 5 - 7, 2009, Göttingen, Germany). Reihe der Universitätsdrucke im Universitätsverlag Göttingen: 33.

Gabbott, S.E., Hou, X.G., Norry, M.J. & Siveter, D.J., 2004. Preservation of Early Cambrian animals of the Chengjiang biota. *Geology 32*, 901–904.

Gaines, R.R., Briggs, D.E.G. & Zhao, Y.L., 2008. Burgess Shale-type deposits share a common mode of fossilization. *Geology*, 36,755-758.

Gaines, R.R. & Droser, M.L., 2010. The paleoredox setting of Burgess Shale-type deposits. *Palaeogeography, Palaeoclimatology, Palaeoecology* 297, 649–661.

Gaines, R.R., Droser, M.L., Orr, P.J., Garson, D., Hammarlund, E., Qi, C. & Canfield, D.E., 2012a. Burgess Shale-type biotas were not entirely burrowed away. *Geology* 40, 283-286.

Gaines, R.R., Hammarlund, E.U., Hou, X, Qi, C., Gabbott, S.E., Zhao, Y., Peng, J. & Canfield, D.E., 2012b. Mechanism for Burgess Shale-type preservation. *Proceedings of the National Academy of Science USA*. 109,5180–5184.

Gaines, R.R., Kennedy, M.J. & Droser, M.L., 2005. A new hypothesis for organic preservation of Burgess Shale taxa in the middle Cambrian Wheeler Formation, House Range, Utah. *Palaeogeography, Palaeoclimatology, Palaeoecology* 220,193–205.

Garson, D.E., Gaines, R.R., Droser, M.L., Liddell, W.D. & Sappenfield, A., 2012. Dynamic palaeoredox and exceptional preservation in the Cambrian Spence Shale of Utah. *Lethaia* 45, 164–177.

Geidies, H., 1954. Abgeänderte Azan-Methoden. *Mikrokosmos* 42: 239-240.

Gehling, J.G., 1999. Microbial Mats in Terminal Proterozoic Siliciclastics: Ediacaran Death Masks. *Palaios* 14, 40–57

Ghadeer, S. G. & Macquaker, J.H.S., 2012. The role of event beds in the preservation of organic carbon in fine-grained sediments: Analyses of the sedimentological processes operating during deposition of the Whitby Mudstone Formation (Toarcian, Lower Jurassic) preserved in northeast England. *Marine and Petroleum Geology* 35, 309-320.

Glaessner M.F., 1984. The dawn of animal life, a biohistorical study. Cambridge University Press, 244pp.

Hammarlund, E., 2007. The ocean chemistry at Cambrian deposits with exceptional preservation & the influence of sulphate on soft-tissue decay. 64pp. Master thesis, Odense, Denmark, University of Southern Denmark.

Han, J., Shu, D., Zhang, Z., Liu, J., Zhang, X. & Yao, Y., 2006. Preliminary notes on soft-bodied fossil concentrations from the Early Cambrian Chengjiang deposits. *Chinese Science Bulletin* 51, 2482-2492.

Hatch, J.R. & Leventhal, J.S., 1992. Relationship between inferred redox potential of the depositional environment and geochemistry of the Upper Pennsylvanian (Missourian) stark shale member of the Dennis Limestone, Wabaunsee County, Kansas, USA. *Chemical Geology* 99, 65– 82.

Hillier, S., 1995. Erosion: Sedimentation and sedimentary origin of clays. In: Velde, B. (Edt.): Origin and mineralogy of clays. Springer, Heidelberg Berlin New York.

Hinds, H.R., 1844-45. The zoology of the voyage of H.M.S. Sulphur, under the command of Capt. Sir Edward Belcher, RN., C.B., F.R.G.S., etc. during 1836-1842, London, Smith, Elder & Co., Mollusca, 2(1): 1-24 (July 1844); 2(2): 25-48 (October 1844); 2(3): 49-72 (January 1845).

Holmer, L.E., 1989. Middle Ordovician phosphatic inarticulate brachiopods from Västergötland and Dalarma, Sweden. *Fossil and strata* 26, 1-172.

Hossain, A., 1975. The occurrence ofpolyframboidal pyrite in a beach sand deposit, Cox's Bazar, Bangladesh. *American Mineralogist* 60, 157–158.

Hou, X., Bergstrom, J. 2003. The Chengjiang fauna- the oldest preserved animal community. *Paleontological research 7(1)*, 55-70

Hou, X.G., Aldrige, R.J., Bergström, J., Sieveter, D.J., Sieveter, D. J. & Feng, X.H., 1988. The Cambrian fossils of Chengjiang, China. The flowering of Early animal life. 246pp. Blackwell Publishing.

Hower, J., Eslinger, E.V., Hower, M.E. & Perry, E.A. 1976. Mechanism of burial metamorphism of argillaceous sediments: I. Mineralogical and chemical evidence. *Geological Society of America Bulletin* 87, 725-737.

Hu, S.X., 2005. Taphonomy and Palaeoecology of the Early Cambrian Chengjiang Biota from Eastern Yunnan, China. *Berliner paläobiologische Abhandlungen* 7, 197pp.

Hu, S.X., Steiner, M., Zhu, M.Y., Erdtmann, B.D., Luo, H.L., Chen, L. &Weber, B., 2007a. Diverse pelagic predators from the Chengjiang Lagerstätte and the establishment of modern-style pelagic ecosystems in the early Cambrian. *Palaeogeography, Palaeoclimatology, Palaeoecology* 254, 307–316

Hu, S., Luo, H., Hou, S. & Erdtmann, B.D., 2007b. Eocrinoid echinoderms from the Lower Cambrian Guanshan Fauna in Wuding, Yunnan, China. *Chinese Science Bulletin* 52, 717-719.

Hu, S., Li, Y., Luo, H., Fu, X., You, T., Pang, J., Liu, Q. & Steiner, M., 2008. New record of palaeoscolecids from the Early Cambrian of Yunnan, China. *Acta geologica Sinica* 82, 244-248.

130

Hu, S.X., Zhu, M.Y., Steiner, M., Luo, H.L., Zhao, F.C. & Liu, Q., 2010a. Biodiversity and taphonomy of the Early Cambrian Guanshan biota, eastern Yunnan. *Science China-Earth Sciences* 53, 1765-1773

Hu, S.X., Zhang, Z., Holmer, L.E. & Skovsted, C.B., 2010b. Soft−part preservation in a linguliform brachiopod from the lower Cambrian Wulongqing Formation (Guanshan Fauna) of Yunnan, southern China. *Acta Palaeontologica Polonica* 55 (3), 495–505

Hu, S.X., Steiner, M., Zhu, M., Luo, H.L., Forchielli, A., Keupp, H., Zhao, F.C. & Liu, Q., 2011. A new priapulid assemblage from the early Cambrian Guanshan fossil Lagerstätte of SW China. *Bulletin of Geosciences* 87(1), 93-106.

Hurst, A., 1985. Diagenetic chlorite formation in some Mesozoic shales from the Sleipner area of the North Sea. *Clay Minerals* 20, 69-79.

Iijima, M. & Moriwaki, Y., 1990. Orientation of apatite and organic matrix in *Lingula unguis* shell. *Calcified Tissue International* 47, 237-242.

Ivantsov, A.Y., Zhuravlev, A.Y., Leguta, A.V., Krassilov, V.A., Melnikova, L.M. & Ushatinskaya, G.T., 2005. Palaeoecology of the Early Cambrian Sinsk biota from the Siberian Platform. *Palaeogeography. Palaeoclimatology, Palaeoecology* 220, 69-88.

Iwata, K., 1981. Ultrastructure and mineralization of the shell of *Lingula unguis* Linneo (inarticulate, brachiopod). *Journal of the Faculty of Sciences, Hokkaido University (Serie 4)* 20, 35-65

Iwata, K., 1982 Ultrastructure and calcification of the shells in inarticulate brachiopods. Part 2. Ultrastructure of the shells of *Glottidia* and *Discinisca* [in Jap.]. *Journal of the geological Society of Japan* 88, 957-966

Jaisi, D.P., Dong, H.L. & Liu, C.X., 2007. Influence of biogenic Fe(II) on the extent of microbial reduction of Fe(III) in clay minerals nontronite, illite, and chlorite. *Geochimica and Cosmochimica Acta* 71, 1145−1158.

Jaisi, D.P., Eberl, D.D., Dong, H. & Kim, J., 2011. The formation of illite from nontronite bymesophilic and thermophilic bacterial reaction. *Clays and Clay Minerals* 59, 21–33.

James, M.A., Ansell, A.D., Collins, M.J., Curry, G.B., Peck, L.S. & Rhodes, M.C., 1992. Biology of living Brachiopods. *Advances in Marine Biology* 28. 175-387.

Jin, Y., Hou, X. & Wang, H., 1993. Lower Cambrian pediculate lingulids from Yunnan, China. *Journal of Paleontology* 67, 788-798.

Jones, B. & Manning, D.A.C., 1994. Comparison of geochemical indices used for the interpretation of palaeoredox conditions in ancient mudstones. *Chemical Gology* 111, 111–129.

Jope, M., 1969. The Protein of Brachiopod Shell III: Comparison with structural protein of soft tissue. *Comparative Biochemistry and Physiology* 30, 209–224.

Jope, M., 1977. Brachiopod shell proteins: their functions and taxonomic significance. *American Zoologist* 17, 133-140.

Kalliokoski, J. & Cathles, L., 1969. Morphology, mode of formation, and diagenetic changes in framboids. *Bulletin of the Geological Society of Finland* 41, 153–133.

Kanehira, K. & Bachinski, D., 1967. Framboidal pyrite and concentric features in ores from the Tilt Cove mine, N. E. Newfoundland. *Canadian Mineralogist* 9, 124–127.

Kaplan, I.R., Emery, K.O. & Rittenberg, S.C., 1963. The distribution and isotopic abundance of sulphur in recent marine sediments off southern California. *Geochimica et Cosmochimica Acta* 27, 297–331.

Kasbohm, J., Tarrah, J. & Henning, K.H., 2002. Transmissionselektronen-mikroskopische Untersuchungen an Feinfraktionen der Ringversuchsprobe „Ton Stoob", in Ottner, F. Gier, S. (Eds.), Beiträge zur Jahrestagung Wien, 18.-20.9. 2002. *Berichte der Deutschen Ton- und Tonmineralgruppe e.V.* 9, 71 – 84.

Keil, R.G., Monlucon, C.B., Prahl, G.F. & Hedges, J. I., 1994. Sorptive preservation of labile organic matter in marine sediments. *Nature* 370, 549 – 552.

Kim, J., Dong, H., Seabaugh, J., Newell, S.W. & Eberl, D.D., 2004. Role of microbes in the smectite-to-illite reaction. *Science* 303, 830-832.

Kleeberg, R., Ufer, K. & Bergmann, J., 2005. The quantification of disordered clay minerals by the Rietveld method - some practical aspects. Presentation at the 42nd Annual Meeting of the Clay Minerals Society, June 11–15, 2005, Burlington/Vermont

Kobluk, D.R. & Mapes, R.H., 1989. The fossil record, function, and possible origins of shell color patterns in Paleozoic marine invertebrates. *Palaios* 4, 63-85

Kostka, J.E., Stucki, J.W., Nealson, K.H. & Wu, J., 1996. Reduction of structural Fe(III) in smectite by a pure culture of Shewanella putrefaciens strain MR-1. *Clays and Clay Minerals* 44, 522−529.

Kowalewski, M. & Flessa, K.W. 1996., Improving with age: the fossil record of lingulide brachiopods and the nature of taphonomic megabiases. *Geology* 24, 977-980.

Kriz, J. & Lukes, P., 1974. Color patterns on Silurian *Platyceras* and Devonian *Merista* from the Barrandian Area, Bohemia, Czechoslovakia. *Journal of Paleontology* 48, 41-48.

Krumm, S., 1994. WINFIT 1.0 - A Computer Program for X-ray Diffraction Line Profile Analysis. XIIIth Conference on Clay Mineralogy and Petrology, Praha. *Acta Universitatis Carolinae Geologica* 38, 253–261.

Laflamme, M.; Schiffbauer, J.D., Narbonne, G. M. & Briggs, D.E.G., 2011. Microbial Biofilms And The Preservation Of The Ediacara Biota. *Lethaia* 44, 203–213.

Li, C.W., Chen, J.Y. & Hua, T.E., 1998. Precambrian Sponges with Cellular Structures *Science* 279 (5352), 879-882 .

Li, Y., Vali, H., Sears, S.K., Yang, J., Deng, B. & Zhang, C.L. 2004. Iron reduction and alteration of nontronite NAu-2 by a sulfate-reducing bacterium. *Geochimica et Cosmochimica Acta* 68, 3251–3260.

Liu J., Ou Q., Han J., Zhang Z., He T., Yao X., Fu D. & Shu D., 2011. New Occurence of the Lower Cambrian (Stage 4, Series 2) Guanshan Biota in Huize, Yunnan, South China. *Bulletin of Geosciences* 87(1), 125-132.

Liu, D., Dong, H., Bishop, M.E., Zhang, J., Wang, H., Xie, S., Wang, S., Huang, L. & Eberl, D.D., 2012. Microbial reduction of structural iron in interstratified illite-smectite minerals by a sulfate-reducing bacterium. *Geobiology* 10, 150-62.

Liu, Q., Luo, H.L., Chen, L.-Z. & Lu, S.-X., 2006. *Panlongia*, a new trilobitomoph from Lower Cambrian, Kunming, Yunnan (in Chinese with English abstract). *Acta Paleontologica Sinica* 45, 384–391

Locquin, M.V. & Weber, C., 1978. Origine et structure des membranes organiques cellulaires des moneres archeo-paleozoiques. 103e Congrès National des Sociétés Savantes, Nancy, sciences fasc. II: 27-38.

Lord III, C.J., 1982. A selective and precise method for pyrite determination in sedimentary materials. *Journal Of Sedimentary Research* 52(2), 664-666.

Lougheed, M.S. & Mancuso, J.J., 1973. Hematite framboids in the Negaunee Iron Formation, Michigan: evidence for their biogenic origin. *Economic Geology* 68, 202–209.

Love, L.G., 1967. Early diagenetic iron sulphide in Recent sediments of the Wash (England). *Sedimentology* 9, 327–352.

Love, L.G. & Amstutz, G.C., 1969. Framboidal pyrite in two andesites. *Neues Jahrbuch für Mineralogie, Monatshefte* 3, 97–108.

Lowenstam, H.A., 1981. Minerals formed by organisms. *Science* 211, 1126-1131.

Luo, H., Hu, S., Chen, L. 1999. Early Cambrian Chengjiang Fauna from Kunming region, China. *Yunnan Science and Technology Press*, Kunming. 130pp.

Luo, H., Fu, X., Hu, S., Li, Y., Chen, L., You, T. & Liu, Q., 2005. New vetulicoliids from the Lower Cambrian Guanshan Fauna, Kunming. *Journal of the Geological Society of China* 79, 1-6.

Luo, H., Fu, X., Hu, S., Li, Y., Chen, L., You, T. & Liu, Q., 2006. New bivalve arthropods from the Lower Cambrian Guanshan Fauna in the Kunming and Wuding areas. *Acta Paleontologica Sinica* 45, 460-472.

Luo, H., Fu, X., Hu, S., Li, Y., Hou, S., You, T., Pang, J. & Liu, Q., 2007. A new Arthropod Guangweicaris Luo, Fu et Hu gen. Nov. from the Early Cambrian Guanshan Fauna, Kunming, China. *Journal of the Geological Society of China* 81, 1-7.

Luo, H., Li, Y., Hu, S.X., Fu, X., Hou, S., Liu, X., Chen, L., Li, F., Pang, J. & Liu, Q., 2008. Early Cambrian Malong Fauna and Guanshan Fauna from Eastern Yunnan, China. *Yunnan Science and Technology Press*, Kunming, China, 134pp.

Lyons, T.W., Werne, J.P., Hollander, D.J. & Murray, R.W., 2003. Contrasting sulfur geochemistry and Fe/Al and Mo/Al ratios across the last oxic-to-anoxic transition in the Cariaco Basin, Venezuela. *Chemical Geology* 195, 131–157

Lyons, T.W. & Severmann, S., 2006. A critical look at iron paleoredox proxies based on new insights from modern euxinic marine basins. *Geochimica et Cosmochimica Acta* 70, 5698–5722.

Lyons, T.W., Anbar, A.D., Severmann, S., Scott, C. & Gill, B.C., 2009. Tracking Euxinia in the Ancient Ocean: A Multiproxy Perspective and Proterozoic Case Study. *Annual review of Earth and Planetary Science* 37, 507–34.

Mackay, S. & Hewitt, R., 1978 Ultrastructural studies on the brachiopod pedicle. *Lethaia* 11, 331-339.

Maclean, L.C.W., Tyliszczak, T., Gilbert, P.U., Zhou, D., Pray, T.J., Onstott, T.C. & Southam, G., 2008. A high-resolution chemical and structural study of framboidal pyrite formed within a low-temperature bacterial biofilm. *Geobiology* 6, 471–480.

McKeague, J.A. & Day, J.H., 1966. Dithionite and oxalate extractable Fe and ai as aids in differentiating various classes of soils. *Canadian journal of soil science*, 46, 13-21.

Manwell, C., 1960. Histological specificity of respiratory pigments-II. Oxygen transfer system involving hemerythrins in sipunculid worms of different ecologies. *Comparative Biochemistry and Physiology* 1, 277-285.

Marshall, R.C., 2006. Explaining the Cambrian "explosion" of animals. *Annual Review of Earth and Planetary Sciences* 34, 355-384.

Martin R. E., 1999. Taphonomy: A Process Approach Cambridge paleobiology series 4. University Press, Cambridge 524pp.

Marynowski, L., Kurkiewicz, S., Rakociński, M. & Simoneit B.R.T., 2011. Effects of weathering on organic matter: I. Changes in molecular composition of extractable

organic compounds caused by paleoweathering of a Lower Carboniferous (Tournaisian) marine black shale. *Chemical Geology* 285, 144–156.

Matthew, G. F., 1902. Notes on Cambrian faunas. *Royal Society of Canada, Transactions* 8, 93-112.

McKirdy, D.M., Hall, P.A., Nedin, C., Halverson, G.P., Michaelsen, B.H., Jago, J.B., Gehling, J.G. & Jenkins, R.J.F., 2011. Paleoredox status and thermal alteration of the lower Cambrian (Series 2) Emu Bay Shale Lagerstätte, South Australia. *Australian Journal of Earth Sciences* 58, 259–272.

Mehl, D., 1999. Die frühe Evolution der Porifera. Phylogenie und Evolutionsökologie der Poriferen im Paläzoikum mit Schwerpunkt der desmentragenden Demospongiae (>Lithistide<). *Münchener Geowissenschaftliche Abhandlungen* 37, 72pp.

Mehl, D. & Reitner, J., 1993. Porifera Grant 1836, *in* Steiner, M., Mehl, D., Reitner, J., and Erdtmann, B.D., Oldest entirely preserved sponges and other fossils from the lowermost Cambrian and a new facies reconstruction of the Yangtze platform (China): *Berliner Geowissenshaftliche Abhandlungen*, series E, 9, 293–329.

Mehl, D. & Erdtmann, B., 1994. *Sanshapentella dapingi* n. gen. n. sp. A new hexactinellid sponge from the Early Cambrian (Tommotian) of China. *Berliner Geowissenshaftliche Abhandlungen 13*, 315–319.

Mehra, O.P. & Jackson, M.L., 1960. Iron oxide removal from soils and clays by a dithionite-citrate system buffered with sodium bicarbonate. *National conference on clays and minerals proceedings*: 317-327.

Menon, K.K., 1967. Origin of diagenetic pyrite in the Quilon Limestone, Kerala, India. *Nature* 213, 1219–1220.

Müller, W.E.G., Wang, X., Burghard, Z., Bill, J., Krasko, A., Boreiko, A., Schloßmacher, U., Schröder, H.C. & Wiens, M., 2009. Bio- sintering processes in hexactinellid sponges: Fusion of bio- silica in giant basal spicules from *Monorhaphis chuni. Journal of Structural Biology* 168, 548-561.

Naimark, E., Kalinina, M., Shokurov, A., Zaytseva, L. & Dzerzhinsky K., 2013. Experimental fossils: Fast mineralization in clay colloids. Proceedings of the 3rd IGCP 591 Annual Meeting, 241-243.

Neary, M.T., Reid, D.G., Mason, M.J., Friscic, T., Duer, M.J. & Cusack, M. 2011. Contrasts between organic participation in apatite biomineralization in brachiopod shell and vertebrate bone identified by nuclear magnetic resonance spectroscopy. *Journal of the Royal Society Interface* 8, 282-288

Nishizawa, A., Sarashina, I., Tsujimoto, Y., Iijima, M. & Endo, K. 2010. Artificial fertilization, early development and chromosome numbers in the brachiopod *Lingula anatina*. *Special Papersin Palaeontology* 84, 309-316.

Orr, P.J., Briggs, D.E.G. & Kearns, S.L., 1998. Cambrian Burgess Shale animals replicated in clay minerals. *Science* 281, 1173–1175.

Passier, H.F., Middelburg, J.J., De Lange, G.J. & Bottcher, M.E., 1997. Pyrite contents, microtextures, and sulfur isotopes in relation to formation of the youngest eastern Mediterranean sapropel. *Geology* 25, 519–522.

Petrovich, R., 2001. Mechanisms of fossilization of the soft-bodied and lightly armored faunas of the Burgess Shale and of some other classical localities. *American Journal of Science* 301, 683–726.

Phillips, E.J.P. and Lovley & D.R., 1987. Determination of Fe(III) and Fe(II) in oxalate extracts of sediment. *Soil Science Society of America journal*, 51(4), 938-941.

Pichevin, L., Bertrand, P., Boussafir, M. & Disnar, J.R., 2004. Organic matter accumulation and preservation controls in a deep sea modern environment: an example from Namibian slope sediments. *Organic Geochemistry* 35, 543–559.

Poch, R.M., Thomas, B.P., Fitzpatrick, R.W., Merry, R.H., 2009. Micromorphological evidence for mineral weathering pathways in a coastal acid sulfate soil sequence with Mediterranean-type climate, South Australia. *Australian Journal of Soil Research* 47, 403–422.

Ponomarenko, A.G., 2010. First record of Dinocarida from Russia. *Paleontological Journal* 44, 503-504.

Poulton, S.W. & Canfield, D.E., 2005. Development of a sequential extraction procedure for iron: Implications for iron partitioning in continentally derived particulates. *Chemical Geology* 214, 209–221.

Poulton, S.W. & Raiswell, R., 2002. The low-temperature geochemical cycle of iron: From continental fluxes to marine sediment deposition. *American Journal of Science* 302, 774–805.

Poulton, S.W., Fralick, P.W. & Canfield, D.E., 2004. The transition to a sulphidic ocean ~ 1, 84 billion years ago. *Nature* 431, 173-177.

Powell, W.G., 2003. Greenschist-facies metamorphism of the Burgess Shale and its implications for model of fossil formation and preservation. *Canadian Journal of Earth Sciences* 40, 13-25.

Powell, W.G., Johnston, P.A. & Collom, C.J., 2003. Geochemical evidence for oxygenated bottom waters during deposition of fossiliferous strata of the Burgess Shale Formation. *Palaeogeography, Palaeoclimatology, Palaeoecology* 201, 249–268.

Raiswell, R., 1982. Pyrite texture, isotopic composition and the availability of iron. *American Journal of Science 82*, 1244–1263.

Raiswell, R. & Berner, R.A., 1986. Pyrite and organic matter in Phanerozoic normal marine shales. *Geochimica et Cosmochimica Acta* 50, 1967–1976

Raiswell, R. & Berner, R.A., 1987. Organic carbon losses during burial and thermal maturation of normal marine shales. *Geology* 15, 853–856.

Raiswell, R., Buckley, F., Berner, R.A. & Anderson, T.F., 1988. Degree of pyritization of iron as a paleoenvironmental indicator of bottom-water oxygenation. *Journal of Sedimentary Petrology* 58, 812–819.

Raiswell, R., Canfield, D. & Berner, R., 1994. A comparison of iron extraction methods for the determination of degree of pyritisation and the recognition of iron-limited pyrite formation. *Chemical Geology*, 111(1-4), 101-110.

Raiswell, R. & Canfield, D.E., 1998. Sources of iron for pyrite formation in marine sediments. *American Journal of Science* 298, 219–245.

Raiswell, R., Newton, R.J. & Wignall, P.B., 2001. An indicator of watercolumn anoxia: resolution of biofacies variations in the Kimmeridge Clay (Upper Jurassic, U.K.). *Journal of Sedimentary Research* 71, 286–294.

Raiswell, R. & Anderson, T.F., 2005. Reactive iron enrichment in sediments deposited beneath euxinic bottom waters: Constraints on supply by shelf recycling, in: McDonald, I., Boyce, A.J., Butler, I.B., Herrington, R.J., Polya, D.A. (Eds), Mineral Deposits and Earth Evolution. *Geological Society Special Publication* 248, 179–194. London.

Rigby, J.K. & Hou, X.G., 1995. Lower Cambrian demosponges and hexactinellid sponges from Yunnan, China: *Journal of Paleontology* 69, 1009–1019.

Rimmer, S.M., 2004. Geochemical paleoredox indicators in Devonian–Mississippian black shales, Central Appalachian Basin (USA). *Chemical Geology* 206, 373– 391.

Rong, J.Y., 1974. Cambrian brachiopods. Nanjing Institute of Geology and Paleontology, Acadamia Sinica, Handbook of Palaeontology and Stratigraphy of Southwest China. *Science Press*, Beijing, pp. 113–114.

Salmon, V., Derenne, S., Lallier-Vergès, E., Largeau, C. & Beaudoin, B., 2000. Protection of organic matter by mineral matrix in a Cenomanian black shale. *Organic Geochemistry* 31, 463–474.

Sawlowicz, Z., 1990. Primary copper sulphides from the Kupferschiefer, Poland. *Mineral Deposita* 25, 262–271.

Sawlowicz, Z., 1993. Pyrite framboids and their development: a new conceptual mechanism. *Geologische Rundschau* 82, 148–156.

Schneiderhoehn, H., 1923. Chalkographische Untersuchung des Mansfelder Kupferschiefers. *Neues Jahrbuch Mineralogie Geologie Palaeontologie* 47, 1–38.

Scott, R., Meffre, S., Woodhead, J., Gilbert, S.E., Berry R.F. & Emsbo, P., 2009. Development of Framboidal Pyrite during Diagenesis, Low-Grade Regional Metamorphism, and Hydrothermal Alteration. *Economic Geology* 104, 1143–1168.

Seilacher, A., 1970. Begriff und Bedeutung der Fossil-Lagerstätten. *Neues Jahrbuch für Geologie und Paläontologie* 34-39.

Seilacher, A., 1990. Die Holzmadener Posidonienschiefer – Entstehung der Fossillagerstätte und eines Erdölmuttergesteins. In: Weidert W.K. (Hrsg.) *Klassische Fundstellen der Paläontologie*, 2, 107–131.

Shen J., Wang Y. & Song F., 2003. Characteristics of the active Xiaojiang fault zone in Yunnan, China: a slip boundary for the southeastward escaping Sichuan–Yunnan Block of the Tibetan Plateau. *Journal of Asian Earth Sciences* 21, 1085–1096.

Shimizu, K., Cha, J., Stucky, G.D. & Morse, D.E., 1998. Silicatein α: Cathepsin L-like protein in sponge biosilica. *Proceeding of the national Academy of Sciences 95*, 6234-6238.

Skripchenko, N.S., 1968. Biogenic pyrite ore deposits. *Dokl Akad Nauk* SSSR 181, 177-179

Środoń, J., Elsass, F., McHardy, W.J. & Morgan, D.J., 1992. Chemistry of illite‑smectite inferred from TEM measurements of fundamental particles. *Clay Minerals* 27, 137‑158.

Steiner, M., 2008. Taphonomy of Early Cambrian phosphatic fossil remains from South China. *Erlanger Geologische Abhandlungen, Sonderband* 6, 64-65.

Steiner, M., Mehl, D., Reitner, J. & Erdtmann, B., 1993. Oldest entirely preserved sponges and other fossils from the lowermost Cambrian and a new facies reconstruction of the Yangtze Platform (China). *Berliner Geowissenshaftliche Abhandlungen,* ser. E, 9, 293–329.

Steiner, M., Zhu, M., Weber, B. & Geyer G., 2001. The Lower Cambrian of Eastern Yunnan: Trilobite-based biostratigraphy and related faunas. *Acta Palaeontologica Sinica*, 40, 63-79.

Steiner, M., Wallis, E., Erdtmann, B., Zhao, Y. & Yang, R., 2001. Submarine- hydrothermal exalative ore layers in black shales from South China and associated fossils- insight into

a Lower Cambrian facies and bio- evolution. *Palaeogeography, Palaeoclimatology, Palaeoecology 169*, 165–191.

Steiner, M., Zhu, M., Zhao, Y. & Erdtmann, B., 2005. Lower Cambrian Burgess shale–type fossil associations of South China. *Palaeogeography, Palaeoclimatology, Palaeoecology* 220, 129–152.

Steiner, M., Li, G., Hu, S. & Keupp, H., 2010. Soft-tissue preservation in small shelly faunas. *Geological Society of America, Annual Meeting, Denver*, 42: 359.

Steiner M., Hu S., Liu J. & Keupp H., 2011. A new species of *Hallucigenia* from the Cambrian Stage 4 Wulongqing Formation of Yunnan (South China) and the structure of sclerites in lobopodians. *Bulletin of Geosciences* 87(1), 107-124.

Steinike, K., 1963. A further remark on biogenic sulfides: inorganic pyrite spheres. *Economic Geology* 58, 998–1000.

Stene, L.P., 1979. Polyframboidal pyrite in the tills of southwestern Alberta. *Canadian Journal of Earth Science* 16, 2053–2057.

Stucki, J.W. & Kostka, J.E., 2006. Microbial reduction of iron in smectite. *Comptes Rendus Geoscience* 338, 468−475.

Stucki, J.W., Komadel, P. & Wilkinson, H.T. 1987. Microbial reduction of structural iron(III) in smectites. *Soil Science Society of America* 51, 1663−1665.

Suk, D., Peacor, D.R. & Van Der Voo, R., 1990. Replacement of pyrite framboids by magnetite in limestone and implications for paleomagnetism. *Nature* 345, 611–613.

Sunagawa, I., Endo, Y. & Nakai, N., 1971. Hydrothermal synthesis of framboidal pyrite. *The Society of Mining Geologists of Japan* (Special Issue) 2, 10-14.

Sweeney, R.E. & Kaplan, I.R., 1973. Pyrite framboid formation: laboratory synthesis and marine sediments. *Economic Geology* 68, 618–634.

Swinehart, J.H. & Smith, K.H., 1979. Iron and manganese deposition in the periostraca of several bivalve molluscs. *Biological Bulletin* 156, 369-381.

Szczepanik, P. & Sawłowicz, Z., 2005. Pyritization of microfossils: Crinoid remains from the middle jurassic of Ogrodzieniec (Kraków-Czestochowa upland, Poland). *Studia Geologica Polonica* 124, 37–52.

Takahashi, Y., Châtellier, X., Hattori, K.H., Kato, K. & Fortin, D., 2005. Adsorption of rare earth elements onto bacterial cell walls and its implication for REE sorption onto natural microbial mats. *Chemical Geology* 219, 53–67.

Takahashi, Y., Hirata, T., Shimizu, H,, Ozaki, T. & Fortin, D. 2007. A rare earth element signature of bacteria in natural waters? *Chemical Geology* 244, 569–583.

Taylor, G.R., 1982. A mechanism for framboid formation as illustrated by a volcanic exhalative sediment. *Mineralium Deposita* 17, 23–36.

Taylor, K.G. & Macquaker, J.H.S., 2000. Early diagenetic pyrite morphology in a mudstone-dominated succession: the Lower Jurassic Cleveland Ironstone Formation, eastern England. *Sedimentary Geology* 131, 77-86.

Taylor, S.R. & McLennan, S.M., 1985. The Continental Crust: Its Composition and Evolution. Blackwell, Oxford.

Tazaki, K., 2000. Formation of Banded Iron-Manganese Structures by Natural Microbial Communities. *Clays and Clay Minerals* 48, 511-520

Tessier, A., Campbell, P.G.C. & Bisson, M., 1979. Sequential extraction procedure for the speciation of particulate trace metals. *Analytical Chemistry*, 51(7), 844-851.

Ufer, K., Roth, G., Kleeberg, R., Stanjek, H., Dohrmann, R. & Bergmann, J., 2004. Descprition and quantification of powder X-ray diffractograms of turbostratically disordered layer structures with a Rietveld compatible approach. *Zeitschrift für Kristallographie* 219, 519–527.

Ufer, K., Kleeberg, R., Bergmann, J., Curtius, H. & Dohrmann, R., 2008a. Refining realstructure parameters of disordered layer structures within the Rietveld method. *Zeitschrift für Kristallographie Supplements* 27, 151–158.

Ufer, K., Stanjek, H., Roth, G., Dohrmann, R., Kleeberg, R. & Kaufhold, S., 2008b. Quantitative phase analysis of bentonites with the rietveld method. *Clays and Clay Minerals* 56, 272–282.

Ufer, K., Kleeberg, R., Bergmann, J. & Dohrmann, R., 2010. Simultaneous Rietveld refinement of multidevice and/or multi-specimen XRD data of mixed layered structures. Book of Abstracts of the 2010 SEA-CSSJ-CMS Trilateral Meeting on Clays. Sevilla, Spain, June 8-10, 2010.

Uzarowicz, Ł., Skiba, S., Skiba, M. & Šegvić, P., 2011. Clay-mineral Formation in Soils Developed in the Weathering Zone of Pyrite-Bearing Schists: A Case Study from the Abandoned Pyrite Mine in Wieściszowice, Lower Silesia, SW Poland *Clays and Clay Minerals* 59, 581-594.

Vallentyne, J.R., 1963. Isolation of pyrite spherules from recent sediments. *Limnology and Oceanography* 8, 16–30.

Van Roy, P., Orr, P.J., Botting, J.P., Muir, L.A., Vinther, J., Lefebvre, B., Hariri K. & Briggs D.E.G., 2010. Ordovician faunas of Burgess Shale type. *Nature* 465, 215-218.

Wang, Q. & Morse, J.W., 1996. Pyrite formation under conditions approximating those in anoxic sediments. I. Pathway and morphology. *Marine Chemistry* 52, 99–121.

Weber B., Hu S. & Steiner, M., 2011. A divers and significant ichnofauna from the Lower Cambrian (Botoman) Wulongqing Fm. near Kunming (Yunnan Prov., S-China). *Bulletin of Geosciences* 87(1), 71-92.

Werne, J.P., Sageman, B.B., Lyons, T.W. & Hollander, D.J., 2002. An integrated assessment of a ''type euxinic'' deposit: evidence for multiple controls on black shale deposition in the Middle Devonian Oatka Creek formation. *American Journal of Science* 302, 110–143.

Wiese, R.G. & Fyfe, W.S., 1986. Occurrences of iron sulfides in Ohio coals. International *Journal of Coastal Geology* 6, 251–276.

Wignall, P.B. & Myers, K.J., 1988. Interpreting benthic oxygen levels in mudrocks: A new approach. *Geology* 16, 452–455.

Wignall, P.B. & Newton, R., 1998. Pyrite framboid diameter as a measure of oxygen deficiency in ancient mudrocks. *American Journal of Science* 298, 537–552.

Wignall, P.B., Newton, R. & Brookfield, M.E., 2005. Pyrite framboid evidence for oxygen-poor deposition during the Permian-Triassic crisis in Kashmir. *Palaeogeography Palaeoclimatology Palaeoecology* 216, 183–188.

Wignall, P.B., Bond, D.P.G., Kuwahara, K., Kakuwa, Y., Newton, R.J. & Poulton, S.W., 2010. An 80 million year oceanic redox history from Permian to Jurassic pelagic sediments of the Mino-Tamba terrane, SW Japan, and the origin of four mass extinctions. *Global and Planetary Change* 71, 109–123.

Wilkin, R.T., Barnes, H.L. & Brantley, S.L., 1996. The size distribution of framboidal pyrite in modern sediments: an indicator of redox conditions. *Geochimica et Cosmochimica Acta* 60, 3897–3912.

Wilkin, R.T. & Barnes, H.L., 1997. Formation processes of framboidal pyrite. *Geochimica et Cosmochimica Acta* 61, 323–339.

Williams, A., 1968. Significance of the Structure of the Brachiopods Periostracum. *Nature* 218, 551-554.

Williams, A., Carlson, S.J., Howard, C., Brunton, C., Holmer, L.E. & Popov, L. 1996. A supra-ordinal classification of the Brachiopoda. *Philosphical Transactions of the Royal Society of London*, Series B 351, 1171–1193.

Williams, A. & Cusack, M. 1997. Lingulid shell mediation in clay formation. *Lethaia* 29, 349-360.

Williams, A., Cusack, M. &Mackay, S. 1994 Collagenous chitinophosphatic shell of the brachiopod *Lingula. Transactions of the Royal Society of London, Series B*, 346: 223-266.

Williams, A., Cusack, M. & Buckman, J.O. 1998. Chemico- structural phylogeny of the discinoid brachiopod shell. *Philosophical Transactions of the Royal Society of London*, Series B 353, 2005-2038.

Williams, A., Lueter, C. & Cusack, M. 2001. The Nature of Siliceous Mosaics Forming the First Shell of the Brachiopod *Discinisca. Journal of Structural Biology* 134, 25–34.

Wilson, L.A., 2006. Food for thought: a morphological and taxonomic study of fossilised digestive systems from Early to Middle Cambrian taxa. University of Cambridge, 275 pp.

Wilson, M.J., 2004. Weathering of primary rock-forming minerals: processes, products and rates. *Clay Minerals* 39, 233_266.

Wu, T., Shelobolina, E., Xu, H., Konishi, H., Kukkadapu, R. & Roden, E.E. 2012. Isolation and Microbial Reduction of Fe (III) Phyllosilicates from Subsurface Sediments. *Environmental Science & Technology* 46, 11618-11626.

Wu, W. 2004. Fossil sponges from the Early Cambrian Chengjiang Fauna, Yunnan, China. Ph. D. Thesis, Nanjing Institute of Geology and Palaeontology, Chinese Academy of Sciences, 181 pp.

Yang, X., Zhao, Y., Wang, Y. & Wang, P., 2005. Discovery of sponge body fossils from the late Meishucunian (Cambrian) at Jinsha, Guizhou, south China: *Progress in Natural Science 15(8)*, 708-712.

Yuan, X., Xiao, S., Parsley, R., Zhan, C., Chen, Z. & Hu J. 2002. Towering sponges in an Early Cambrian Lagerstätte: Disparity between nonbilaterian and bilaterian epifaunal tierers at the Neoproterozoic- Cambrian transition, *Geology 30*, 363-366.

Zhang, X., 2007. Phosphatized Bradoriids (Arthropoda) from the Cambrian of China. *Palaeontographica Abteilung* A 281, 1-173.

Zhang W.T. & Babcock L.E., 2001. New extraordinarily preserved enigmatic fossils, possibly with Ediacaran affinities, from the Lower Cambrian of Yunnan, China. *Acta Palaeontologica Sinica,* 40(Suppl), 201–213

Zhang, X., Hou, X. & Emig, C.C. 2003. Evidence of lophophora diversity in Early Cambrian Brachiopoda. *Proceeding of the Royal Society of London Series B (Supplement)* 270, 65–68.

Zhang, Y., Meng, Q., Jiang, T., Wang, H., Xie, L. &Zhang, R. 2003. A novel ferritin subunit involved in shell formation from the pearl oyster (*Pinctada fucata*). *Comparative Biochemistry and Physiology Part B: Biochemistry and Molecular Biology* 135: 43-54

Zhang, Z.F., Han, J., Zhang, X.L., Liu, J.N. &Shu, D.G. 2004a. Soft tissue preservation in the Lower Cambrian linguloid brachiopod from South China. *Acta Palaeontologica Polonica* 49, 259–266.

Zhang, Z.F., Shu, D.G., Han, J. & Liu, J.N. 2004b. New data on the lophophora anatomy of Early Cambrian linguloids from the Chengjiang Lagerstätte, Southwest China. *Carnets de Géologie – Notebooks on Geology, Letter* 04**,** 7 pp.

Zhang, Z.F., Shu, D.G., Han, J. &Liu, J.N. 2005. Morpho-anatomical differences of the Early Cambrian Chengjiang and Recent linguloids and their implications. *Acta Zoologica* 86, 277–288.

Zhao, Y., Zhu, M., Babcock, L.E., Yuan, J., Parsley, R.L., Peng, J., Yang, X. & Wang, Y., 2005. Kaili Biota: A Taphonomic Window on Diversification of Metazoans from the Basal Middle Cambrian: Guizhou, China. *Acta Geologica Sinica* - English Edition, 79, 751–765.

Zhang, X.G., Bergström, J., Bromley, R.G. &Hou, X.G., 2007. Diminutive trace fossils in the Chengjiang Lagerstätte. *Terra Nova* 19, 407–412.

Zhang, Z.F., Han, J., Zhang, X.L., Liu, J.N. &Shu, D.G. 2007. Note on the gut preserved in the Lower Cambrian Lingulellotreta (Lingulata, Brachiopoda) from South China. *Acta Zoologica (Stockholm)* 88, 65–70.

Zhang, X., Liu, W. &Zhao, L. 2008. Cambrian Burgess Shale-type Lagerstätten in South China:Distribution and significance. *Gondwana Research* 14, 255–262.

Zhang, Z., Robson, S.P., Emig, C. &Shu, D. 2008. Early Cambrian radiation of brachiopods: a prespective from South China. *Gondwana Research* 14, 241-254.

Zhao, F., Caron, J.B., Hu, S.X. & Zhu, M.Y. 2009. Quantitative analysis of taphofacies and paleocommunities in the Early Cambrian Chengjiang Lagerstätte. *Palaios* 24, 826-839.

Zhao, F., Zhu, M. & Hu, S., 2012. Diverse responses of Cambrian organisms to sedimentary events: Evidence from the Chengjiang Lagerstätte of eastern Yunnan. *Acta Palaeontologica Sinica* 51, 265-280.

Zhu, M., Zhang, J.M. & Li, G.X., 2001. Sedimentary environments of the Early Cambrian Chengjiang Biota: Sedimentology of the Yu'anshan Formation in Chengjiang County, eastern Yunnan. *Acta Palaeontologica Sinica*, 40(sup.):80-105.

Zhu, M., Babcock, L. & Steiner, M., 2005. Fossilization modes in the Chengjiang Lagerstätte (Cambrian of China): testing the role of organic preservation and diagenetic alteration in exceptional preservation. *Palaeogeography, Palaeoclimatology, Palaeoecology* 220, 31-46.

Zöller, M.H., 1993. Charakterisierung von Illitkristallen durch konvergente Elektronenbeugung. In: Berichte der Deutschen Ton‐ und Tonmineralgruppe e.V.: 211‐220 [Beiträge zur Jahrestagung der DTTG 1992].

<u>CURRICULUM VITAE</u>

September 2013

Personal Details:
Dipl. Geol. Angela Forchielli

<u>E-mail</u>:   <u>Nationality</u>:

<u>Date and place of birth</u>:   <u>Marital status</u>:

                     <u>Private Address</u>:

<u>Education</u>:

2008- present

Ph.D. student in Palaeontology at the Institute of Geological Science, Freie Universität Berlin, Ph.D. topic:Taphonomy of exceptional Cambrian fossil Lagerstätten of China exemplified by the Chengjiang Biota.

Supervisors: Prof. H. Keupp and Dr. M. Steiner

1999 - 2006

Master degree ("Laurea") in Geological Science at the University of Rome "La Sapienza". Specialization in Paleontology.

Qualification mark: 110 cum laude /110

- <u>Experimental thesis in Paleontology</u>: "Similitudini nelle modalitá di formazione dei gusci di alcuni cefalopodi: il caso di *Atractites*". [Similarity in the modalities of formation of some cephalopod shells: the *Atractites* case.]".

Supervisor: Professor Umberto Nicosia, University of Rome "La Sapienza".

- <u>Second Thesis in Geophysics</u>: "Tomografia sismica e profili gravimetrici nella caldera di Nisyros". [Seismic tomography and gravimetric profiles in the caldera of Nisyros]", 2006.

Supervisor: Professor Michele Di Filippo, University of Rome "La Sapienza"

1994-1999

High-school degree at the Liceo statale (Classical high school: among others humanistic subjects, 5 years of Latin and Greek) "Augusto", Rome (Italy), 1999. Specialization in English.

Research Activities and scholarships:

- **2011- 2012**

Ernst Mach Scholarship (OEAD) at Department of Palaeontology, Universität Wien

Reserch Topic: Taphonomic pathways of the arthropods from the Polzberg fossil *Lagerstätte*

- **2008 –2011**

Researcher in the international project FOR 736 at Freie Universität Berlin

Research topic: Biology and taphonomy of exceptional Cambrian fossil Lagerstätten of China exemplified by the Chengjiang Biota

- **2007 - 2008**

Praktikum at Museum für Naturkunde Leibniz-Institut für Evolutions- und Biodiversitätsforschung, Berlin

- **2003-2006**

Scholarship at the library of the Department of Earth Sciences of the University "La Sapienza", Rome

- **2001-2002**

Scholarship at the fossil collections of the Department of Earth Sciences of the University "La Sapienza", Rome

Attended meetings:

July 2008
Talk given at Freie Universität Berlin: "Taphonomy of the Chengjiang Biota and field campaign 2008"
March 2009
Seminar given at Freie Universität Berlin: "Taphonomy of the Chengjiang Biota"
June 2009
Talk given at Freie Universität Berlin: "Taphonomy of exceptional Cambrian fossil lagerstätten of China exemplified by Chengjiang Biota"

October 2009
Earth Control on Planetary Life and Environment: Geologische Vereinigung e. V. -
05.10.-07.10. Göttingen- Poster presentation.
May 2010
Invited talk given at Museum für Naturkunde Leibniz-Institut für Evolutions- und
Biodiversitätsforschung, Berlin:"Taphonomy of the Chengjiang Fauna"
June 2010
Talk given at Charles University Prague: "Taphonomy of the sponges of Burgess Shale –
type fossil Lagerstätten of South China"
July 2010
International palaeontological congress- (IPC3) London 26.6-03.7.-Two poster
presentations
October 2010
Geological Society of America (GSA) Denver Annual Meeting (31 October –3
November)- Oral presentation
November 2010
Poster presentation in internal international meeting in Nanjing-China
January 2012
Invited talk given at University of Vienna
July 2012
Invited talk given at Natural History museum of Kyoto: "The Chengjiang Fauna (SW
China): overview and latest results from an Early Cambrian Burgess Shale-type fossil
Lagerstätte".
September 2012
Pangeo 2012- Salzburg (17-18.9)-Oral presentation
Palges Berlin 2012 German Paleontological association (24-29.9)- Oral presentation
May 2013
SPI- Paleodays 2013-Perugia (22-25.5) Oral and Poster presentations

Publication list:

Forchielli, A., Steiner**,** M., Keupp**,** H., Hu**,** S., Li**,** G., (2009): Taphonomy of Early
Cambrian Chengjiang fossils and phosphatized organic tissues. in: Eynatten, Reitner and
Wörner (Eds.), Abstracts (GV Annual Meeting 2009, Earth Control on Planetary Life and
Environment, October 5 - 7, 2009, Göttingen, Germany). Page 33. Reihe der
Universitätsdrucke im Universitätsverlag Göttingen 2009, 158 S.; Göttingen. [ISBN 978-
3-941875-09-8]

Keupp, H., Steiner, M. and **Forchielli** A., (2010): Back to the roots of modern life-
studies in the Lower Cambrian of China. Fossilien 4 (pp. 218-224).

Briguglio A., & **Forchielli** A., 2010: Transportability of Larger Benthic Foraminifera.
Third International Palaeontological Congress IPC3, London. Abstract Volume: p. 102

Forchielli, A., Steiner, M., Hu S. and Keupp, H., (2010): Taphonomic pathways of the early Cambrian Chengjiang Biota. Third International Palaeontological Congress IPC3, London. Abstract Volume: p. 170

Forchielli, A., Steiner**, M., Hu S., Keupp**, H., (2010): Recent brachiopods as a tool to understand the taphonomic pathways of the earliest Cambrian Chengjiang linguliform brachiopods. Geological Society of America Abstract with program Vol 42, N. 5 p 360.

Hu S., Steiner M., Zhu M., Luo H., **Forchielli** A., Keupp H., Zhao F., Liu Q. (2012): A new priapulid assemblage from the early Cambrian Guanshan Lagerstätte of SW China. Czech Bulletin of Geosciences 87, 93-106.

Forchielli A., Steiner M., Hu S., Keupp H. (2012): Taphonomy of Cambrian (Stage 3/ 4) sponges from Yunnan (South China). Czech Bulletin of Geosciences 87, 133-142.

Forchielli, A., Steiner**, M., Hu S., Lüter C., Keupp**, H. (in press): Taphonomy of the earliest Cambrian linguliform brachiopods. Acta Paleontologica Polonica, available online 04 May 2012 doi: http://dx.doi.org/10.4202/app.2011.0182

Forchielli A., Steiner M., Hu S., Keupp H. (2012): The Chengjiang Biota (Cambrian Stage 3) of Yunnan Province (South China): taphonomy of a Burgess Shale-type fossil Lagerstätte. Terra Nostra 3/2012, 55-56.

Forchielli A. and Pervesler P. (2012): The Polzberg Fauna (Lower Austria): overview and preliminary taphonomic results from a Carnian Fossillagerstätte. Pangeo Austria 2012 Abstract Volume p. 42.

Forchielli A. and Pervesler P. (2013): Phosphatic cuticle in thylacocephalans: a taphonomic case study of *Austriocaris* (Arthropoda, Thylacocephala) from the Fossillagerstätte Polzberg (Raingraben shales, Carnian, Upper Triassic, Lower Austria). Austrian Journal of Earth Sciences 106, 46-61.

Forchielli, A., Steiner**, M., Kasbohm J., Hu S., Keupp**, H. (in press): Taphonomic traits of clay- hosted early Cambrian Burgess Shale- type fossil Lagerstätten in South China. Palaeogeography, Palaeoclimatology, Palaeoecology, (2013), doi: 10.1016/j.palaeo.2013.08.001

Prizes and Awards:

Student Poster Award at the international Conference 2009 Göttingen Earth Control on

  Planetary Life and Environment**. Poster title:** "Taphonomy of the early Cambrian

  Chengjiang fossils and phosphatized organic tissues".

Software:

- Software Applications: MS-Office applications (2003 and 2007)
- Windows environment, vectorial and image processing programs (Adobe Photoshop, ACD Canvas)
- w.w.w. surfing, computer mechanics
- Sebina software (open library OPAC)
- Inca software (Element mapping and EDX analyses)
- Past (data analysis package)

Languages:

- Italian (mother tongue)
- German (fluent)
- English (fluent)
- Spanish (intermediate)
- French (basic)

Field work experiences:

- Mesozoic and Cenozoic of Center and South Italy
- Proterozoic (Ediacarian) of Estremadura (Spain)
- Cambrian (Stage 3 and 4) of South China
- Paleozoic of Barrandium
- Mesozoic of South Germany
- Paleozoic of Utah-USA

Attended curses, Longer stay abroad (>3 weeks) and personal interests

- **Summer Schools** funding by the DAAD to develop elements of a joint Ph.D.-program via joint field summer schools.
    - June 2009- South Germany
    - June 2010- Germany and Czech Republic
- 1.4.2009-30.4.2009: Yunnan Geological Survey, Kunming, Yunnan China
- 31.3.2008-5.5.2008: Yunnan Geological Survey, Kunming, Yunnan China
- Advanced sewing (4 Semesters at VHS WIEN)
- 3 years of oil paint school (in Rome)
- Experience in designer markets in Germany (Berlin) and Italy (Rome) as seller
- Photography

Drive license: cat. B
H-index (stand Scopus September 2013): 2